Calhoun
Institutional Archive of the Naval Postgraduate School

Calhoun: The NPS Institutional Archive

DSpace Repository

Theses and Dissertations | 1. Thesis and Dissertation Collection, all items

1993-06

Ionospheric photoelectrons measured at geosynchronous orbit

Laszakovits, John Samuel.

Monterey, California. Naval Postgraduate School

http://hdl.handle.net/10945/39804

This publication is a work of the U.S. Government as defined in Title 17, United States Code, Section 101. Copyright protection is not available for this work in the United States.

Downloaded from NPS Archive: Calhoun

http://www.nps.edu/library

Calhoun is the Naval Postgraduate School's public access digital repository for research materials and institutional publications created by the NPS community. Calhoun is named for Professor of Mathematics Guy K. Calhoun, NPS's first appointed -- and published -- scholarly author.

Dudley Knox Library / Naval Postgraduate School
411 Dyer Road / 1 University Circle
Monterey, California USA 93943

AD-A272 431

NAVAL POSTGRADUATE SCHOOL
Monterey, California

NOV 12 1993

THESIS

Ionospheric Photoelectrons Measured at Geosynchronous Orbit

by

John Samuel Laszakovits

June 1993

Thesis Advisor: R. C. Olsen

Approved for public release; distribution is unlimited.

93-27503

REPORT DOCUMENTATION PAGE

Form Approved
OMB No 0704-0188

Public reporting burden for this collection of information is estimated to average 1 hour per response, including the time for reviewing instructions, searching existing data sources, gathering and maintaining the data needed, and completing and reviewing the collection of information. Send comments regarding this burden estimate or any other aspect of this collection of information, including suggestions for reducing this burden, to Washington Headquarters Services, Directorate for Information Operations and Reports, 1215 Jefferson Davis Highway, Suite 1204, Arlington, VA 22202-4302, and to the Office of Management and Budget, Paperwork Reduction Project (0704-0188), Washington, DC 20503.

1. AGENCY USE ONLY (Leave blank)	2. REPORT DATE	3. REPORT TYPE AND DATES COVERED
	17 June 1993	Final

4. TITLE AND SUBTITLE

Ionospheric Photoelectrons Measured at Geosynchronous Orbit

5. FUNDING NUMBERS

6. AUTHOR(S)

John S. Laszakovits, LT, USN

7. PERFORMING ORGANIZATION NAME(S) AND ADDRESS(ES)

Naval Postgraduate School
Monterey, CA 93943

8. PERFORMING ORGANIZATION REPORT NUMBER

9. SPONSORING / MONITORING AGENCY NAME(S) AND ADDRESS(ES)

10. SPONSORING / MONITORING AGENCY REPORT NUMBER

11. SUPPLEMENTARY NOTES

The views expressed in this thesis are those of the author and do not reflect the official policy of the Department of Defense or the U.S. Government.

12a. DISTRIBUTION / AVAILABILITY STATEMENT

12b. DISTRIBUTION CODE

13. ABSTRACT (Maximum 200 words)

Measurements of ions and electrons were made by the Los Alamos National Laboratory instrument, the Magnetospheric Plasma Analyzer, onboard spacecraft 1989-046. Observations from five days indicated the presence of both field aligned electrons and equatorially trapped electrons. Correlation existed between occurrences and location in the magnetosphere. Field aligned electrons were measured in the plasmasphere during daylight. On two days, field aligned electrons were also noted in the midnight region of the magnetosphere. Field aligned electrons at energies between 1 and 50 eV were characterized. These electron's spectrum were shown to be similar in shape to the ionospheric photoelectron distribution. Conic distributions of photoelectrons were observed between 08:00 and 10:00 local time on days when both photoelectrons and equatroially trapped electrons were present. $V_{parallel}$ versus $V_{perpendicular}$ spectrograms clearly indicated that photoelectrons undergo perpendicular acceleration. Lack of any magnetic field measurements or collection of wave data prevented determinig the source of the acceleration.

14. SUBJECT TERMS	15. NUMBER OF PAGES
Ionospheric Photoelectrons, Plasmasphere, Electron Spectra, Magnetospheric Plasma Analyzer (MPA), Geosynchronous Orbit.	174
	16. PRICE CODE

17. SECURITY CLASSIFICATION OF REPORT	18. SECURITY CLASSIFICATION OF THIS PAGE	19. SECURITY CLASSIFICATION OF ABSTRACT	20. LIMITATION OF ABSTRACT
UNCLASSIFIED			

NSN 7540-01-280-5500

Standard Form 298 (Rev 2-89)
Prescribed by ANSI Std 239-18

Approved for public release; distribution is unlimited.

Ionospheric Photoelectrons Measured at Geosynchronous Orbit

by

John Samuel Laszakovits
Lieutenant, United States Navy
B.S., University of Kansas, 1982
M.B.A., San Jose State University, 1992

Submitted in partial fulfillment of the
requirements for the degree of

MASTER OF SCIENCE IN PHYSICS

from the

NAVAL POSTGRADUATE SCHOOL
June, 1993

Author: [redacted]
John Samuel Laszakovits

Approved By: [redacted]
R. C. Olsen, Thesis Advisor

[redacted]
S. Gnanalingam, Second Reader

[redacted]
K. E. Woehler, Chairman, Department of Physics

ABSTRACT

Measurements of ions and electrons were made by the Los Alamos National Laboratory instrument, the Magnetospheric Plasma Analyzer, onboard spacecraft 1989-046. Observations from five days indicated the presence of both field aligned electrons and equatorially trapped electrons. Correlation existed between occurrences and location in the magnetosphere. Field aligned electrons were measured in the plasmasphere during daylight. On two days, field aligned electrons were also noted in the midnight region of the magnetosphere. Field aligned electrons at energies between 1 and 50 eV were characterized. These electron's spectrum were shown to be similar in shape to the ionospheric photoelectron distribution. Conic distributions of photoelectrons were observed between 08:00 and 10:00 local time on days when both photoelectrons and equatorially trapped electrons were present. $V_{parallel}$ versus $V_{perpendicular}$ spectrograms clearly indicated that photoelectrons undergo perpendicular acceleration. Lack of any magnetic field measurements or collection of wave data prevented determining the source of the perpendicular acceleration.

Table of Contents

Acknowledgement

This research work could not have been completed in such a short period of time without the significant efforts of Professor R. C. Olsen. All of the courses completed in the Physics Department provided an invaluable background for the theoretical understanding necessary for this research. All of the professors of the Physics Department were very inspiring to me. My special thanks to Professors Otto Heinz and Rudolph Panholzer for their guidance and contributions to my education.

As is true of all of my accomplishments, I am thankful to my parents for instilling in me the desire to always do my best and an optimistic outlook on life. I thank my children for giving me a reason to get up in the morning. And I thank my faith.

But most of all, I thank my wife Laurie Anne for keeping my rudder straight and my sails always full. My every achievement would not be realized without her love, support, and encouragement.

DTIC QUALITY INSPECTED 4

Accession For
NTIS GRA&I ☑
DTIC TAB ☐
Unannounced ☐
Justification
By
Distribution/
Availability Codes
Dist Avail and/or Special
A-1

I. INTRODUCTION

It is important to monitor the plasma environment in which satellites are immersed. Longevity and performance are characteristics that need continual evaluation for "resource-limited" space programs. Distinguishing plasma regions and measuring their properties accurately, within the available resources of current spacecraft, continue to provide a challenge for researchers and spacecraft designers.

In some parts of the magnetosphere and under certain conditions, a satellite may charge to several kilovolts relative to its environment. If the charging is not uniform over the spacecraft, electrical discharges between adjacent unlike components occurs. These discharges may result in physical and irreparable damage or in single event upsets. Dielectric materials found in today's electronics provide another mode for particle deposition and subsequent spurious electronic upsets. These upsets can inject false

commands or degrade information and ultimately cause a mission failure.

There are many missions today that would benefit from properly identifying the plasma region in which they are operating. The goal of some research today is the characterization of the plasma regions in space and their effects on spacecraft. In the future, a spacecraft might measure the electrons and ions to identify its own relative location. Then, depending on the local plasma region, the spacecraft would employ an optimal strategy for the operation of spacecraft systems.

There have been many measurements of electrons above the ionosphere at energies greater than 100 eV. In contrast, the measurements taken below 100 eV have produced relatively few research papers. One such paper was by Coates (1985), who reported that field aligned fluxes measured by GEOS 1 and GEOS 2 were similar to what would be expected from photoelectrons escaping from the ionosphere. Cicerone (1974) wrote that numerical models were low by as much as a factor of two or three in flux magnitude and in related quantities when compared to measured

data from Millstone Hill. There exists a need for research on the low energy electrons generated in the ionosphere as they move upward into the magnetosphere.

Today's instruments are producing a great deal of data in a much larger energy spectrum, including below 100 eV. Faster computers and more powerful interactive software are now providing the tools to study such vast amounts of data effectively and efficiently.

Data studied in this research effort was obtained from a Los Alamos National Laboratory (Los Alamos) instrument mounted onboard spacecraft 1989-046. Particle count data from its Magnetospheric Plasma Analyzer (MPA), presented herein provides an energy spectrum of 1 to 40,000 eV in three dimensions at geosynchronous orbit for both electrons and ions. The work done here has focused on the low energy field aligned electrons. The sections that follow will describe the background science that is understood today, a literature research on photoelectron characteristics and detection, the Los Alamos instrument, observations about the data analyzed, and a discussion of the pertinent characteristics of the low energy field aligned electrons.

II. BACKGROUND PHYSICS

Most research must present the reader with background information before delving into observations and discussions. Understanding the processes which produce the fluxes being analyzed is as important as having the fluxes to analyze. The spectrograms presented are rich with phenomena. This section will discuss the nominal environment experienced by spacecraft at geosynchronous orbits, the production of photoelectrons in the ionosphere, previous detections of photoelectron at geosynchronous orbit, the transport of electrons along field lines in the magnetosphere, and the complicated detection of particles in space.

A. NOMINAL GEOSYNCHRONOUS ENVIRONMENT

During most orbits of a geosynchronous satellite, it encounters various regions and currents that make up earth's magnetosphere, detailed in Figure 1. On a nominal day at geosynchronous orbit, after passing through the outer plasmasphere's dusk bulge, the satellite encounters the plasma sheet currents in the dusk and midnight

regions. The high energy plasma sheet electrons result in the spacecraft charging up to the negative kilovolt range within the midnight region. On the day side, the sunlit spacecraft surfaces charge to a few volts positive due to photoemission. Throughout the day, the spacecraft encounters the ring current while outside the plasmasphere, and co-rotating currents while inside the plasmasphere. The fourth type of currents experienced are the field aligned currents which connect the ionosphere to the magnetosphere. There is an observed net flow of current into the ionosphere in the morning and a net outflow in the evening.

The plasmasphere is the region surrounding the earth between the auroral regions, shaped in a non-symmetrical torus. The interior is filled with ionospheric plasma which is cold and dense compared to the hot plasma in the inner magnetosphere or plasma sheet. The plasmasphere boundary with the plasma sheet is called the plasmapause. McComas (1992) found that the plasmapause moves back and forth across the geosynchronous orbit in very short periods of time. The geosynchronous spacecraft encounters a different environment when it is inside the plasmasphere than when it is

outside the plasmasphere. With a fast moving plasmapause, the environment experienced by the spacecraft becomes unpredictable.

The plasmasphere has a bulge at dusk that has been explained by Chappell (1971). As can be seen in Figure 2, the dusk bulge typically includes the geosynchronous orbit between 15:00 and 22:00 local time. The night side plasmasphere is larger than the day side plasmasphere due to magnetospheric compression from the pressure applied on the magnetosphere by the solar wind. Magnetic activity causes the plasmasphere to be compressed. The plasmashere expands as the magnetic activity secedes. Consequently, the plasmasphere will be larger on days of low magnetic activity. A geosynchronous orbit is most likely to be in the plasmasphere in the dusk region, between 15:00 and 22:00 local time.

B. IONOSPHERIC PHOTOELECTRON PRODUCTION

One of the sources of the field aligned currents in the magnetosphere is the ionospheric photoelectrons. Photons from the sun cause ionization of atoms and molecules that makeup the ionosphere. Photoelectrons are those freed electrons produced during the ionization process. Most photoelectrons possess energies below

60 eV. Above 300 kilometers altitude the dominant constituent for ionization is atomic oxygen, as is indicated in Figure 3 by Tascione (1988). The ionization of atomic oxygen determines the fine structure seen in the flux versus energy distribution of the electrons.

Many studies and measurements have determined expected energy and angular distributions at different altitudes for photoelectrons produced in the upper atmosphere. Cicerone (1973) modeled the atmosphere to determine the energy spectra of photoelectrons in the ionosphere, Figure 4. According to Peterson (1977a), the peaks at 22 and 26 eV correspond to the energy levels attained by electrons from the photoionization of oxygen atoms by extreme ultraviolet (EUV) light at 304Å (He II). Two curves are plotted to illustrate the decrease in photoionization rate with increasing altitude. This decrease is attributed to the decreasing density with increasing altitude. Around 60 eV, both curves have an increase in negative slope.

Lee used data from three Atmosphere Explorer (AE) satellites to complete two comprehensive reports discussing the photoelectron spectrum from below 300 km (1980a) and the photoelectron

spectrum from 300 to 1,000 km (1980b). He divided the day time ionosphere into two regions for the discussion of photoelectrons. Below 300 km, photoelectrons are produced and lost locally. According to Doering (1976), below 300 km, transport processes are not important because coulomb scattering is clearly observable between 200 and 300 km. While above 300 km, local production of photoelectrons is negligible due to the low neutral density. Photoelectrons observed in this region have escaped from lower altitudes.

In Figure 5, Lee (1980b) shows data from AE-E at an altitude of 350 km for the energy range of 0 to 100 eV. Three spectra were plotted for different background plasma densities. For illustrative purposes, the spectra are offset upwards by multiplicative factors of x 3 and x 18. The spectra are arranged from top to bottom in increasing plasma densities. There is a noticeable difference in the intensity and the detailed shape. The structure is more apparent at the lowest density. Lee also noted that at consistent plasma densities, the flux decreases with increasing altitude.

Singhal (1984) did a comprehensive study of photoelectrons produced in the ionosphere. He compared calculated photoelectron fluxes by Singhal (1984) and Oran (1978) with the measured photoelectron fluxes from Lee (1980a) and (1980b). Singhal's calculations use two different models. The "2 D Present" refers to the application of a two dimensional yield spectrum for photoelectron production. Photoelectron transport in altitude is not allowed in this model. It assumes that photoelectrons are produced and absorbed at the observation altitude. In the "3 D Present" model, photoelectron transport to different altitudes is allowed.

Figure 6 has four plots that vary by the model values plotted and in their altitude. In Figure 6A, three curves were plotted for an altitude of approximately 150 km. The solid line represented experimentally measured data, the dash--dot--dot line represented calculations from Oran's model, and the dashed line represented Singhal's "2 D Present" model. There was an exponential decease in photoelectron flux with increasing energy, structure near 25 eV, and a sudden drop in flux beyond 55 eV. Between 10 and 35 eV, measured data by Lee compared favorably with the calculated

curves. Singhal attributed the slight differences between the plotted values of Oran's and Singhal's models to the difference in the inelastic cross sections used in each model.

In Figure 6B, curves obtained from the same three sources, were plotted for an altitude of approximately 187 km. The same general shape of the curves was present: an exponential decease in photoelectron flux with increasing energy; structure near 25 eV; and a sudden drop influx beyond 55 eV. Between 10 and 35 eV, the measured data compared favorably with the calculated values. From Figure 6A to Figure 6B, the increase in structure near 25 eV was attributed to the dominance of atomic oxygen at 187 km: while at 150 km, N_2 and O had almost equal densities.

In Figure 6C, four curves were plotted for an altitude of approximately 247 km. Three of the four curves were obtained from the same sources used for Figures 6A and 6B. The fourth curve, represented by the dash--dot line, was obtained from Singhal's "3 D Present" model. Again the same general shape of the curves was present with an especially remarkable similarity to Figure 6B. Between 10 and 35 eV, the measured data compares favorably with

the calculated data. There was little difference noted between the two curves calculated from the Singhal models. Singhal explained that between 187 and 247 km, almost all photoelectrons are absorbed at the same altitude at which they are produced. Therefore, the difference between the "2 D Present" and the "3 D Present" models produced a very slight difference in the calculated values.

In Figure 6D, curves obtained from the same four models were plotted for an altitude of approximately 350 km. While the curves had the same general shape, there were several noticeable differences: the entire curve was shifted down in photoelectron flux compared to previous Figures; the structure near 25 eV was not as prominent; and the slope was slightly less negative. Again there was favorable agreement between the measured data and the calculated data for the 10 and 35 eV energy range. The sequence of four Figures indicates that the photoelectron flux drops and the features become less prominent as altitude increases.

The photoelectron flux distributions in Figures 4, 5, and 6 illustrated a general consensus from numerous references as to the

shape of the flux versus energy below 60 eV. Some structure is expected in the 22 and 26 eV energy range associated with the ionization of oxygen. A sharp dropoff in flux below 60 eV is expected as well. The major characteristics found in the measured spectra were reproduced by the theoretical models. The inconsistencies in data beyond 70 eV were attributed by Singhal to instrumentation inaccuracies and to stray photons and cosmic ray counts.

C. PHOTOELECTRON TRANSPORT ABOVE THE IONOSPHERE

We know that charged particles in motion in a magnetic field gyrate about the magnetic field lines, as illustrated in Figure 7. Pitch angle refers to that angle between the direction of a field line and the direction of motion for a particle streaming along the field line. All of the photoelectrons produced in the earth's upper ionosphere with an upward velocity component will move along the magnetic field lines and have the potential to "escape" into the magnetosphere. However, most photoelectrons will undergo collision and become absorbed in the ionosphere before escaping into the magnetosphere.

The magnetic mirror force on charged particles is in the upward direction along the magnetic field line. As the particles gyrate along the magnetic field line, the isotropic distribution of the photoelectrons escaping the ionosphere becomes focused into a narrow pitch angle distribution. The distribution continues to narrow as long as there is a negative magnetic field gradient.

In Figure 8, analytical calculations by Krinberg (1978) showed the evolution of the photoelectron pitch angle distribution in a series of five polar plots. Along the field line L = 2, the evolution of the pitch angle distributions ranges from ionosphere escape at the bottom, equatorial plane in the middle, to the conjugate point reentry at the top. At geosynchronous orbit, the pitch angle distribution was shown to be within several degrees of the field aligned direction. The reentry flux at the conjugate point will be less than the escaping photoelectron flux. The flux decrease occurred because Krinberg's model takes into account the coulomb scattering.

Wrenn's analysis (1974) showed that there is considerable pitch angle scattering of photoelectrons taking place between the ionosphere and the spacecraft mounted instrument. Wrenn

concluded that photoelectron flux transport from the ionosphere to the magnetosphere was a function of local time at the source region and that the escape flux was greatest during the morning. Shawhan, Block, and Falthammar (1970) concluded that at mid-latitudes, the dawn escape flux exceeded the dusk escape flux and that the escape flux in summer should exceed the escape flux in winter. Galperin and Mulyarchik (1966) had shown that the upward photoelectron flux decreased below about 600 to 700 kilometers.

Lee (1980a) showed that the upward photoelectron flux decreased as latitude increases. Table I summarizes the 7 to 9 eV photoelectron flux for six altitudes between 148 and 280 km and for seven solar zenith angles (SZA) ranging from 10° to 95°. The SZA is a function of the latitude. When the sun is directly overhead, the SZA is 0°. When the sun is below the local horizon at sea level, the sun will be visible at significant altitudes and the SZA will be greater than 90°. At every altitude, as SZA was increased, the average flux decreased. The table also shows that at every SZA except 95°, at 280 km, the average flux was decreasing as altitude was increasing.

Other contributing factors to decreasing escape flux intensity with increased latitude are the contributions from precipitating electrons and electric fields in the auroral regions. Their effects are inconsistent and cause high latitude fluxes to be more variable compared to the mid latitude fluxes. Lee (1980a) noted that the fluxes were extremely stable for the latitudes analyzed by AE-E. Ground tracks of the samples used by Lee cover latitudes of about 30° North to 30° south.

Wrenn (1974) reported that ISIS 1 spectrograms clearly established that there is little difference between upward traveling and downward traveling photoelectric fluxes when both ends of the flux tube are sunlit. The ISIS 1 data also showed that significant upgoing fluxes can be seen when the local ionosphere is in darkness. As Figure 9 illustrates, when the conjugate point is sunlit, an upward photoelectric flux is measured due to the ionosphere's albedo. When these data sets were measured, the base of the field line was in darkness while the conjugate point was sunlit. The upper plot in Figure 9 shows the total number flux versus latitude for both the downward conjugate flux and the upward albedo flux. This plot

illustrates that for the longer flux tubes found at higher latitudes, the transmission of photoelectrons decreases. The lower plot in Figure 9 shows the differential number flux versus energy between 9.5 and 54 eV for both the downward conjugate flux and the upward albedo flux. Both curves have a rough similarity to the characteristic shape of ionospheric photoelectrons. The apparent deterioration of the curves' shapes were attributed to transmission losses in the plasmasphere and the poor resolution of the instrument. Although the albedo flux was approximately a factor of three lower than the conjugate flux, both fluxes were clearly present. Consequently, at geosynchronous orbit, photoelectrons will appear to be coming from both ends of the flux tube even though only one end is sunlit.

Measurements from ISIS 1 led Wrenn to the argument that since electrons easily cross the protonosphere (plasmasphere) and are reflected at both ends of the flux tube, a pseudo-trapped population is established. Figure 10 shows the model developed by Wrenn (1974) for the calculation of the trapped fluxes. Production P_1 and P_2 occurred at the ends of each flux tubes, escape levels were set to h_1 and h_2 , and magnetic field strengths were assumed to be B_1 and

B_2. μ was specified as the transparency coefficient and β_1 and β_2 were the reflection coefficients.

An estimation of μ was made by comparing ISIS 1 data and up and down fluxes in a balanced situation, where $P_1 = P_2$ and $B_1 = B_2$. A value of $\mu = 0.7$ was obtained and applied to the equations in Figure 10 to calculate the losses occurring in the plasmasphere and at the ends of the flux tubes for two specific cases. When there was production and reflection at both ends of the flux tube: $P_1 = P_2 = P$, $\beta_1 = \beta_2$, and $F_1 = F_2 = F = 1.54 \times P$; the loss to the plasmasphere equaled $0.6 \times F$ and $0.92 \times P$ and the loss at the ends of the flux tubes equaled $0.35 \times F$ and $0.54 \times P$. When there was production at only one end of the flux tube: $P_2 = 0$, $F_1 = 1.14 \times P_1$, $F_2 = 0.4 \times P_1$, $\beta_1 = \beta_2$; the loss to the plasmasphere equaled $0.46 \times P_1$, and loss at the ends of the flux tubes equaled $0.14 \times P_1$ and $0.4 \times P_1$.

Wrenn showed that the loss in the plasmasphere was caused by the pitch angle scattering and thermalization of the plasmasphere above the escape and reflection altitudes. Wrenn concluded that his simple model was only useful at middle latitudes. The concepts of μ and β became indistinguishable at low latitudes.

Krinberg (1978) calculated values for plasmaspheric transparency based on the premise that rare coulomb collisions occurring in the plasmasphere may cause electrons to leave the loss cone. Only the photoelectrons in the loss cone along the field lines fall to the conjugate point of the flux tube. Figure 11 compares the analytical calculated transparency values by Krinberg with the numerical calculated transparency values by Takahashi (1973 and 1974). Plotted are the average plasmaspheric transparency values for L values of 1.5 and 4 against the energy range of 0 to 50 eV. All of the calculations showed that higher values of energy have a higher average transmission. Also, the average transparency decreased as the L value increased. This agrees with Lee's (1980a) research that showed increasing latitude resulted in decreasing flux at geosynchronous orbit. Krinberg concluded that the results of analytical and numerical calculations were in fairly good agreement.

Mantas (1978) showed radar data that illustrated the relative impacts on flux from the effects of plasmaspheric transparency and from ionospheric surface albedo. In Figure 12, Mantas plotted seven traces of ionospheric photoelectron differential flux versus energy

measured with radar at an L value of 1.42, from Arecibo, Puerto Rico. Solid lines indicate upward traveling electrons and dashed lines indicate downward traveling electrons. The $\emptyset_{tau}^{+}$ curve represented the steady state upward flux when both ends of the flux tube were sunlit. The subscript numbers represented the number of reflections that the electrons had experienced.

The difference between the $\emptyset_0^{-}$ and $\emptyset_1^{+}$ curves illustrates the effect ionospheric reflection has on electron flux, while the difference between the $\emptyset_1^{+}$ and $\emptyset_1^{-}$ curves illustrates the effect the plasmaspheric transparency has on electron flux. Mantas' data showed that both ionospheric reflection and plasmaspheric transparency increased with energy. Above approximately 20 eV, transparency was greater than 0.80 and reflection reduced flux by a factor of two to three. The measured values by Mantas (1978) are higher than both the analytical calculations by Krinberg (1978) and numerical calculations by Takahashi (1973 and 1974).

Peterson (1977a) reported measurements taken with the AE-C spacecraft. Figure 13 illustrates upward streaming photoelectron flux plotted against energy. Data were plotted for two sets of

measurements. The solar zenith angles (SZA) of 95° to 88° and 101° to 95° for for these data indicate that the near end of the field line was just barely in the sunlight. The high values for conjugate SZA (CSZA) indicate that the conjugate point was in darkness for both data sets. Both curves have the characteristic shape expected for photoelectrons: exponentially decreasing flux; structure near 25 eV; and increasing negative flux above 55 eV.

Figure 14 shows downward streaming photoelectrons versus energy. Data are again plotted for two measurement sets. The CSZA and SZA for both traces indicate that the field line ends were at high latitudes, that the near field line ends were in darkness, and that the conjugate points were sunlit. Although both traces have the characteristic shape expected of photoelectrons, the structure is less apparent and the slope less negative than the traces in Figure 13.

The SZA's in Figures 13 and 14 are close enough for a direct comparison of their flux values. They are remarkably similar in shape. The downward flowing electron flux is less than the upward flowing electron flux by a factor of two to three. These ratios were lower than those presented by Krinberg (1978).

Figure 15 illustrates the loss of electron flux during ionospheric surface reflection (Peterson, 1977a). The trace indicated by x's represents the electron flux flowing downward from the conjugate point. The trace indicated by o's represents the electron flux flowing upward after reflection from the ionosphere's surface. The SZA of 123° to 120° indicate that the local ionosphere was in darkness. The CSZA of 100° to 81° indicate that the conjugate point was sunlit. Compared to the conjugate electron flux, the reflected electron flux is almost the same at an energy of 15 eV, and lower by a factor of two to three at an energy of 50 eV. These measurements are consistent with the measurements of Mantas (1978).

AE-C data presented by Peterson (1977b) have also been considered as tracers of field aligned potentials. In Figure 16, conjugate photoelectron flux from two consecutive 48 second intervals were plotted against energy. The latitude range for the two observations increased. The higher latitude observation line was shifted slightly downward in energy. Peterson noted that on some occasions, the sensor detected normal fluxes of electrons at energies greater than 200 eV in regions where conjugate photoelectrons were

expected but not observed. Peterson further noted that on these occasions, a net field aligned potential difference of ≈100 eV would be sufficient to exclude the conjugate photoelectrons. A much smaller potential difference of a few volts was speculated to cause the shift in observed photoelectron spectra. Of particular interest is the fact that these measurements were taken at latitudes corresponding closely to L values of 6.6, the same as geosynchronous orbit.

When both ends of the flux tube are in darkness, no photoelectrons are expected at geosynchronous orbit. However, after sunset, the pseudo-trapped population will continue to mirror because of the ionosphere's surface albedo. This phenomenon will persist for a short period of time as the flux decreases with every mirror at the ionosphere's surface.

Once out of the ionosphere, ionospheric photoelectrons are expected to flow along the flux tube to the conjugate point in the ionosphere. Calculations by Krinberg (1978) showed that the plasmaspheric transparency will allow it and measurements by Peterson (1977a), Wrenn (1974), and Mantas (1978) showed that it

happens. Therefore, at geosynchronous orbit, the upward flowing, low energy electrons will be detected as "field-aligned electrons" streaming from the northern and southern magnetic poles.

The aforementioned literature presented ionospheric measurements and calculations. The subsequent literature discusses magnetospheric measurements.

D. PHOTOELECTRON DETECTION AT GEOSYNCHRONOUS ORBIT

Coates (1985) reported that GEOS 1 and GEOS 2 satellites detected field aligned electrons below 100 eV whenever the ionosphere at the base of the field line was sunlit and magnetic conditions were quiet. Figure 17 shows energy spectra measured when the spin angle is constant over a 20° range centered on the field aligned direction on GEOS 1. The peak between 0 and 5 eV is due to locally produced photoelectrons and ambient cold plasma. The real feature noted by Coates in the spectrum measured by Analyzer A, the upper curve, is the peak at approximately 23 eV and the dip in energies above 50 eV.

Figure 18 shows the GEOS 2 data measured when the Analyzer A is fairly closely aligned with the field aligned direction. The eight

traces plotted on the counts versus energy field correspond to eight half hour time bins between 02:00 and 06:30 universal time (UT) (between 02:36 and 07:06 (LT)). All of the traces have the characteristic shape of photoelectrons for counts (or flux) versus energy. The variations between traces illustrate the dependence on local time of the field aligned electron flux. For energies greater than approximately 10 eV, the counts are greater after 05:06 than the counts before 05:06 (LT). Traces with the greater counts correspond to the time bins during which the base of the field line was sunlit.

Coates used the following four points to compare the field aligned electrons measured on GOES 1 and GOES 2 with photoelectrons measured on the AE satellites by Lee (1980b):

(1) The fluxes were confined to within a few degrees of the atmospheric source cone in direction.

(2) The energy spectrum was similar to the smoothed photoelectron escape energy spectrum above the ionosphere with a peak at 20 eV and an increase in the negative slope above 60 eV.

(3) The fluxes appeared at a local time corresponding to sunrise at an altitude of 300 km in the sunlit conjugate hemisphere.

(4) The radial variation in intensity was in agreement with theoretical estimates of the escape flux and with a simple model of propagation along the magnetic field line.

Based or four points of comparison, Coates concluded that field aligned electrons measured by GEOS 1 and GEOS 2 were photoelectrons escaping from the ionosphere. Using the measurements of photoelectrons at geosynchronous orbit, Coates deduced the following two aspects of the transport process in the magnetosphere.

(1) The maximum possible field aligned electric potential is less than 2 volts for magnetic field lines passing through geosynchronous orbit. This limit was based on the observation that the energy of the peak in the spectrum was identical to the peak in the photoelectron spectrum within the accuracy of the instrument.

(2) The photoelectrons are subject to scattering processes on their journey along the field line. Based on the field of view and the accuracy of the GEOS instrument, the mean scattering angle was as much as 3° to 6°.

E. CONIC SHAPED DISTRIBUTIONS

An important result of the analysis done for this thesis was the occurrence of conical distributions of low energy electrons.

A literature search found several articles presenting discussions on ion conic generation. No articles were found dealing with electron conic generation. However, the concepts for the generation of both are similar. While this section only describes the generation of ion conics, the concepts can also be applied to the generation of electron conics.

Sharp (1977) examined the characteristics of ionospheric acceleration mechanisms which operated on the velocity component perpendicular to the magnetic field. Data was obtained by an energetic mass spectrometer on board satellite 1976-65B. Figure 19 showed count versus pitch angle for three consecutive spacecraft

revolutions. The top plot in Figure 19 provides measurements of O^+ and the other two figures provided measurements of H^+ from two different instruments. All of the traces clearly indicate minimums at about 180°. Distribution peaks occur on both sides of the minimum at pitch angles of about 130° to 140°. The data for O^+ is much more ordered then the H^+ data. Sharp concluded that the distribution resulted from an acceleration mechanism that operated on the perpendicular velocity component. Subsequent upward motion due to the magnetic mirror force results in the distribution shown in Figure 19.

Dusenbery (1981) studied the mechanism for producing ion-conic distributions of the upward flowing ions in the auroral zone. The theory of particle interaction with ion-cyclotron waves was applied for a specific path length of upward flowing ions. Since ion cyclotron waves had been measured at altitudes ≈ 6,000 km by the S3-3 satellite, they were assumed to exist at lower altitudes. Quasi-linear diffusion theory was used to solve for the time evolution of the ion distribution during the time of interaction. The calculated H^+

distributions found reasonable agreement with measurements from S3-3.

Klumpar (1984) presented evidence that ions were accelerated in both the parallel and perpendicular directions. Figure 20 showed a stacked line plot of the time averaged, oxygen ion flux versus pitch angle as a function of energy. Measurements were made by the energetic ion composition spectrometer on board the Dynamic Explorer (DE) 1 satellite. The flux levels greater than 1 x 10^5 ions $(cm^2 \text{ sec sr keV})^{-1}$ were shaded for emphasis. Ten flux traces correspond to decreasing energy levels from 5.03 keV at the top to 0.23 keV at the bottom. This figure illustrated the classic profile for a conic distribution. At the lowest energy levels, the pitch angle distribution is nearly field aligned. As energy increased, the amount of perpendicular acceleration experienced per particle increased and the difference in pitch angle from the field aligned direction increased.

In considering the low energy field aligned component, Klumpar deduced that the ions had experienced a parallel acceleration of approximately 310 eV. After removing the parallel acceleration, the

pitch angle distribution was what would be expected as a result of adiabatic transport through a primarily transverse heating region. Klumpar concluded that the multistage acceleration mechanism was a common feature of the acceleration of ionospheric ions from the auroral topside ionosphere.

Possibly related processes involving electron pitch angle diffusion have been considered at high altitude. Kennel (1970) argued that pitch angle diffusion from a whistler wave would only occur at energies greater than the characteristic energy of 10 keV. Johnstone (1993) studied the interaction between low energy electrons and whistler mode waves. His premise was that there was no justification for this lower limit of 10 keV. Measurements made by the low energy plasma analyzer an board the CRRES spacecraft showed that pitch angle diffusion of electrons occurred at energy levels down to 100 eV, which was the lowest energy measurable by the instrument. The pitch angle diffusion was found to be driven by the whistler interaction.

The shape of an electron conic distribution would be the same as that for the ion conic distribution, illustrated by Figures 19 and 20.

F. PARTICLE DETECTION AT GEOSYNCHRONOUS ORBIT

Wrenn described two basic types of instruments which have been used to study photoelectrons: retarding potential analyzers (RPA) and electrostatic analyzers (EA). Typical RPA's are described in detail by Rao (1969) and by Knudsen (1972). A high transparency grid is swept or stepped in potential such that it creates a variable threshold energy for electrons to pass through to a collector. The collector current is detected with a logarithmic electrometer and is a measure of the integral electron flux with energy above the threshold. RPA's suffer from a number of disadvantages. They collect over an extended solid angle which results in data that lacks pitch angle distribution information. The energy spectrum can only be derived by assuming an angular distribution. Also, the collection current is contaminated by electrons that are photoemitted either inside the instrument or from nearby spacecraft surfaces.

Different electrostatic analyzers are described in detail by several sources: each EA employing a different geometry. Bame (1993) and McComas (1992) each describe the magnetospheric plasma analyzer (MPA) which has flown by Los Alamos aboard three

geosynchronous satellites with the International Designators of 1989-046, 1990-095, and 1991-080.

Since the data used in this study was measured by the MPA, its description is provided. As illustrated in Figure 21, the MPA instrument is composed of a single EA coupled to an array of six channel electron multipliers (CEM) to measure three dimensional E/q distributions of both ions and electrons in an energy range of one to 40,000 eV/q.

The EA is composed of a set of curved plates with spherical section geometry such that the bending angle is a constant 60 degrees, and is independent of the polar angle of entry. After transiting the EA, the particles are directed and post accelerated into the array of CEM's, set at nominal geometric angles with respect to the entrance aperture of ±11.5°, ± 34.5°, and ± 57.5°. Each CEM covers a separate polar angle field of view (FOV). Figure 22 provides a visualization of the effective look angles of the fan shaped FOV with respect to the spacecraft spin axis. The top plot in Figure 22 illustrates the calibrated relative response between CEM's. The number three and four channels, at ±11.5°, have the highest relative

transmission through the EA section. The bottom plot in Figure 22 illustrates on a sphere the expected FOV coverage for each CEM. The rings of CEM transmission response indicate, from the center outward,10%, 40%, and 80% of the peak relative transmission for each CEM. During each complete spin of the spacecraft, the MPA observes 92% of the unit sphere. This large percent coverage allows development of three dimensional energy spectrograms.

The operation of the MPA results in five types of data sets. Each set takes 10.15 seconds for a complete sweep of 365.5° of spacecraft revolution. Only two of the five types of data sets were analyzed in this study. Both of these data sets consist of 24 uniformly spaced exponential sweeps from the top energy level to the bottom. Each sweep collects counts in 40 nine-millisecond counting bins. Thus, the data set for a three dimensional observation of either ions or electrons contains spacecraft ephemeris data and six 24 by 40 matrices of particle counts, one for each CEM.

There is a sun shade on the instrument that prevents direct UV radiation from entering the aperture. The sun shade does not completely prevent the corruption of electron data as a result of

solar illumination. Photoemission from the shield and instrument surfaces results in a characteristic sun signature (pulse) in the energy versus angle spectrograms. It covers an energy band of 1 to 10 eV and a roll angle width of 40°. It also varies in angle from before noon to after noon, due to the sun's position relative to the spacecraft's spin axis. The angle difference between the field aligned direction and the sun signature also varies as a function of the time of year.

Carrying the MPA is a secondary function for its host satellites. Observations are routinely not telemetered to the ground station when primary functions of the satellite preempt the telemetry links. This precludes obtaining MPA data during some events that are of scientific interest. The events that trigger the primary functions into full and overriding service are the same as those of scientific interest. The remaining data does however provide ample opportunity for magnetosphere physics research.

An important characteristic of the magnetosphere plasma is the angle distribution. On most scientific satellites, pitch angle for particle measurements are obtained by means of onboard

magnetometers. The spacecraft platform utilized for this study does not have a magnetometer. Consequently, the spacecraft roll angle is used to determine the field aligned direction and electron pitch angles.

The roll angle for this spacecraft is defined as the angle of rotation completed since the MPA aperture had passed a northward facing orientation. Spacecraft 1989-046 is a spin stabilized spacecraft with its spin axis oriented toward the center of the earth and is in a geosynchronous orbit within 10° latitude of the equatorial plane. At geosynchronous orbit, the magnetic field lines are approximately perpendicular to both the orbital plane and the spin axis and parallel to the local vertical. Consequently, the roll angle from magnetic field line direction is approximately equal to pitch angle. Roll angle is used as pitch angle in the data analysis.

Using this study's frame of reference, plasma sheet currents, ring currents, co-rotating currents, and trapped electrons will all be measured at pitch angles of approximately 90° and 270°. While field aligned electrons will be measured at pitch angles of approximately 0°, 180°, and 360°.

Typical energy versus roll angle spectrograms indicate the presence of isotropic electrons at energies between 5 and 40 keV. These electrons are believed to be hot background electrons originating in the tail of the magnetosphere.

The energy versus time spectrograms indicate hot plasma injections into the magnetosphere as a result of magnetic storms. These are characterized by spontaneous high fluxes at high energies that slowly decrease in energy and flux over time. The signature appears as a high-energy, high-flux curve that is downward sloping to the right.

The energy versus time spectrograms also portray a characteristic spacecraft charging signature discussed by Fiely (1992). Fiely's research used data measured by the same MPA used for this study. He performed a detailed evaluation of algorithms which determine a spacecraft's potential.

Figure 23 illustrates the characteristic spacecraft potential signature in an energy versus time spectrogram with the estimated potential overplotted. The top spectrogram plotted electron energy spectra versus time for one complete day, while the bottom

spectrogram plotted ion energy spectra versus time. The quality of this figure is poor due to the reproduction of a color spectrogram into black and white. The OBSERVATION section will display better figures of the same information using a gray scale instead of the color scale. The characteristic to notice in this spectrogram is that the shape of the overplot. The shape followed flux variations which were readily apparent on color spectrograms.

Further discussion of the details found in Figure 23 is delayed until the OBSERVATION Subsection for Case Study Day One.

With this background physics understood, the next section will note observations made of electrons at geosynchronous orbit with the MPA.

III. OBSERVATIONS

In order to determine the environment that the spacecraft was passing through, several parameters were evaluated for either a qualitative or quantitative value. Five days were selected to be surveyed for characterization of the low energy field aligned electrons based on the variety of environmental conditions that they provided. Five days of data from satellite 1989-046 were surveyed for a total of about 470 observations for each day. Table II shows a portion of the survey data table taken for April 12, 1990.

The table consisted of about 470 rows of observations and 8 columns and is described as follows. The index was a sequential number assigned to each observation ordered in time. The plasmasphere column indicates whether or not the spacecraft is in the plasmasphere. This was determined qualitatively by noting the presence of cold ions. The plasma sheet column indicates the presence of hot electrons characteristic of the plasma sheet. This was determined qualitatively by the presence of electrons with energies

of several keV and at pitch angles of approximately 90° and 180°. The trapped column indicates the presence of either equatorially trapped or trapped electrons. The conic column indicates the presence of low energy electrons exhibiting a conic shaped distribution. The field aligned column indicates both a qualitative and quantitative value. A numerical value indicates the presence of field aligned electrons at an approximate peak energy value, as determined by best estimate from the observation spectrograms. No numerical value indicates that no field aligned electrons were noted. The storm column indicates that a magnetic storm had occurred. Observations during magnetic storms are characterized on the energy versus roll angle spectrograms by a high electron flux at all pitch angles and in most of the measured energy bands. The time column indicates the time of the observation in universal time. To convert to local time, add 13:00 hours to the universal time for the April days and 13:20 hours for December 10, 1989. The mean time interval between observations was 3 minutes while the median time interval was 2 minutes and 52 seconds. Large time intervals between

successive observations indicates that the satellite's primary mission had preempted the telemetry channel.

Figure 24 illustrates a ten day period in April of 1990, during which the magnetic activity increased rapidly to a peak and then slowly decreased over a period of a few days. April 12th and 14th were analyzed to provide data from the period of moderate solar activity. April 20th and 21st were analyzed to provide data from a period where the magnetosphere is returning to a less turbulent state. December 10, 1989 was chosen because the satellite never leaves the plasmasphere during the entire day.

Details from three of the five days are presented below to provide an indication of the various environmental circumstances. The first day represents a period of moderate solar activity, the second provides a day where the satellite never leaves the plasmasphere, and the third represents a nominal day in a series of several days of decreasing solar activity.

A. CASE STUDY DAY ONE--APRIL 14, 1990

The energy versus time spectrograms, Figures 25 and 26, illustrate all of the features that a spacecraft might encounter during

a complete geosynchronous orbit. Figure 25 shows field aligned measurements and was created by integrating the counts collected within 45° of the field aligned directions, while Figure 26 shows the perpendicular flux by integrating data measured within 45° of the perpendicular directions. Both Figures together comprise an entire day of charged particle counts collected by CEM numbers three and four.

The high flux of low energy ions between 01:00 and 04:00 UT (14:00 and 17:00 LT) in Figure 26 indicates that the spacecraft is inside the plasmasphere. Between 08:00 and 17:00 UT (between 21:00 and 06:00 LT), the spacecraft is charged negatively to greater than 200 volts. From 04:30 to 05:45 (17:30 and 18:45 LT) and from 16:30 UT (05:30 LT) into the next day, there are trapped electrons present between 100 and 1,000 eV. The one hour vertical stripe about 11:00 UT (24:00 LT) shows the effect of eclipse. The high energy electrons across the top between 07:00 and 13:00 UT (20:00 and 02:00 LT) are indicative of the hot plasma injections resulting from magnetic activity. The step feature seen in the ion spectrogram is indicative of the spacecraft potential signature. From 00:00 to

06:30 (13:00 and 19:30 LT) and from 18:30 UT (07:30 LT) until day end there are field aligned electrons present. These are not readily obvious on gray scale spectrograms but are clearly seen on color spectrograms.

The following four observation sets are typical for data processed from the MPA. These observations describe the interesting periods found on April 14, 1990 and include

(1) spacecraft in the plasmasphere,

(2) trapped perpendicular electrons,

(3) both trapped and field aligned electrons, and

(4) a conic distribution of field aligned electrons connected to the trapped electrons.

At universal time 02:26:22 (15:26 LT), the spacecraft is inside the plasmasphere. The energy versus pitch angle spectrogram, Figure 27, shows that no trapped electrons or plasma sheet electrons were present. The characteristic sun pulse is present at the lower right, between 200° and 285° in roll angle and 0 and 20 eV in energy. High energy background electrons are seen across the top. The field aligned electrons, found at angles of about 180° and 360° (which is

the same as 0° on these plots), are present from both the south and north, respectively. Inside the plasmasphere, the transmission of electrons along magnetic field lines is good and detection at geosynchronous orbit is highly probable on the day side.

A more detailed analysis of these field aligned electrons is seen in Figure 28. The distribution functions were least square fitted with maxwellian distribution curves to provide estimates of the density and temperature. This method is described in Olsen (1981). The density is approximately 4.33 cm^{-3} while the temperature (kT) is 6.91 eV. Figures 27 and 28 represent typical spectrograms and calculated values for the period of time that the spacecraft spends inside the plasmasphere.

At universal time 18:35:31 (07:35 LT), the MPA measured trapped perpendicular electron populations. The energy versus pitch angle spectrogram, Figure 29, shows the plasma sheet electrons above 1,000 eV. It illustrates equatorially trapped electrons which are characterized by the narrow distribution found about the 90° and 270° roll angles. The characteristic sun pulse is present as expected at the lower left, between 15° and 95° in roll angle and 0 and 15 eV

in energy. This differs from Figure 27 because the sun-earth-spacecraft spin axis orientation has shifted approximately 180°, the difference between late afternoon and early morning. Faint field aligned electrons are present at pitch angles of about 180° and 360°.

A more detailed analysis of these field aligned electrons is seen in Figures 30 and 31. A maxwellian distribution curve was again least squares fitted to the distribution function data. The density is approximately 2.49 cm^{-3} and the temperature (kT) is 6.69 eV. The peak in differential flux is not very distinct, since there is a significant amount of noise in the data.

Figure 31 provides another perspective of the data that can readily be compared to figures in the literature. The stacked line traces plot the flux for five of the forty energy bins versus spacecraft roll angle. The peak on the 7.4 eV trace indicates the characteristic sun pulse found in the MPA data. The slight flux peak at 180° of roll angle on the 21.4 eV trace indicates the faint field aligned electron population. The peaks at 90° and 270° of roll angle on the other three traces indicate the equatorially trapped electrons. The small

peaks at 150° and 195° of roll angle on the 61.7 eV trace resembles the conic distribution illustrated by Figure 20.

At universal time 19:27:07 (08:27 LT), the MPA measures both the narrow distribution of equatorially trapped electrons and highly collimated field aligned electrons. The energy versus roll angle spectrogram, Figure 32, shows both of these populations. At this early morning observation time, the ionosphere is sunlit and escaping photoelectrons are expected to be measured along the field aligned direction. Figure 32 also shows a lack of plasma sheet electrons. The characteristic sun pulse is at the bottom left between 350° and 85° of roll angle and 0 and 12 eV in energy.

In Figure 32, the $V_{parallel}$ versus $V_{perpendicular}$ plot indicates two distinct and separate electron populations. The dark circle near the center is the sun response. The high fluxes at $V_{parallel} = \pm$ 2,200 km/sec and $V_{perpendicular} \approx 0$ km/sec are the field aligned electrons, since most of their velocity is parallel to the field aligned direction. The high fluxes at $V_{perpendicular} = \pm$ 6,000 km/sec and $V_{parallel} \approx 0$ km/sec are the equatorially trapped electrons, since most of their velocity is perpendicular to the field aligned direction.

The detailed analysis of the field aligned electrons is presented in Figures 33 and 34. A maxwellian distribution curve was least squares fitted to the distribution function data. The curve fit is reasonably good considering the scatter in the data. The density is approximately 4.97 cm^{-3} and the temperature (kT) is 6.93 eV. These values are typical for the field aligned electrons observed outside of the plasmasphere.

Figure 34 is a stacked line plot of the flux for five of the forty energy bins versus spacecraft roll angle. The peak on the 7.4 eV trace indicates the characteristic sun pulse found in the MPA data. The slight flux peak at 165° of roll angle on the 21.4 eV trace indicates the field aligned electron population. The peaks at 90° and 270° of roll angle on the top four traces indicate the equatorially trapped electrons. Since the width of these peaks is narrow, these trapped electrons are equatorially trapped rather than simply trapped. In concurrent research at the Naval Postgraduate School by Lantto (1993), trapped electrons are classified as equatorially trapped electrons if their orbits remain within 10° latitude of the

equatorial plane. This distinction results in a narrow signature on the energy versus roll angle spectrograms.

At universal time 20:01:32 (09:01 LT), the MPA again measured both the trapped perpendicular electrons and the field aligned electrons. The energy versus angle spectrogram, Figure 35, shows a faint population of plasma sheet electrons between 2 and 10 keV. It shows the characteristic sun pulse at the bottom left between 355° and 90° in roll angle and 0 and 14 eV. This figure differs from Figure 32 in that the field aligned electrons extend into a conic distribution at increasing energies, connecting the trapped and field aligned distributions. The $V_{parallel}$ versus $V_{perpendicular}$ plot also indicates that the two distinct electron populations are connected. The field aligned electrons appear to experience a perpendicular acceleration, signified by the horizontal features in the Figure.

More detailed analysis of the field aligned electrons is presented in Figures 36 and 37. A maxwellian distribution curve was least squares fitted to the distribution function data. The density is approximately 4.24 cm^{-3} and the temperature (kT) is 11.16 eV. This

temperature is higher than other observations taken outside of the plasmasphere.

Figure 37 is a stacked line plot of the flux versus spacecraft roll angle. The peak on the 7.4 eV trace indicates the characteristic sun pulse found in the MPA data. The broad flux peak ranging from 120° and 225° of roll angle on the 21.4 eV trace indicates the large field aligned electron population. The peaks at 90° and 270° of roll angle on the 512.7 eV trace indicate the trapped electrons. The small peaks at 150° and 210° of roll angle on the 61.7 eV trace results from the ridge of higher flux that connects the conic distribution to the trapped electrons.

B. CASE STUDY DAY TWO--DECEMBER 10, 1989

The energy versus time spectrogram for the entire day, Figures 38 and 39, illustrates a day during which the spacecraft's entire geosynchronous orbit remains inside the plasmasphere. This day provided a baseline of photoelectron distributions to compare against in analyzing the photoelectron distributions observed on other days. Once again, the field aligned figure integrates the counts collected within 45° of the field aligned directions, while the perpendicular

figure integrates the counts collected within 45° of the perpendicular directions. The flux data in the parallel figure appears to be contaminated by the sun response.

The isotropic, high flux of low energy ions measured all day long are indicative of the plasmasphere. A moderate flux of low energy field aligned electrons are present throughout the local afternoon, a few observations during the local night time, and slightly increased flux during the last seven hours, from local sunrise on. There are very infrequent perpendicular electrons present within the characteristic energy band of the trapped electrons. The isotropic background fluxes of ions and electrons at the top of the plots are remnants of some distant phenomena and appear to be drifting and gradually losing energy.

Data from universal time 16:07:50 (05:27 LT) illustrates the typical plasmasphere data. The energy versus angle spectrogram, Figure 40, shows no trapped electrons or plasma sheet electrons present. The characteristic sun pulse is present at the lower left between 5° and 110° of roll angle and 1 to 20 eV in energy. Faint

high energy background electrons are seen in the top half. Low energy field aligned electrons are present at about 170° of roll angle.

The $V_{parallel}$ versus $V_{perpendicular}$ plot indicates field aligned electrons at a $V_{parallel} \approx 0$ km/sec and $V_{perpendicular} \approx -2{,}000$ km/sec. The dark circle near the center is the sun response. The faint figure at $V_{parallel} \approx 0$ km/sec and $V_{perpendicular} \approx +2{,}000$ km/sec is a low flux population of field aligned electrons originating from the conjugate hemisphere.

A more detailed analysis of the field aligned electrons is presented as Figure 41. The distribution functions were least square fitted with maxwellian distribution curves to provide estimates of the density and temperature. The density is ≈ 2.01 cm^{-3} while the temperature (kT) is ≈ 8.36 eV. These density and temperature values represent typical values deduced from the plasmasphere day measurements. The density calculations do not take into account the -4 to -5 volt spacecraft potential, which is present all day long.

A second observation from the plasmasphere day is presented for universal time 23:36:34 (12:56 LT). Figure 42, the energy versus angle spectrogram, shows no trapped electrons or plasma sheet

electrons present. The characteristic sun pulse is present at the lower center between 135° and 235° of roll angle and 1 to 20 eV in energy. The location of the sun response partially blocks out the low flux, field aligned electrons present at about 170° of roll angle. Field aligned electrons are present at about 355° of roll angle. Low flux, high energy background electrons are seen in the top half.

The $V_{parallel}$ versus $V_{perpendicular}$ plot is dominated by the large sun response circle. The form found at $V_{parallel} \approx 0$ km/sec and $V_{perpendicular} \approx +2{,}000$ km/sec is the field aligned electron population found on the spectrogram at about 355° of roll angle. The conjugate field aligned electron population is masked by the sun response.

A more detailed analysis of the field aligned electrons is presented as Figure 43. The distribution functions were least square fitted with maxwellian distribution curves to provide estimates of the density and temperature. The estimated density is ≈ 1.65 cm^{-3} while the estimated temperature (kT) is ≈ 6.52 eV. The curve fit is reasonably good considering the scatter in the data.

The spectrograms and calculated densities and temperatures remained consistent throughout the plasmasphere day. The average

calculated density of the field aligned electrons was 2.0 cm^{-3}, which is lower than the average density of 5.8 cm^{-3} calculated for the April 14^{th} observations taken inside the plasmasphere. The average calculated temperature (kT) of the field aligned electrons of 8.3 eV was nearly the same as the April 14 average of 8.6 eV, also calculated from measurements taken inside of the plasmasphere.

C. CASE STUDY DAY THREE--APRIL 21, 1990

The energy versus time spectrogram for April 21, Figures 44 and 45, illustrate the features of a day when the magnetosphere is rebounding from several days of moderate magnetic activity. Low energy field aligned electrons are present during most of the midnight region passage, making this an anomalous day in the analysis set.

Fiely (1992) analyzed the same MPA data for this day and determined that the spacecraft potential was between -1 and -10 volts from 00:00 to about 04:10 UT (13:00 until 17:10 LT) and between ± 2 volts for the remainder of the day.

The low energy ions indicate that the spacecraft is in the plasmasphere during the first five hours and last two hours of the

day. Between 07:30 and 10:00 UT (10:30 and 23:00 LT), the high energy electrons across the top indicate hot plasma injections from magnetic activity. From 10:00 UT until the end of the day (23:00 until 13:00 LT), there is a constant perpendicular electron population between 30 and 800 eV. From 00:00 to 07:15 UT (13:00 to 20:15 LT) and from 10:00 UT until the end of the day (23:00 until 13:00 LT), there are low energy field aligned electrons present between 2 and 50 eV. Again, these electrons are not readily obvious on gray scale spectrograms but are clearly seen on color spectrograms.

At universal time 04:16:34 (17:16 LT) the spacecraft is inside the plasmasphere. The energy versus angle spectrogram, Figure 46, shows that no trapped electrons or plasma sheet electrons are present. The characteristic sun signature is present at the lower center between 200° and 285° of roll angle and 1 and 30 eV in energy. High energy background electrons are seen across the top. The field aligned electrons are present from both the south and north.

A more detailed analysis of these field aligned electrons is seen in Figure 47. The distribution functions were again least squares

fitted with maxwellian distribution curves to provide estimates of the density and temperature. For the observations taken from inside the plasmasphere, the density is 3.28 cm^{-3} and the temperature (kT) is 7.11 eV. The average density is 5.6 cm^{-3} and the average temperature (kT) is 8.2 eV for the period of time that the spacecraft spends inside the plasmasphere on this day.

At universal time 14:38:46 (03:38 LT), the spacecraft is outside the plasmasphere and in the early local morning, predawn region. The energy versus angle spectrogram, Figure 48, shows that both trapped electrons and plasma sheet electrons were present. High energy background electrons are not seen across the top only because of the gray scale that was selected. The characteristic sun signature is present at the lower left between 0° and 85° in roll angle and 1 and 20 eV in energy. The field aligned electrons are present from the 180° direction only. The gray scale in this figure was adjusted to better illustrate the the conic distribution of the field aligned electrons, the Christmas tree shaped distribution of the trapped electrons, and the connection between the two populations.

The $V_{parallel}$ versus $V_{perpendicular}$ plot appears to show that the field aligned populations experience a perpendicular acceleration. The perpendicular acceleration is seen on this plot as a band of horizontal features. The electron flux does not exceed absolute values greater than ≈ 5,000 km/sec in the field aligned directions.

The detailed analysis of the field aligned electrons is presented in Figures 49 and 50. The distribution functions were again least squares fitted with maxwellian distribution curves to provide estimates of the density and temperature. The estimated density is 4.99 cm^{-3} and the estimated temperature (kT) is 6.7 eV. When the spacecraft was outside of the plasmasphere, the average estimated density is 4.2 cm^{-3} and the average estimated temperature (kT) is 6.6 eV. These values are only slightly lower than the average estimated values based on data taken when the spacecraft is in the plasmasphere.

In Figure 50, the stacked differential energy flux versus roll angle plot is similar to the conic distribution shown by Klumpar in Figure 20. The peak on the 7.4 eV trace at 45° is the sun response. The peaks at about 170° on the bottom two traces are the field

aligned electrons. The peaks at 90° and 270° on the top three traces are the trapped electrons. The small peaks at 135° and 225° on the 61.7 eV trace are the ridge of flux that connects the field aligned electrons to the trapped electrons.

D. OBSERVED CONIC--APRIL 12, 1990

The best illustration of a conic seen in the five days of observations occurred at 19:11:12 UT (08:11 LT) on April 12, 1990. The energy versus angle spectrogram, Figure 51, shows that both trapped electrons and plasma sheet electrons were present. The characteristic sun signature is present at the lower left between 10° and 85° in roll angle and 1 and 12 eV in energy. The low energy, field aligned electrons are present at about 180° and 355°. There is a ridge of higher than background flux between the trapped electron distribution and the conic shaped, low energy, field aligned electron distribution.

The $V_{parallel}$ versus $V_{perpendicular}$ plot appears to show that the field aligned populations experience a perpendicular acceleration. The horizontal feature seen in Figure 35 is also present in this figure.

The measured electron flux is much lower at absolute $V_{parallel}$ values greater than ≈ 4,000 km/sec.

The detailed analysis of the field aligned electrons is presented in Figures 52 and 53. The distribution functions were again least squares fitted with maxwellian distribution curves to provide estimates of the density and temperature. The estimated density is 7.28 cm-3 and the estimated temperature (kT) is 7.32 eV. The curve was a very good fit of the data between 2 and 30 eV. The estimated values are only slightly lower than the average estimated values based on data taken when the spacecraft was outside of the plasmasphere on April 21, 1990. However, these values are typical for April 12, 1990.

In Figure 53, the stacked differential energy flux versus roll angle plot is similar to the conic distribution shown by Klumpar in Figure 20. The peak on the 7.4 eV trace at 60° of roll angle is the sun response. The broad peaks at about 170° on the bottom two traces are field aligned electrons with a great deal of pitch angle diffusion. The peaks at 90° and 270° on the top two traces are the trapped electrons. The small peaks at 135° and 225° on the 61.7 eV trace are

the ridge of flux that connects the field aligned electrons to the trapped electrons.

E. STATISTICAL STUDY FOR DAY THREE--APRIL 21, 1990

A statistical analysis was conducted on all five days. Analysis for April 21, 1990 is presented for illustrative purposes. Plots for the other four days is provided in Appendix C, Other Statistical Plots.

Quantitative data of the instances of the trapped electrons, field aligned electrons, and conic distributions of field aligned electrons were plotted against time and compared.

Using the data provided in the thesis by Fiely, the presence of a high spacecraft potential was used to discount data that might have been misleading. Measuring low energy electron counts with an instrument mounted on a platform with a large potential is impossible. The low energy electrons do not have enough energy to penetrate the potential barrier. Thus, observations that are contaminated with a high spacecraft potential will slew the analysis results toward few occurrences. To remove the contaminated data, any observation that occur while the spacecraft potential is high is not counted as an observation.

Figure 54 provides the count of observations taken during 30 minute intervals that had trapped electrons present. Observation counts per half hour ranged from zero counts found between 00:00 and 03:30 UT (between 13:00 and 16:30 LT), to 11 counts found between 11:00 and 22:00 UT (00:00 and 11:00 LT).

Figure 55 provides the count of observations taken during 30 minute intervals that had low energy, field aligned electrons present. Observation counts per half hour ranged from zero counts found between 00:00 and 03:30 (13:00 and 16:30 LT), to 11 counts found between 11:00 and 22:00 (00:00 and 11:00 LT).

Figure 56 provides the count of observations taken during 30 minute intervals that had conical distributions of electrons connecting the low energy, field aligned electrons to the trapped electrons. There were no conical distributions observed during the first 6 hours (from 13:00 to 19:00 LT). Observation counts per half hour ranged from zero to 11 counts between 06:00 and 21:30 (19:00 and 10:30 LT). The figure peaks at 14:30 (03:30 LT) with 11 counts. The last 5 intervals (10:30 to 13:00 LT) contain only one count.

The process of counting observations can average out details in a distribution. The peak energy values of the field aligned electron distributions provide another opportunity for evaluation. The peak energy versus time plot for April 21, 1990 is discussed below. Plots for the other four days are found in Appendix D, Peak Energy versus Time Plots.

In Figure 57, the solid line plot represents the peak energy values of the field aligned electron distributions. The zero values indicate that no field aligned electrons were noted. On April 21st, the spacecraft never charged to more than -10 volts. Consequently, there was no potential barrier to prevent low energy electrons from being measure by the MPA. Also the data presented was void of contamination that previously discussed as attributed to high spacecraft potential charging. The data in Figure 57 was typical for the five days analyzed. The peaks were consistent during the day time when there was no magnetic activity.

The peak values were erratic during the first four hours (13:00 to 17:00 LT), when the spacecraft potential was most volatile. During those hours, the potential varied between -1 and -10 volts. Between

04:00 and 07:00 UT (17:00 and 20:00 LT), the peak values then ramps upward from 8 to 11 eV. Few field aligned electrons are observed between 07:00 and 10:00 UT (20:00 and 23:00 LT). The higher value peaks between 10:00 and 12:00 UT (23:00 and 01:00 LT) represent electrons that appear to have gone through an acceleration process. The observations were consistent for the remainder of the day. From 12:30 until 24:00 UT (01:30 until 13:00 LT), the peak values ramp downward from 11 to 9 eV.

F. STATISTICAL SUMMARY

The next logical step in the analysis process was to combine the statistical data prepared for each day onto one plot. The combined plots were plotted against local time. This method results in identification of trends that are dependent on local time.

Figure 58 provides a percentage of the cumulative observations that noted the presence of trapped electrons. The plot indicated that trapped electrons can be observed anytime during the day. The distribution has a mid morning peak after a steady upward ramp through the night time region. The minimum occurs in the late afternoon when the spacecraft is in the plasmasphere's dusk bulge.

Figure 59 provides the cumulative statistics for field aligned electron observations. During the five days surveyed, field aligned electrons were noted far more often then trapped electrons. In general, field aligned electrons are observed greater than 58 percent of the time during the daylight hours from 05:00 to 19:00 (LT). Conversely, field aligned electrons are observed less than 48 percent of the time during the dark hours from 19:00 to 05:00 (LT). The distribution has a bell shape with a peak at about 10:00 LT and a minimum at around 22:00 LT.

Figure 60 provides the cumulative statistics for the conical distributions of field aligned electrons that connect to the trapped electrons. By the criteria imposed on the definition of a conical distribution in this research, conics can only occur when both field aligned and trapped electron populations are present. The distribution exhibits a double peaked curved shape with peaks of 40 percent and 14 percent at 08:00 and 20:00 (LT), respectively. The minimums drop to one percent at about 15:00 and 22:00 (LT). The morning peak at 08:00 LT coincides with the peak values for both the trapped and field aligned electron populations. The number of

conics drops off with the same slope as the drop in trapped electrons following their respective peaks. The percentage of observations noting conical distributions was not a function of either the of trapped electron observation percentage or the field aligned electron observation percentage. With these observations noted, the next step in the analysis is to discuss the findings.

IV. DISCUSSIONS

From the five days analyzed a number of important findings deserve more discussion. Trapped electrons are present during most of the day, with the consistent exception of observations made inside of the plasmasphere. Low energy field aligned electrons are consistently present during the day time observations and frequently absent during night time observations. The distribution functions for field aligned electrons are remarkably similar to the distribution functions for photoelectrons that are produced above an altitude of 300 kilometers in the ionosphere. At the time when most trapped electron observations occur, 40 percent of the field aligned electron observations have a conic shaped pitch angle distribution. These conic distributions connect the field aligned electron population with the trapped electron population.

Observations made by Coates on the GEOS 1 and GEOS 2 satellites concluded that the field aligned electron fluxes below 100 eV were the photoelectrons escaping from the ionosphere. Based on Coates'

four points of comparison, analysis of the field aligned electron flux measured by the MPA draws the following comments:

(1) The fluxes are always within a few degrees of the field aligned direction.

(2) The distribution function versus energy plots have the same characteristic shape found in Figures 4 through 6, the ionospheric photoelectrons and Figures 17 and 18, the field aligned electrons measured by GEOS 1 and GEOS 2.

(3) The fluxes are consistently observed during sunlit hours and frequently absent during dark hours. And

(4) The radial variation in intensity was not evaluated in this data set since the spacecraft was in a geosynchronous orbit of non-varying radius.

These observations lead to the conclusion that the measured field aligned electron populations resulted from the transport of escaping ionospheric photoelectron populations.

Much of the research literature presented in the BACKGROUND PHYSICS' Subsection on photoelectrons' Transport from the Ionosphere to Geosynchronous Orbit showed that the photoelectrons

were able to traverse the magnetosphere from a conjugate hemisphere. At high L values, like 6.6 at geosynchronous orbit, it is a good assumption that photoelectrons will also traverse the magnetosphere. Any spacecraft of low potential will be able to measure these photoelectrons along their path.

Figures 54 and 55 showed that trapped electron and field aligned photoelectron occurrence peaks closely coincide during the local midmorning. Both populations broadened in pitch angle within the energy band that lies between the respective energy distribution peaks. The conic shaped distribution of photoelectrons was noted in 40 percent of the observations taken during the midmorning occurrence peak. No trapped electrons were noted by observations taken inside of the plasmasphere. Conic distributions were never noted by observations taken inside of the plasmasphere. These conic distributions were noted only when both trapped electron and field aligned photoelectron populations were present.

Based on these observations, the trapped electron and field aligned photoelectron populations must be related. Statistically, the occurrence peaks appear in close proximity to each other on the time

line. The spectrograms clearly indicate a ridge of higher than background flux connecting the two populations. The $V_{parallel}$ versus $V_{perpendicular}$ plots suggested that some perpendicular acceleration of the field aligned photoelectrons existed.

The literature research discussed in the BACKGROUND PHYSICS' Subsection on Conic Shaped Distributions the formation of ion conics. The implication is that electron conics should also occur. This research has shown many examples of flux versus pitch angle spectra that resemble the traditional conic presented by Klumpar in Figure 20.

The presence of a conic distribution of photoelectrons signified that an acceleration process had occurred. In this process, the field aligned photoelectrons are accelerated in the perpendicular direction. The highest energy field aligned photoelectrons became the lowest energy trapped electrons.

The acceleration process probably occurred during the transport from the ionosphere to the geosynchronous orbit. Collision along the flux tube has been assumed to cause the apparent angular diffusion. This research produced no evidence to either support or oppose this

assumption. Others have suggested that waves are responsible for the apparent angular diffusion. However, this research has no evidence to support or oppose this assumption as well. Energy distributions, angular distributions, and wave measurements taken at points along the transport path might shed some light on the acceleration process.

The two observations that seem irrefutable are that the two populations are related and that the conic distributions signified a process that relates the two populations.

One undesirable observation noted was that field aligned electrons are observed on two separate days in the midnight region. This was inconsistent with the theory presented herein and leads to the question: What is the physical mechanism that extracts low energy electrons out of the ionosphere at night? The writer acknowledges the fact that more research of this topic is required.

V. CONCLUSIONS

Measurements of ions and electrons were made by the MPA onboard spacecraft 1989-046. Observations from five days indicated the presence of both field aligned electrons and trapped electrons. Some 2,350 observations were analyzed to create a statistical data base for further detailed analysis

The occurrences of the field aligned and equatorially trapped electrons were statistically analyzed to determine if any correlation existed between their occurrences and local time, or location in the magnetosphere. Field aligned electrons were found present when the base of the magnetic field line was sunlit and the instrument was inside the plasmasphere.

Field aligned electron populations at low energies between 1 and 50 eV were characterized. Electron density ranged from 1.0 to 6.7 cm^{-3} and electron temperature varied between 4.7 and 8.9 eV. The low energy field aligned electrons were shown to be ionospheric

photoelectrons because their distributions showed a good match in shape.

Conical distributions of the photoelectrons were observed between 08:00 and 10:00 (LT) on days when both photoelectrons and equatorially trapped electrons are present. The conic distribution is present when some interaction between the photoelectrons and equatorially trapped electrons is hypothesized to be occurring. $V_{parallel}$ versus $V_{perpendicular}$ spectrograms clearly indicated that photoelectrons undergo perpendicular acceleration. Lack of any magnetic field measurements or collection of wave data onboard spacecraft 1989-046 prevented determining the source of the perpendicular acceleration.

On two days, field aligned electrons were also noted during the midnight region of the magnetosphere. The physical mechanism that extracts low energy electrons out of the ionosphere at night remains in question.

APPENDIX A TABLES

J. S. Lee, J. P. Doering, T. A. Potemra and L. H. Brace

TABLE 2. 7–9 eV AVERAGE FLUX ($\times 10^7$ (cm^2 s sr eV)$^{-1}$
(VARIATIONS OF ≈45% ARE COMMON)

	Alt.					
SZA	148 km	170 km	190 km	215 km	245 km	280 km
95°	2.9×10^{-2}	3.3×10^{-2}	7.8×10^{-2}	0.26	1.0	2.0
90	8.5×10^{-2}	0.2	0.6	2.1	3.2	2.8
80	0.51	2.5	4.8	5.9	5.1	2.9
70	1.5	6.1	9.0	8.5	5.9	2.9
50	5.3	12.0	12.0	10.0	6.4	2.9
30	10.0	15.0	14.0	11.0	6.5	2.9
10	13.0	16.0	15.0	11.0	6.5	2.9

TABLE I 7 TO 9 eV AVERAGE FLUX [x10^7 (cm^2 sec sr eV)$^{-1}$]
Lee (1980a)

	12-Apr-90							
	Plasma-	Plasma-	Trapped	Conic	Field Align	Magnetic		Universal
	sphere	sheet e's	Electrons	Distribution	Electrons	Storm		Time
1	no	yes	√	√	12	no		0:01:26
2	no	yes	√		15	no		0:04:18
3	no	yes	√		18	no		0:07:10
4	no	yes	√	√	10	no		0:10:02
5	no	yes	√		11	no		0:14:20
6	no	yes	√		11	no		0:17:12
7	no	yes	√		11	no		0:20:04
8	no	yes	√		11	no		0:22:56
9	no	yes	√	√	11	no		0:25:48
10	no	yes	√		11	no		0:28:40
11	no	yes	√	√	10	no		0:31:32
12	no	yes	√		10	no		0:34:24
13	no	yes	√		10	no		0:37:16
14	no	yes	√		11	no		0:40:08
15	no	yes	√		11	no		0:43:00
16	no	yes	√		11	no		0:45:52
17	no	yes	√		14	no		0:48:44

TABLE II SUBSET OF THE OBSERVATION TABLE FOR APRIL 12, 1990

APPENDIX B FIGURES

Magnetosphere

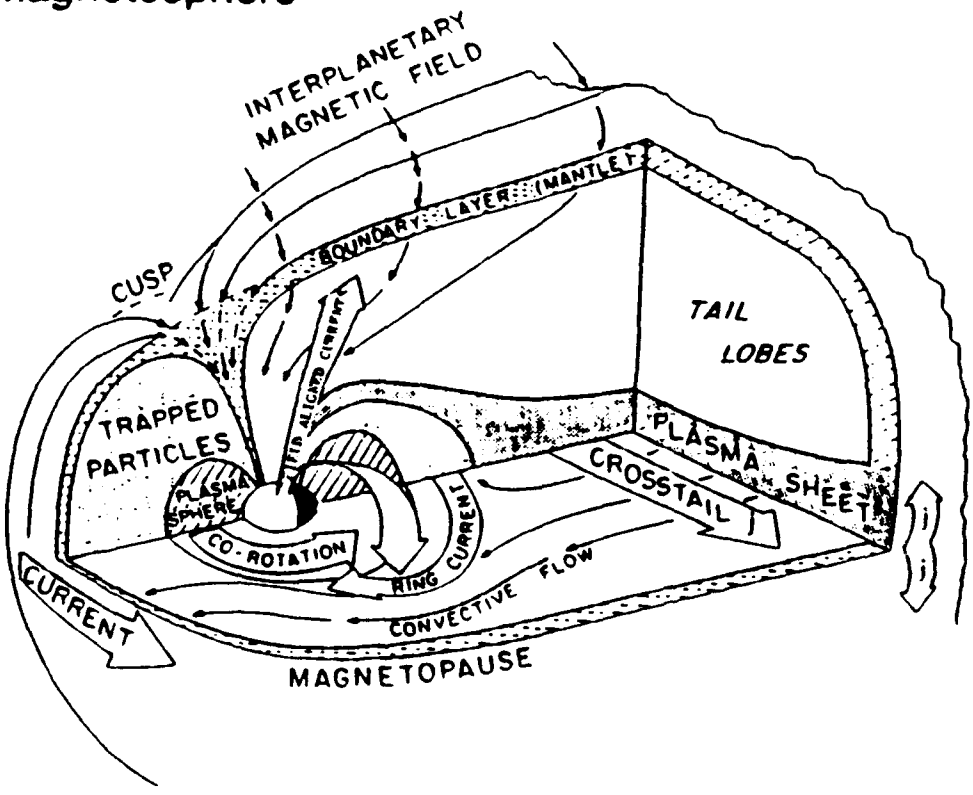

Figure 5.4 Cross section of the magnetosphere showing the principal current systems: magnetopause current, cross-tail (or neutral) current sheet, ring current, and field aligned currents. Also shown are the regions of convective and co-rotation plasma flow directions *(after Stern and Ness, 1981).*

Figure 1 Cross Section of the Earth's Magnetosphere, Tascione (1988)

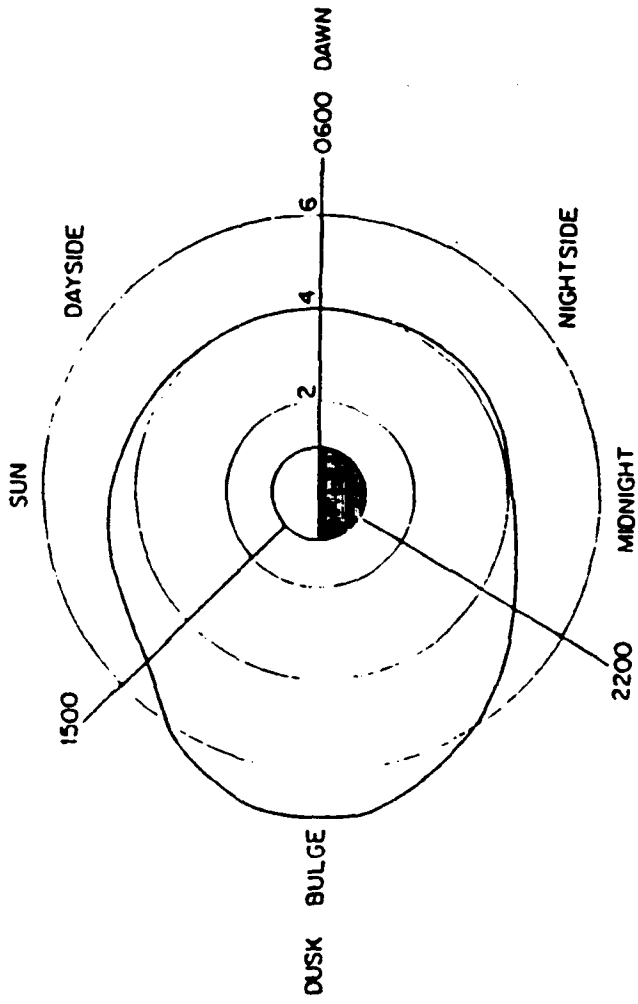

Fig. 1. An L local-time plot showing the different local-time sectors of the plasmasphere, dayside, nightside, and bulge. The dark line shows the average plasmapause position determined from more than 150 Ogo 5 profiles.

Figure 2 Plasmasphere Dusk Bulge, Chappell (1971)

SOLAR RADIATION

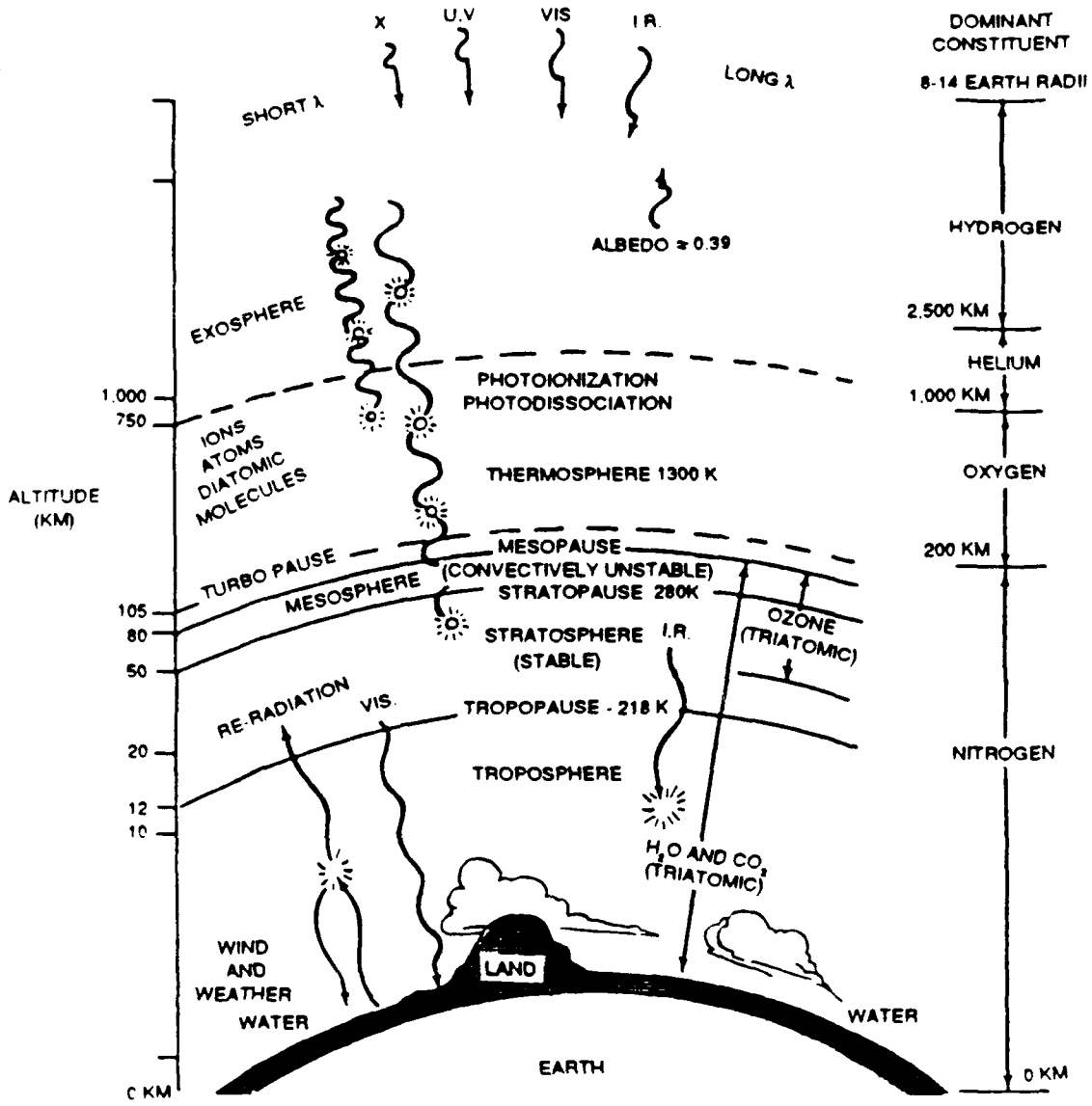

Figure 6.2 Atmospheric chemical regimes *(after Carpenter et al., 1978)*

Figure 3 Atmospheric Chemical Regimes, Tascione (1988)

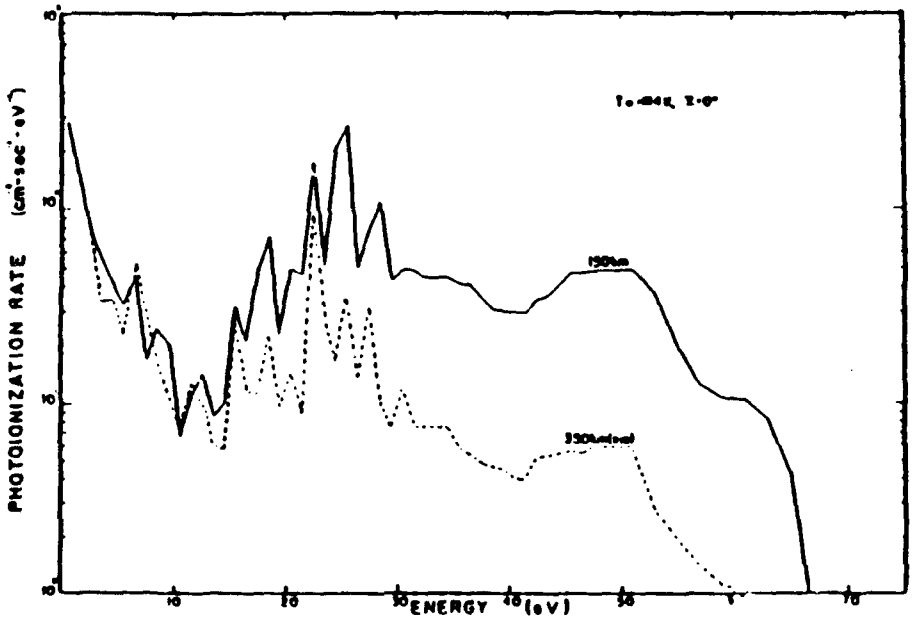

Fig. 1. Energy spectra of fresh photoelectrons at two altitudes in an overhead sun model atmosphere (after *Cicerone et al* [1973]).

Figure 4 Photoionization Rate vs Energy for Overhead Sun Model. Cicerone (1973)

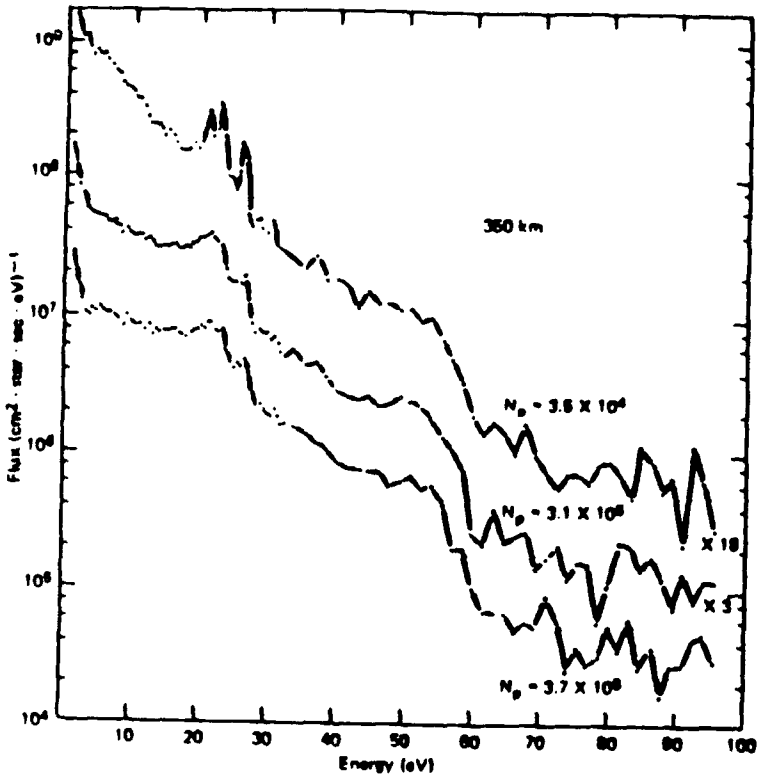

FIG. 1. PHOTOELECTRON SPECTRA FROM 0 TO 100 eV AT 350 km FOR VARIOUS PLASMA DENSITIES. For clarity the spectra have been offset upwards by the multiplicative factors shown. From top to bottom: $N_p = 3.5 \times 10^4$, 3.1×10^5, 3.7×10^5 cm^{-3}; Dip latitude = 13°, 2.4°, −3.2°; L.T. = 6.4, 7.7, 11.4; Solar zenith angle = 89°, 69°, 29°.

Figure 5 Photoelectron spectra from 0 to 100 eV from AE-E, Lee (1980b)

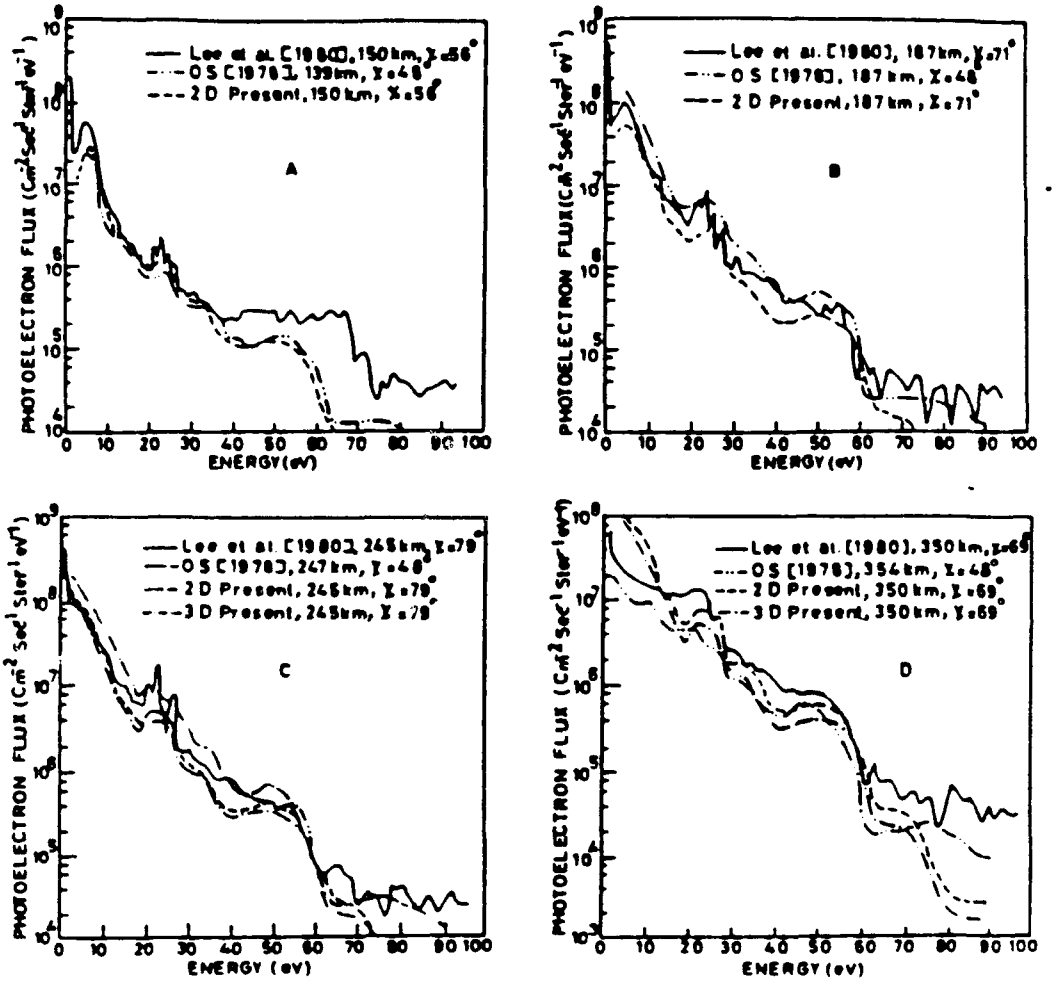

Fig. 3. Photoelectron flux spectra in earth's atmosphere at selected altitudes, (a) approximately 150 km, (b) approximately 187 km, (c) approximately 247 km, (d)

Figure 6 Photoelectron Flux Spectra at Selected Altitudes, Singhal (1984)

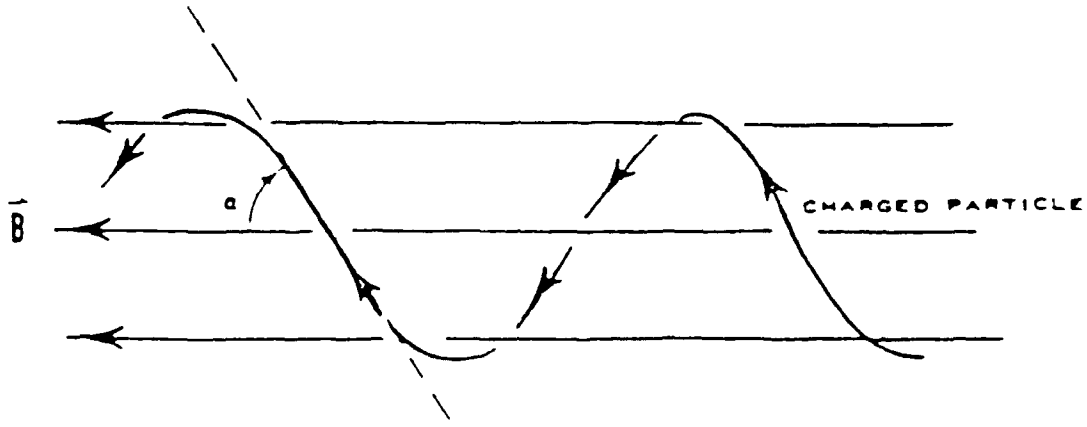

Figure 1.5 Pitch angle α, the angle between the magnetic line of force and the direction of the charged particle's motion.

Figure 7 Description of Pitch Angle, Tascione (1988)

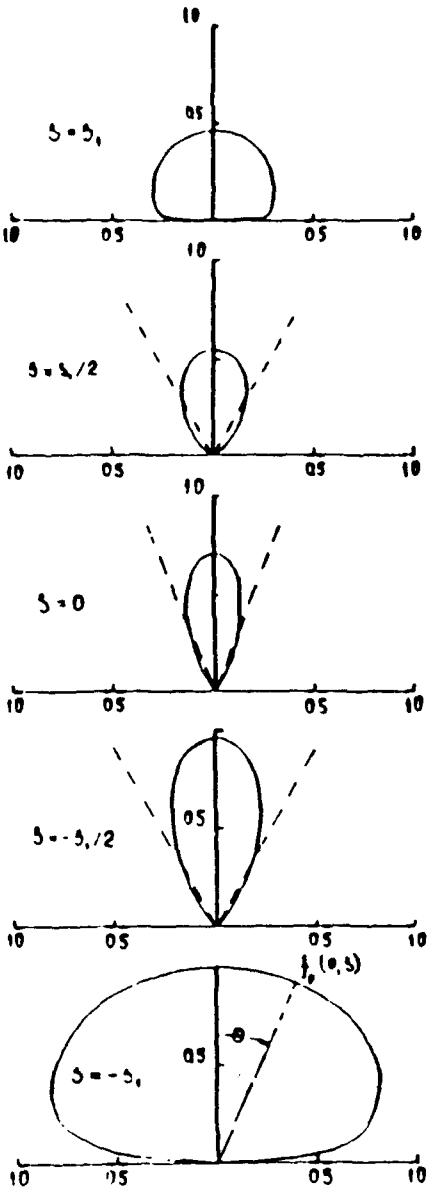

Fig. 6

Polar diagrams of variation of pitch-angle distribution of photoelectrons when they move along the field line with $L = 2$. The pitch-angle distribution of the photoelectrons escaping from the ionosphere ($s = -s_1$) is taken from the paper by I.A. Krinberg (1974).

Figure 8 Polar Diagrams of Pitch Angle Distributions Variations. Krinberg (1978)

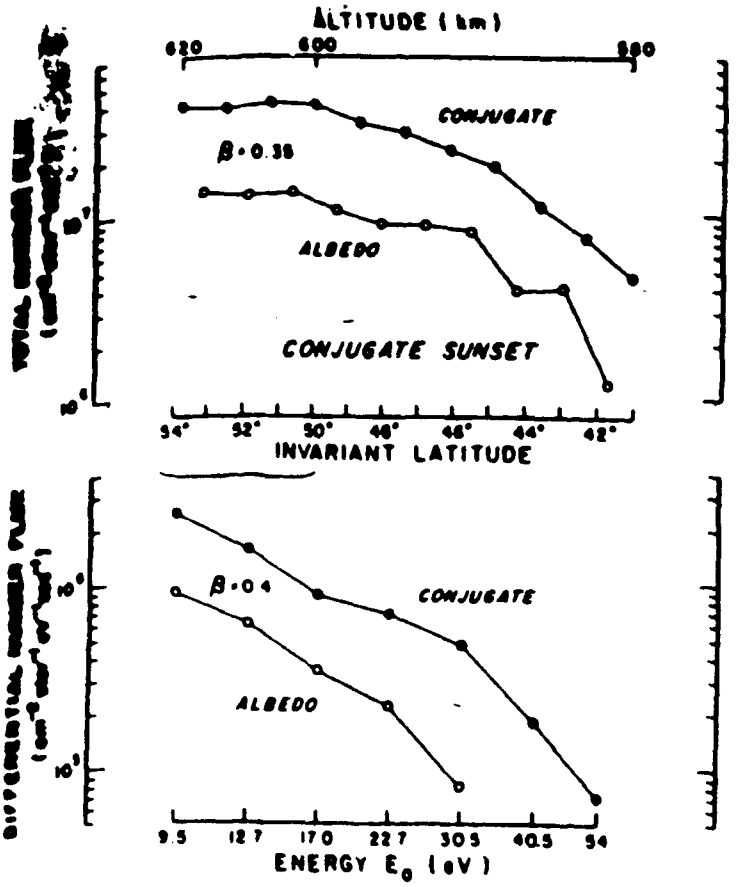

Fig. 6

ISIS I field aligned photoelectrons measured at conjugate sunset with no local production. β = reflection coefficient.

Figure 9 Photoelectrons Measured at Conjugate Sunset, ISIS 1, Wrenn (1974)

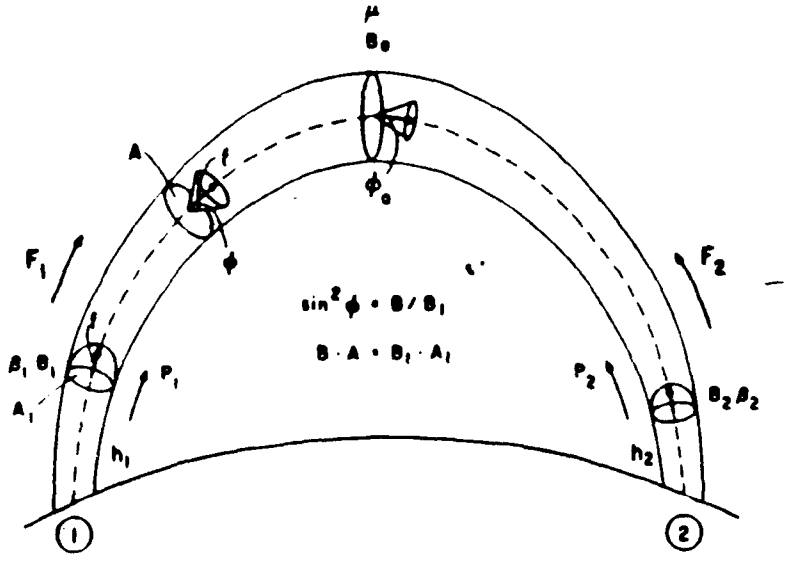

$$F = A \cdot \pi \cdot \int_0^{\phi} f \cdot \sin 2\alpha \cdot d\alpha = A \cdot \pi \cdot f \cdot \sin^2\phi = \pi \cdot f \cdot A_1$$

$$F_1 = \frac{P_1 + \mu\beta_1 P_2}{1-\mu^2\beta_1\beta_2} \quad , \quad F_2 = \frac{P_2 + \mu\beta_2 P_1}{1-\mu^2\beta_1\beta_2}$$

$$\text{LOSS TO PROTONOSPHERE} = (1-\mu)\cdot(F_1 + F_2)$$

$$\text{LOSS TO } (2) = (1-\beta_2)\cdot\mu\cdot F_1$$

$$\text{LOSS TO } (1) = (1-\beta_1)\cdot\mu\cdot F_2$$

Fig. 7

Model of photoelectron trapping with equations for flux determination

Figure 10 Model of Photoelectron Trapping with Equations, Wrenn (1974)

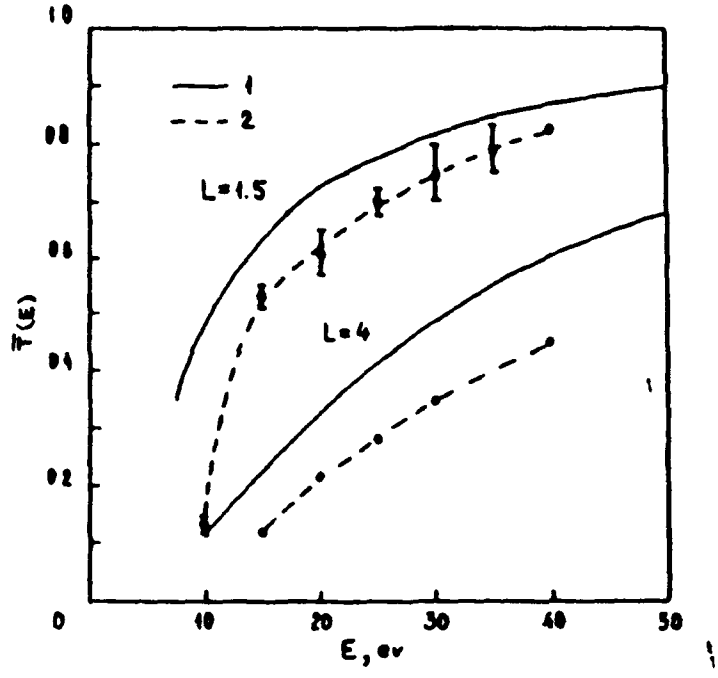

Fig. 5

Transparency of the force tube for isotropic pitch-angle distribution of entering photoelectrons; 1 – the calculation using formula (20); 2 – the results of Takahashi's calculations (1973, 1974).

Figure 11 Calculated Plasmaspheric Transparency versus Energy. Krinberg (1978)

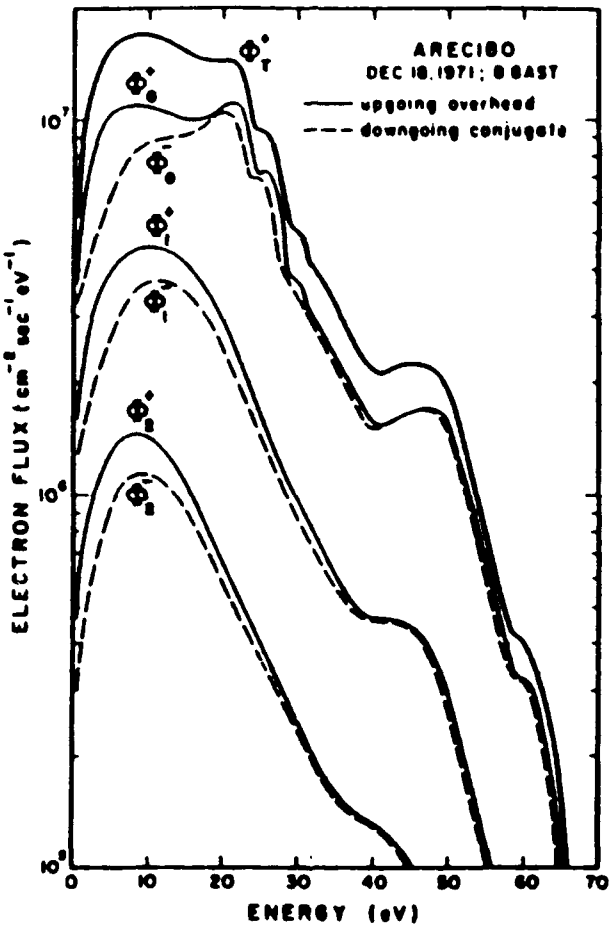

Fig. 2. Energy spectra of the escape photoelectron flux and of its two first reflections between local and conjugate hemispheres. The solid curves represent upward flux components at 1000 km over Arecibo. The dashed curves represent downward flux components at the other end of the magnetic field line at 1000 km. The curve denoted Φ_T^* represents the steady state upward flux at 1000 km, when both local and conjugate hemispheres are sunlit.

Figure 12 Energy Spectra of Reflected Electrons from Arecibo. Mantas (1978)

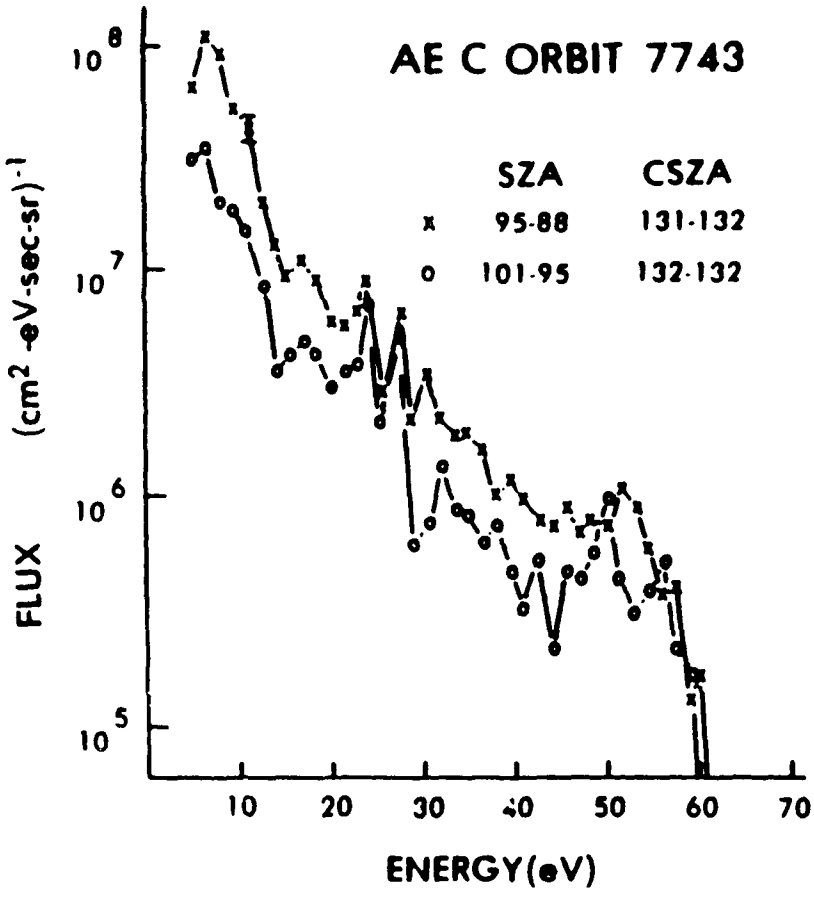

Fig. 1. Energy spectra of photoelectrons observed streaming up the magnetic field lines when the magnetic conjugate point was not illuminated. These are average data for the solar zenith angles (SZA) and conjugate solar zenith angles (CSZA) indicated. Other orbit parameters are given in Fig. 2. The error bar shown represents the error due to the finite number of counts.

Figure 13 Upward Streaming Electron Energy Spectra from AE-C, Peterson (1977a)

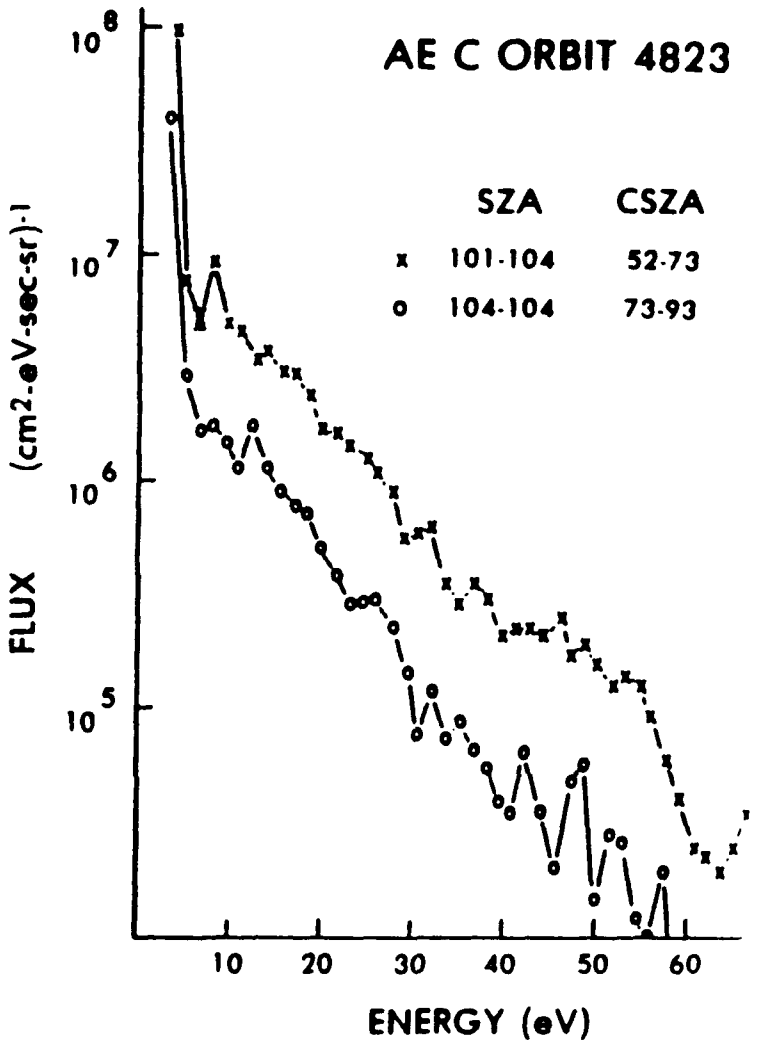

Fig. 3. Energy spectra of electrons observed precipitating into the atmosphere when the magnetic conjugate point was illuminated. These are average data for the solar zenith angles (SZA) and conjugate solar zenith angles (CSZA) indicated. Other orbital parameters are given in Fig. 4.

Figure 14 Downward Streaming Electron Energy Spectra from AE-C, Peterson (1977a)

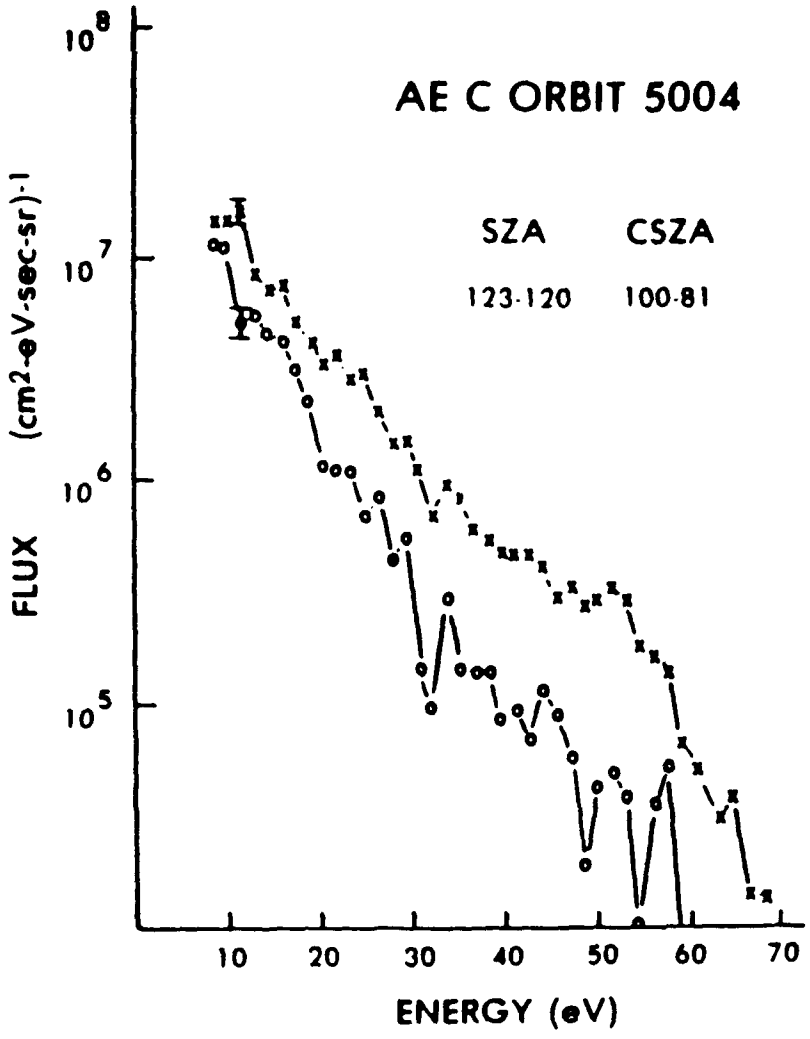

Fig. 5. Average energy spectra of electrons observed at 263 km for a range of solar zenith angles (SZA) when the zenith angles at the magnetic conjugate point (CSZA) varied from 100° to 81°, taken on January 12, 1975. Precipitating electrons are indicated by x's (pitch angles less than 60°) and backscattered electrons are indicated by open circles (pitch angles greater than 120°). The dip latitude varied from 34° to 54° during the time these data were acquired.

Figure 15 Energy Spectra for Reflected Electrons from AE-C, Peterson (1977a)

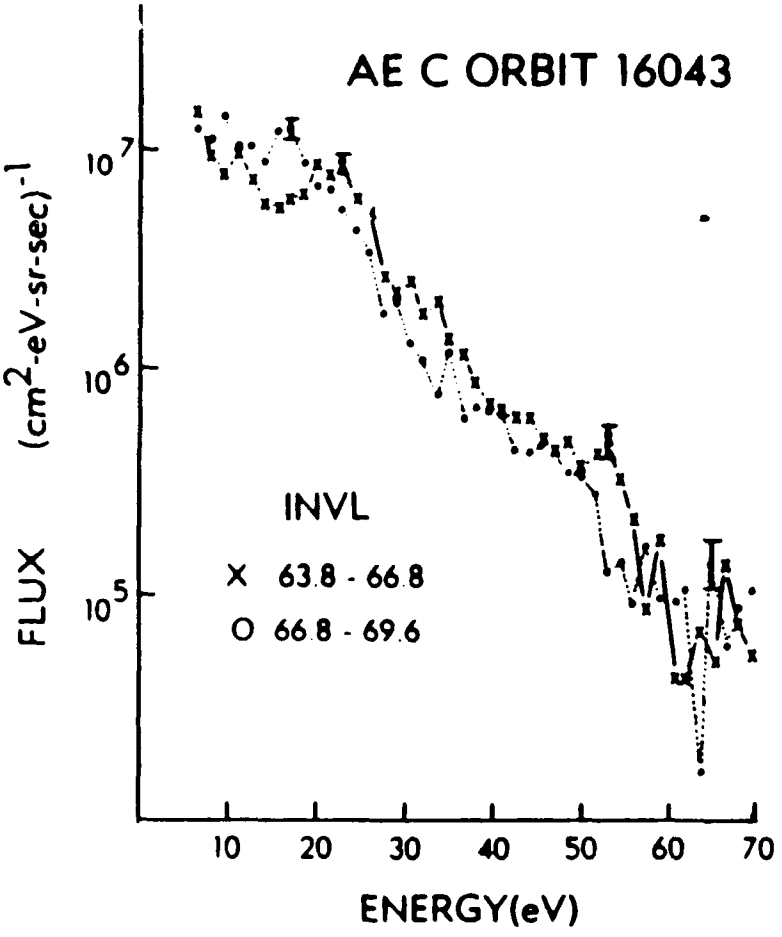

Figure 4. Average flux of conjugate photoelectrons observed as a function of energy for two consecutive 48 second intervals on AE-C Orbit 16043, and the corresponding ranges of invariant latitude (INVL) during these periods. The error bars shown are for the uncertainties due to the finite number of counts only.

Figure 16 Average Flux for Two Consecutive Intervals on AE-C, Peterson (1977b)

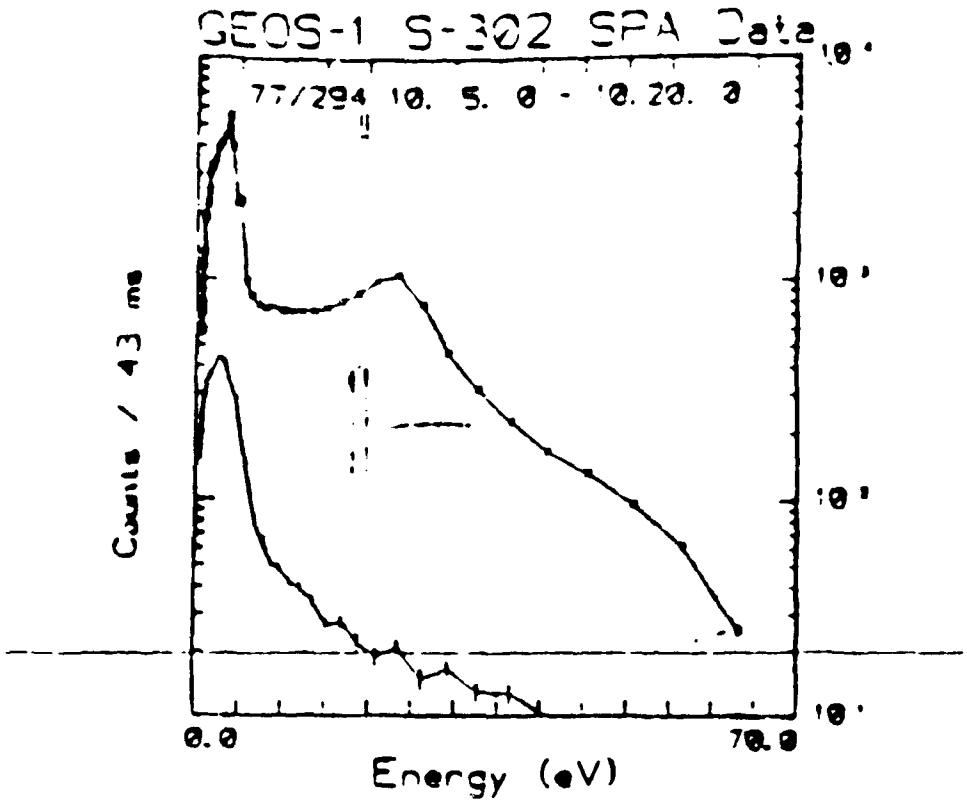

FIG. 2. CROSS-SECTION OF FIG. 1 SHOWING THE VARIATION OF THE COUNT RATE WITH ENERGY IN THE ZERO PITCH ANGLE REGION.
Peaks are visible at ~ 3 and 23 eV.

Figure 17 Counts versus Energy Plot from GEOS 1, Coates (1985)

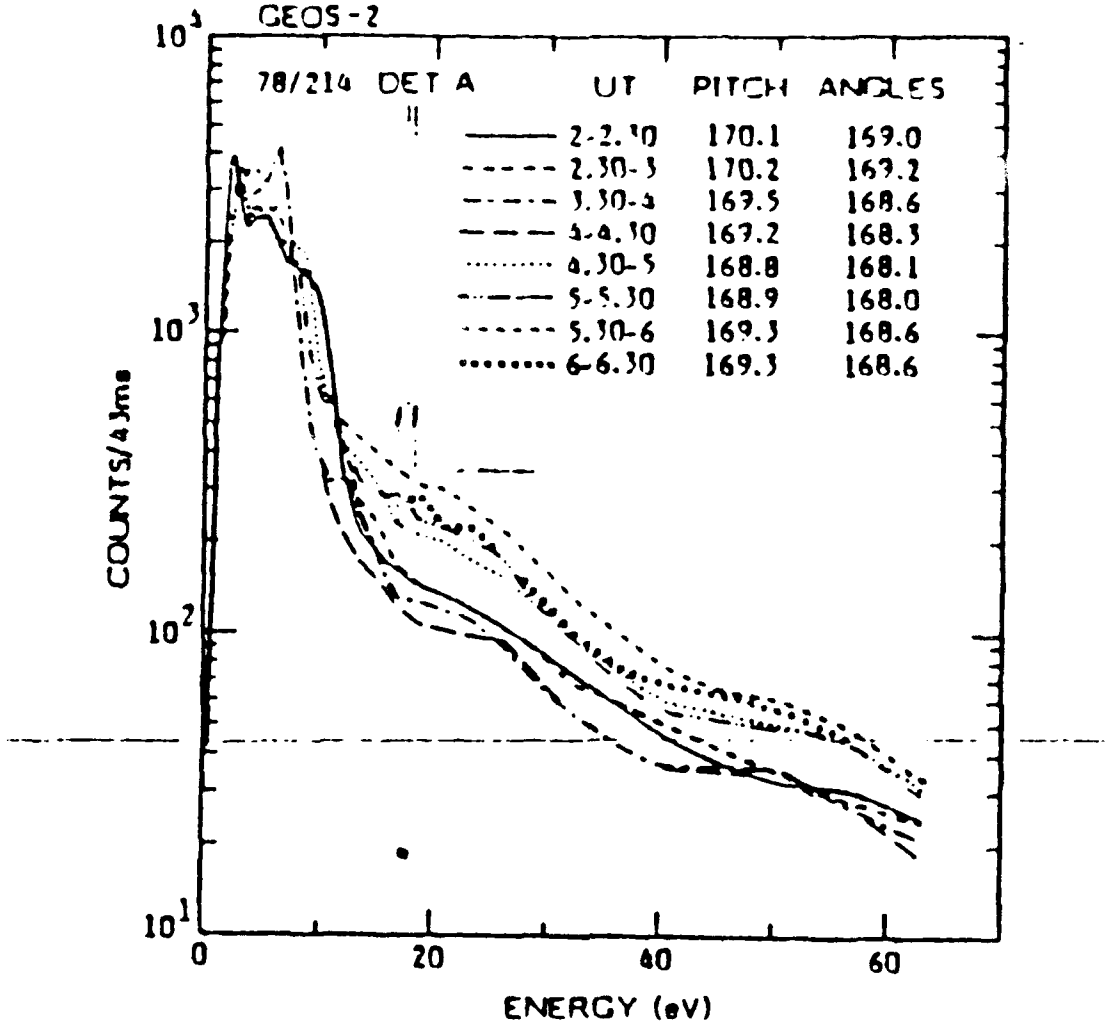

FIG. 6. *GEOS*-2 MEASUREMENTS SHOWING THE VARIATION OF THE ANALYSER A FIELD-ALIGNED ENERGY SPECTRUM WITH TIME. The 20 eV peak occurs after 04.30 U.T.

Figure 18 Counts versus Energy Plot from GEOS 2, Coates (1985)

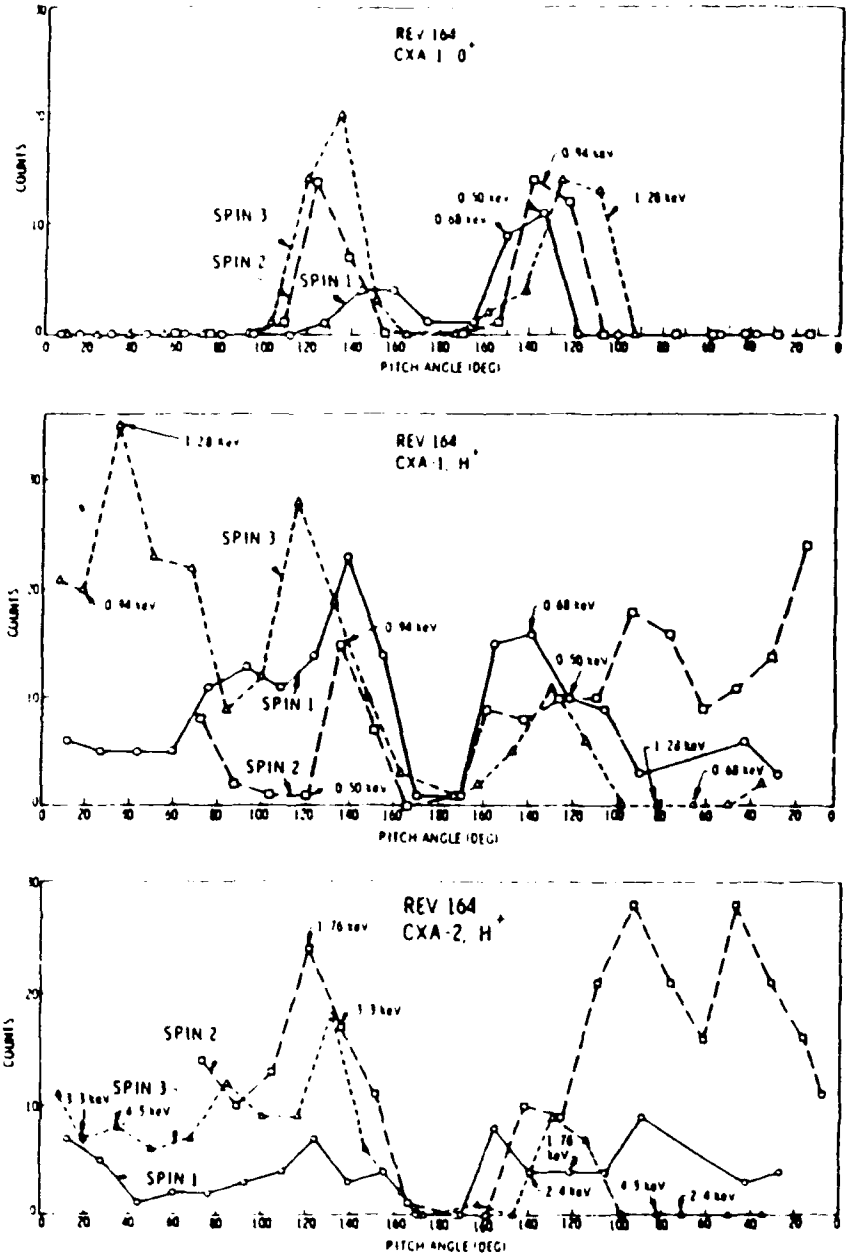

Fig. 3. Ion data showing detailed pitch angle dependence of the low-energy O^+ and H^+ fluxes during the three spins indicated in Figure 1.

Figure 19 Ion Flux versus Pitch Angle from Satellite 1976-65B, Sharp (1977)

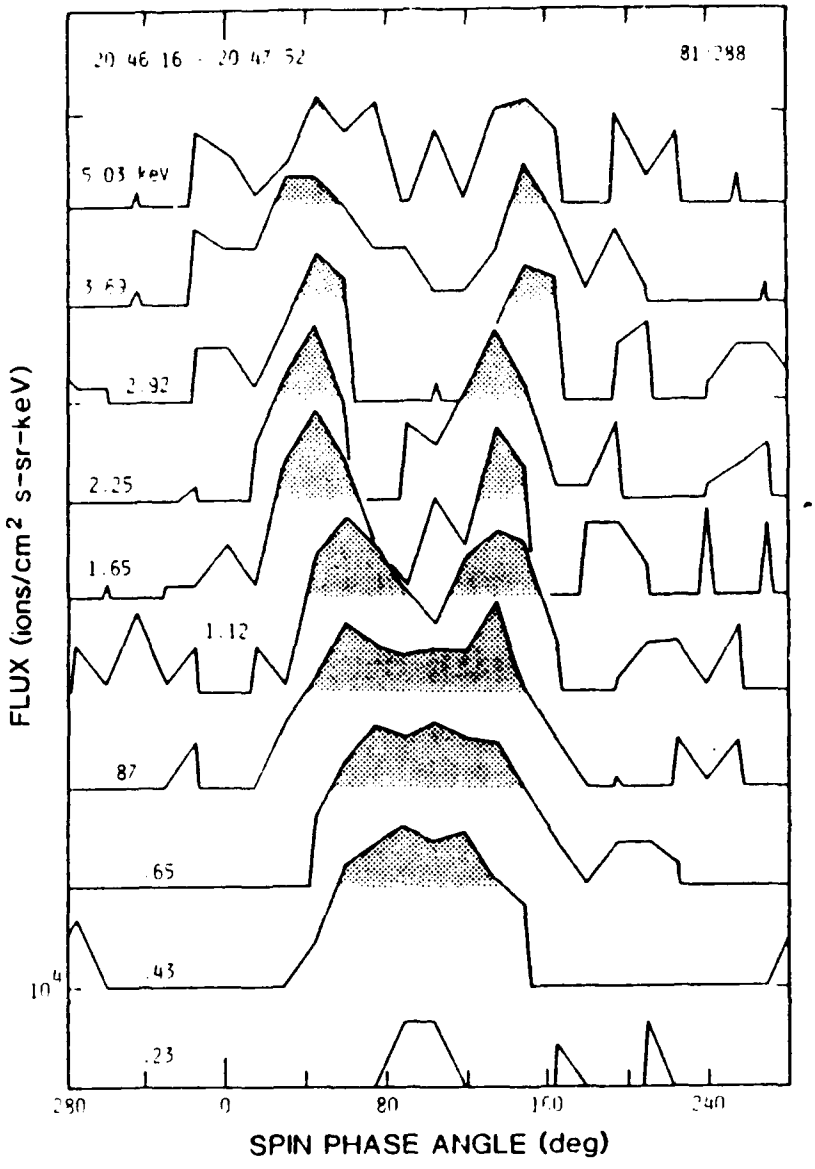

Fig. 2. Stack plot of log oxygen ion flux versus spin phase angle at the 10 successive energy levels sampled between 0.23 and 5.03 keV. The baseline of each curve is at 10^4 ions cm^{-2} s^{-1} sr^{-1} keV^{-1} and each successive curve is displaced upward by one decade. Flux levels in excess of 10^5 ions cm^{-2} s^{-1} sr^{-1} keV^{-1} have been shaded for emphasis. The magnetic field direction is at a spin phase angle of 100.

Figure 20 Conic Flux Distribution vs Pitch Angle Stacked Plot, DE 1, Klumpar (1984)

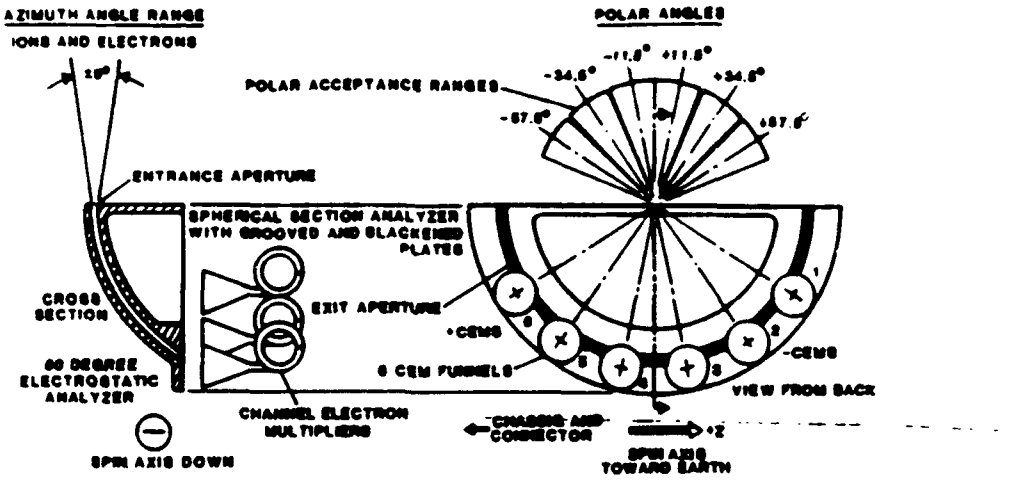

FIG. 1. Cross-sectional view of the MPA charged particle optics system, on the left. A view of the system on the right, taken from behind the analyzer, shows the locations of the six CEM funnels and their nominal polar angle fields-of-view.

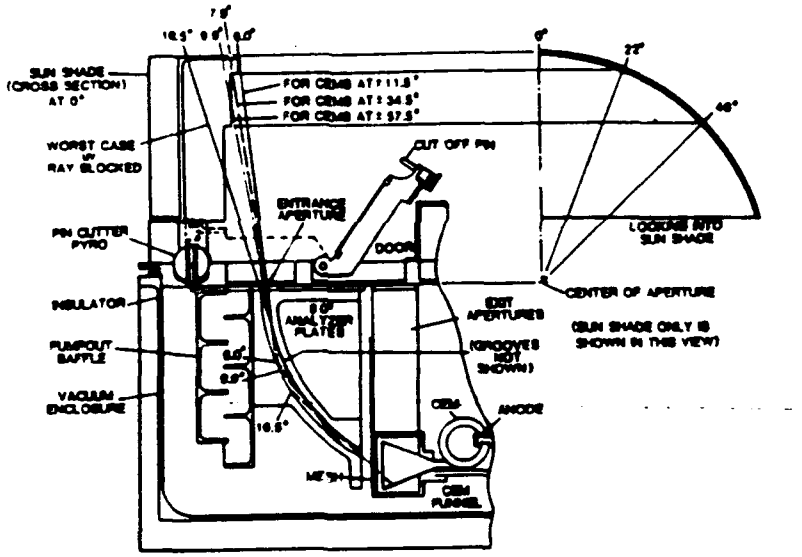

FIG. 2. Cross-sectional view of the entrance aperture end of MPA showing the cylindrically shaped sun shade which limits how deep into the gap solar UV can fall before scattering or producing photoelectrons, as well as other features of the sensor package. Grooving of the plates, not shown in the drawing, reduces the area from which UV can scatter into the CEMs or produce photoelectrons that might reach the CEMs.

Figure 21 Cross Sectional Views of the MPA, Bame (1993)

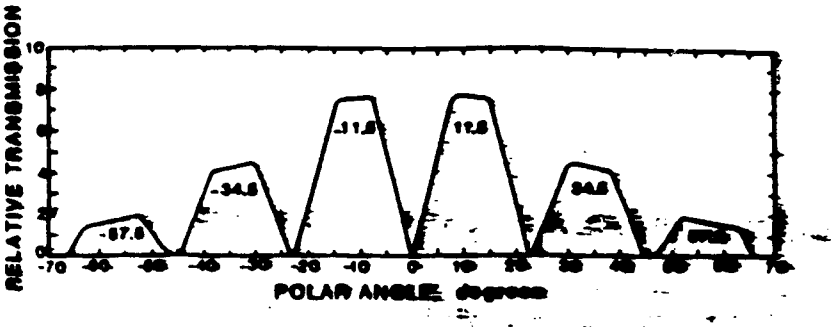

FIG. 6. Calculated MPA response profiles vs. polar angle, integrated over

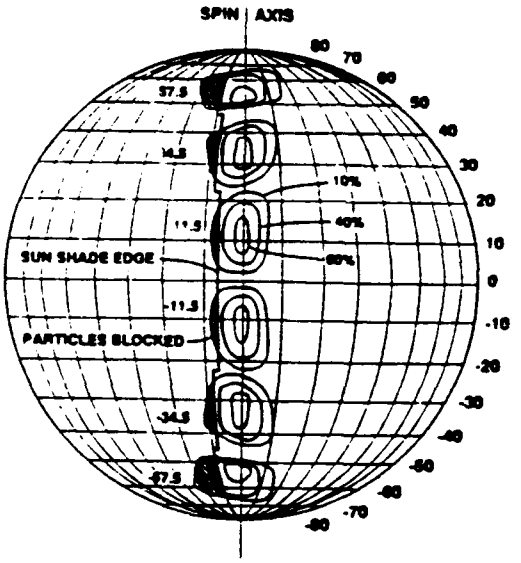

FIG. 8. Contours of MPA transmission response shown on the unit sphere at the 10%, 40%, and 80% transmission levels.

Figure 22 MPA Transmission Response Curves and Unit Sphere, Bame (1993)

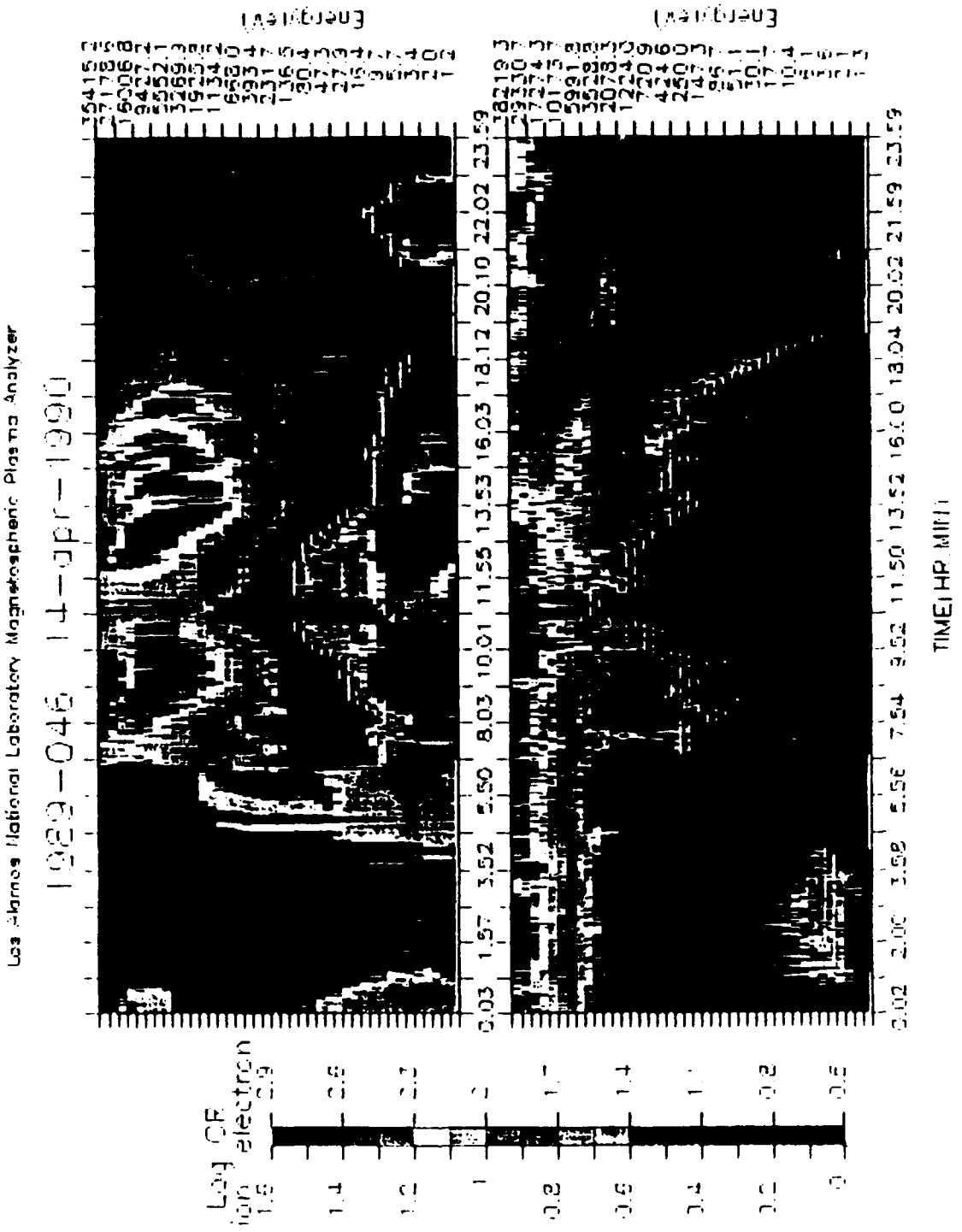

Figure 23 14 April Energy Spectrogram and Potential Overplot, Fiely (1992)

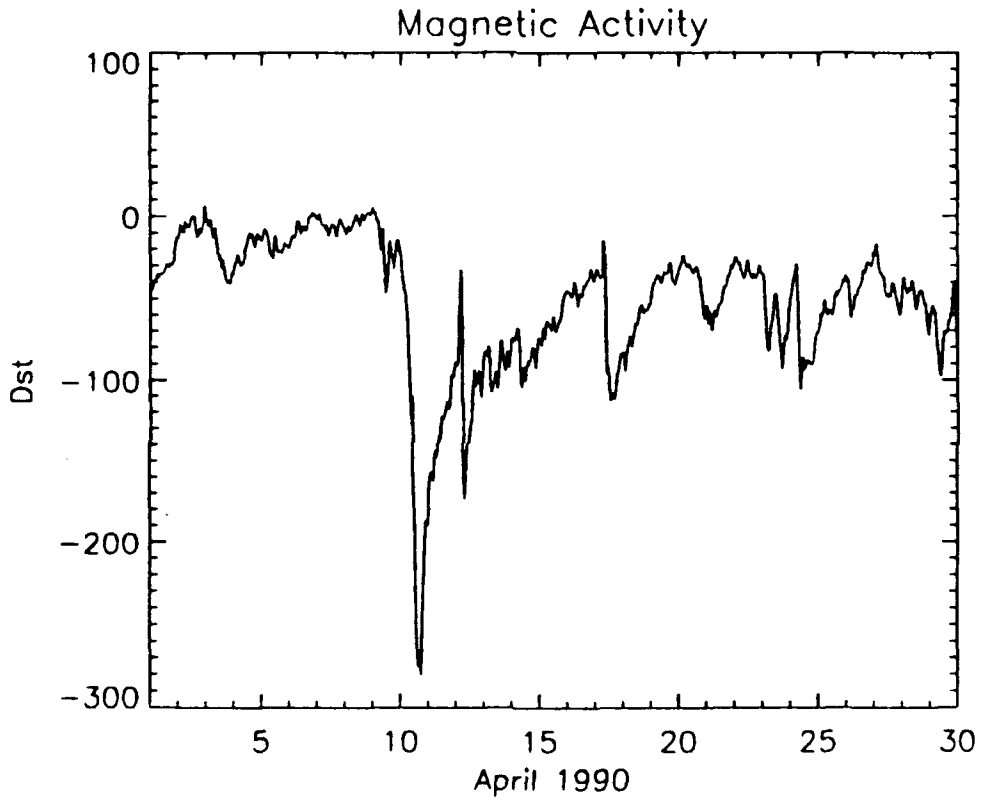

Figure 24 Magnetic Activity for April 12 through April 21, 1990

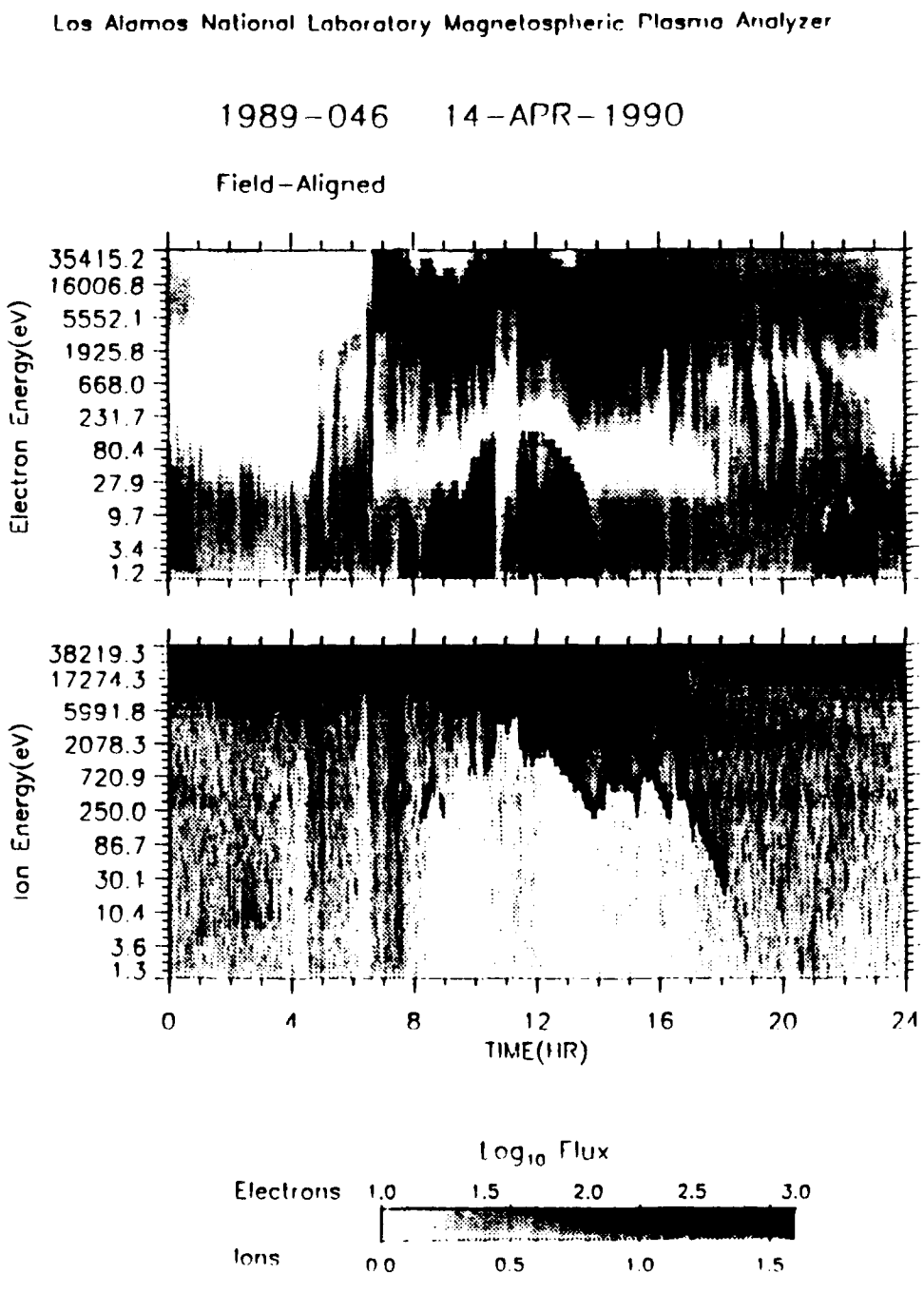

Figure 25 Energy vs Time Spectrogram--Field Aligned--4/14/90

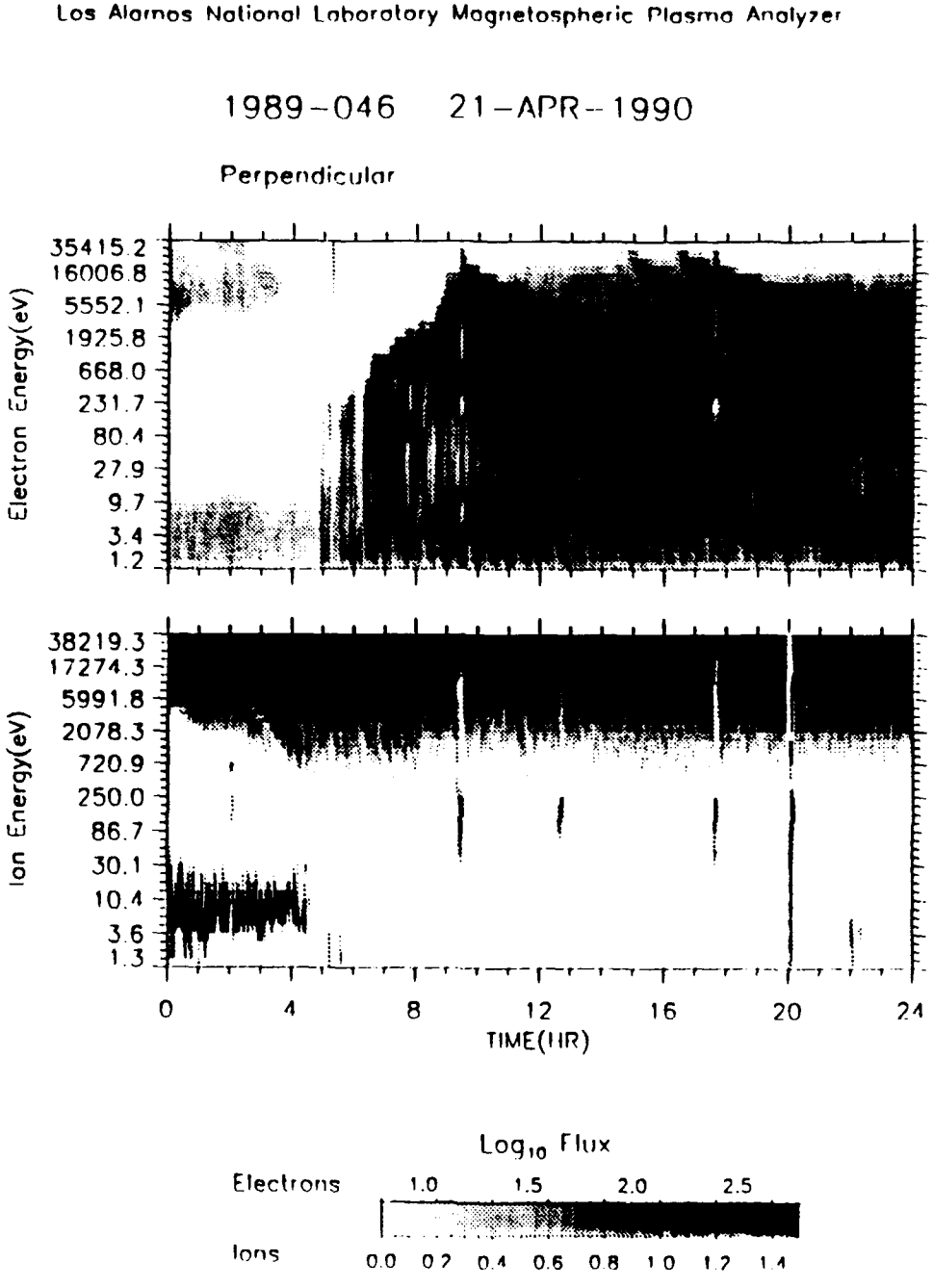

Figure 26 Energy vs Time Spectrogram--Perpendicular--4/14/90

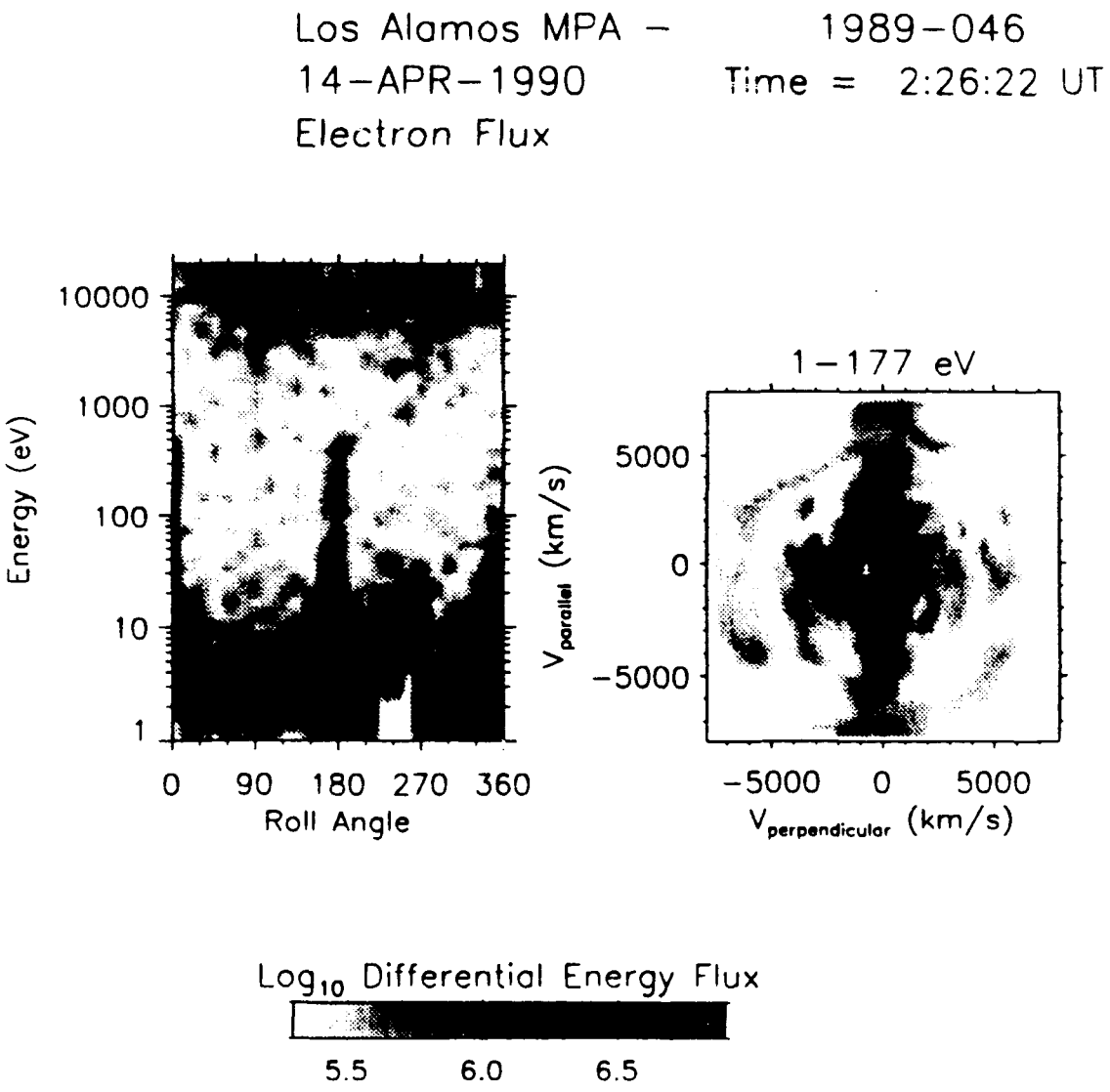

Figure 27 Energy versus Angle Spectrogram for 02:26:22 UT on April 14, 1990 (Spacecraft in Plasmasphere)

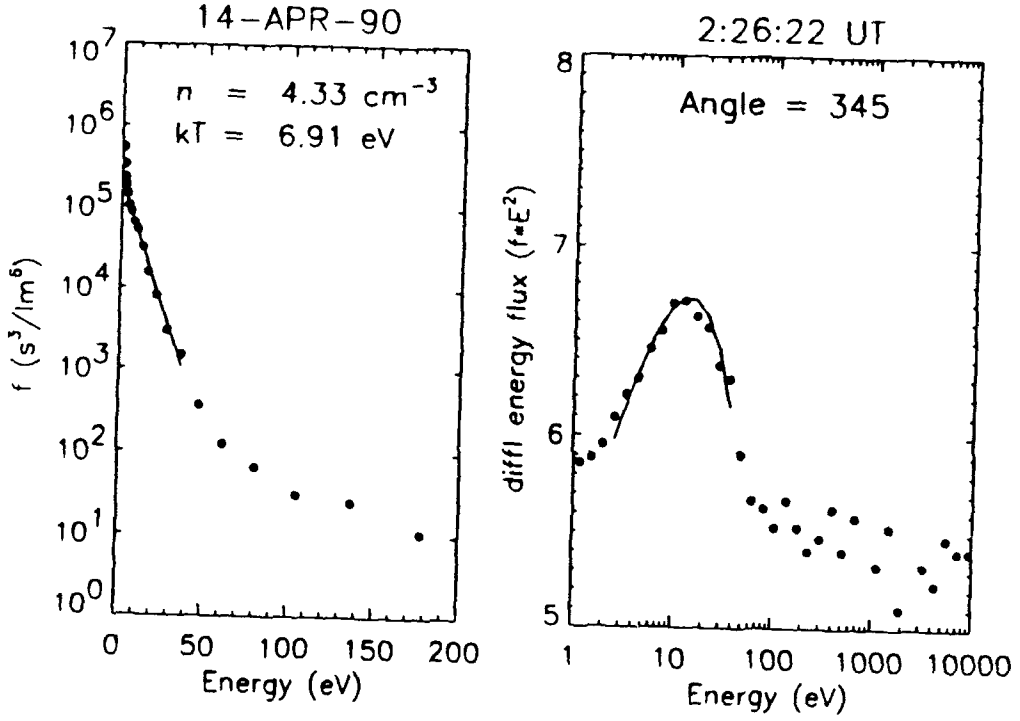

Figure 28 f vs Energy and Differential Energy Flux vs Energy Plots for 02:26:22 UT on April 14, 1990

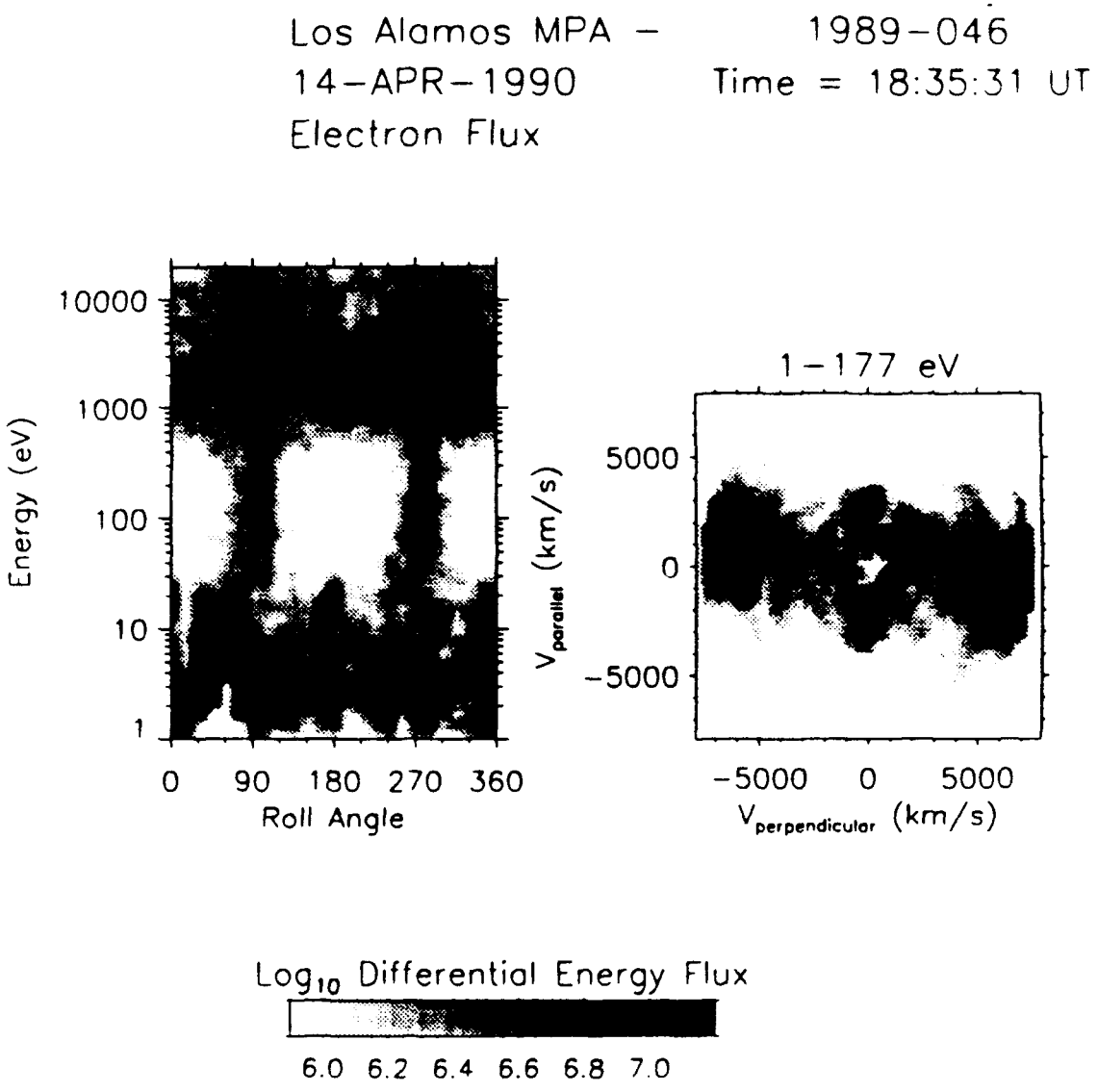

Figure 29 Energy versus Angle Spectrogram for 18:35:31 UT on April 14, 1990

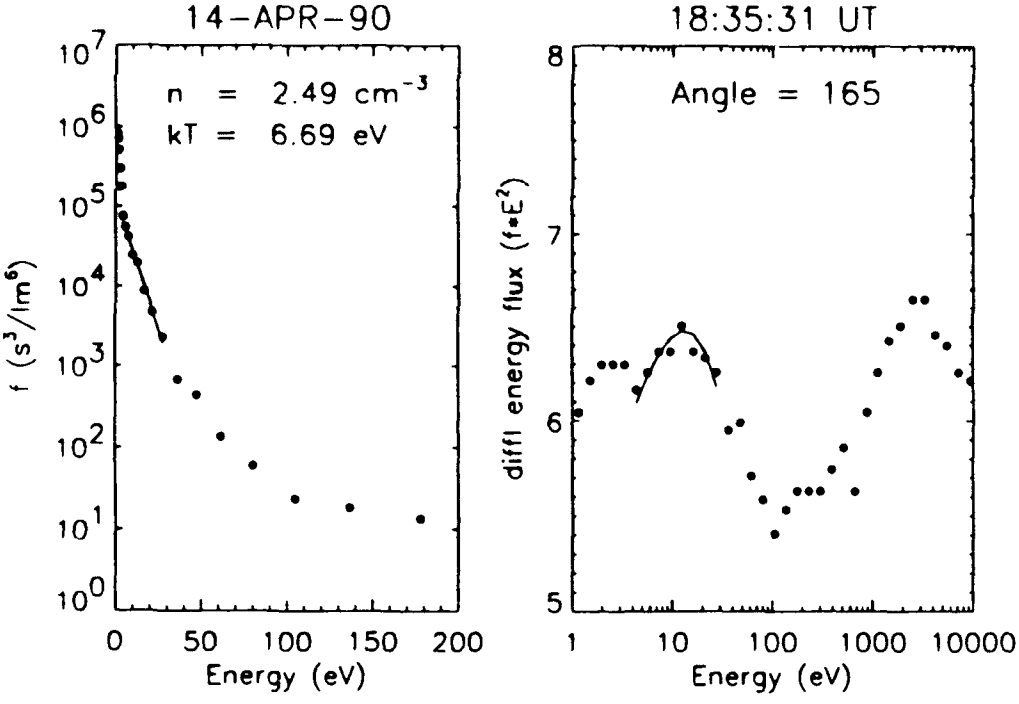

Figure 30 f vs Energy and Differential Energy Flux vs Energy Plots for 18:35:31 UT on April 14, 1990

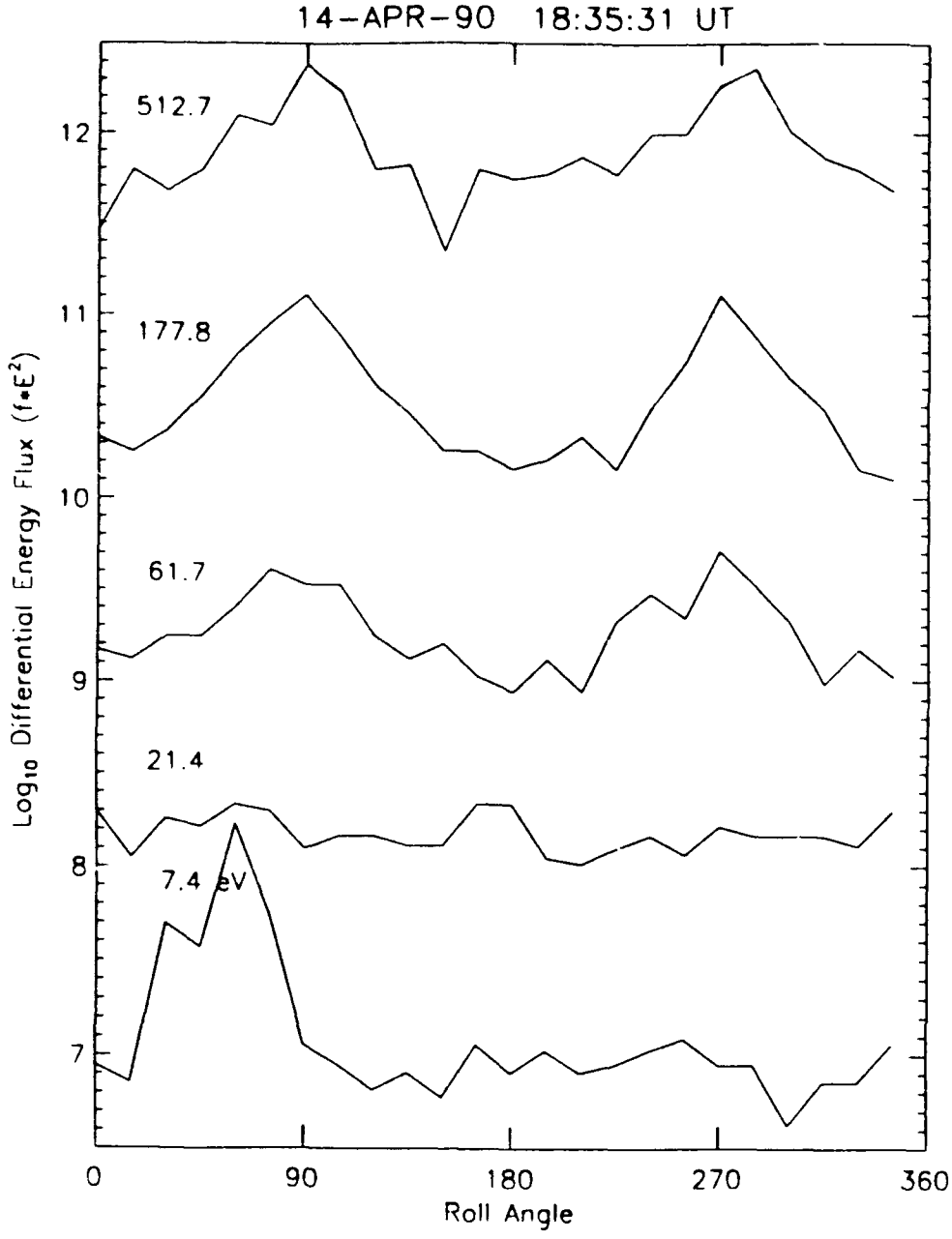

Figure 31 Stacked Line Plots of Diff. Energy Flux vs Roll Angle for 18:35:31 UT on April 14, 1990

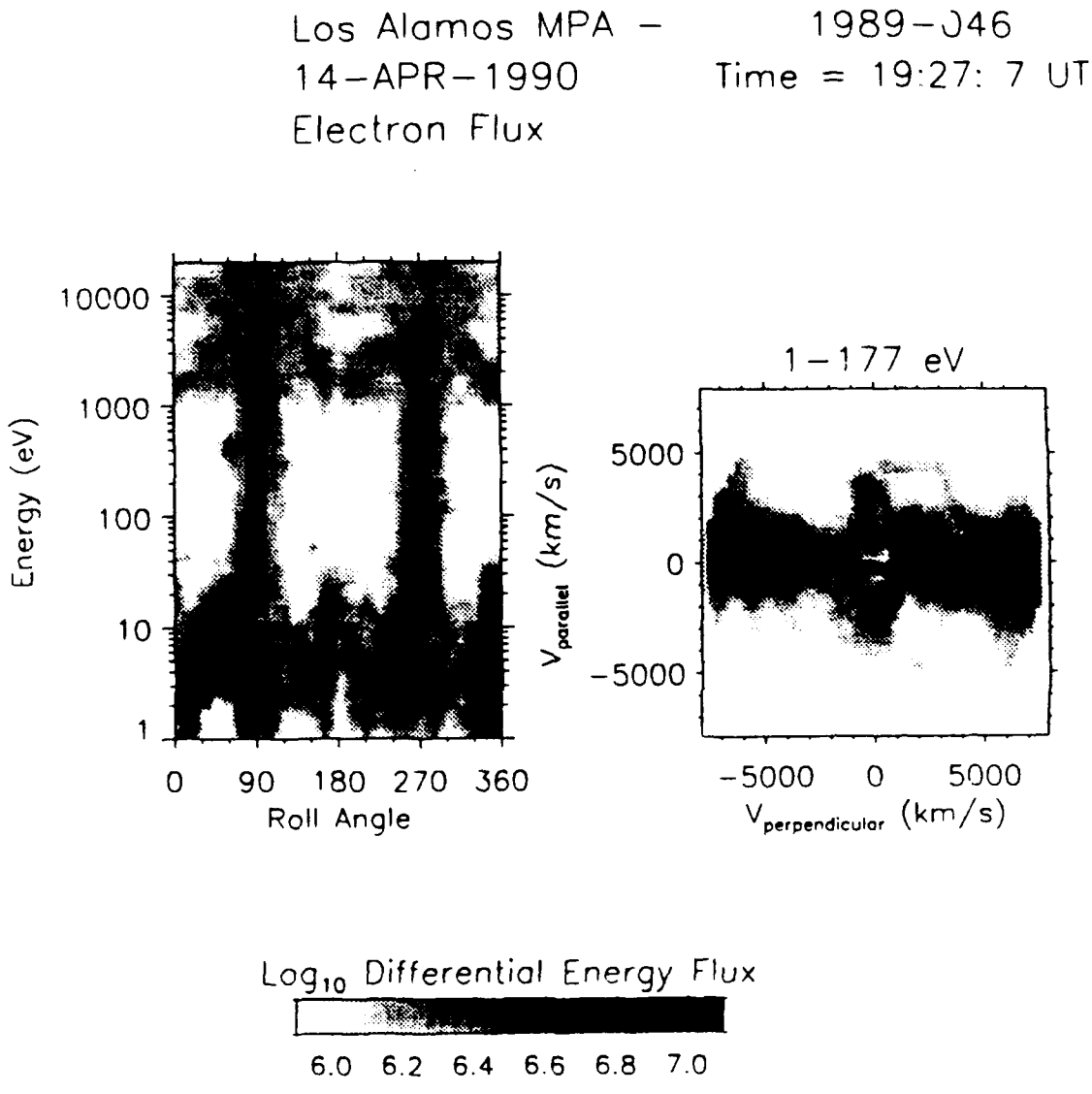

Figure 32 Energy versus Angle Spectrogram for 19:27:07 UT on April 14, 1990

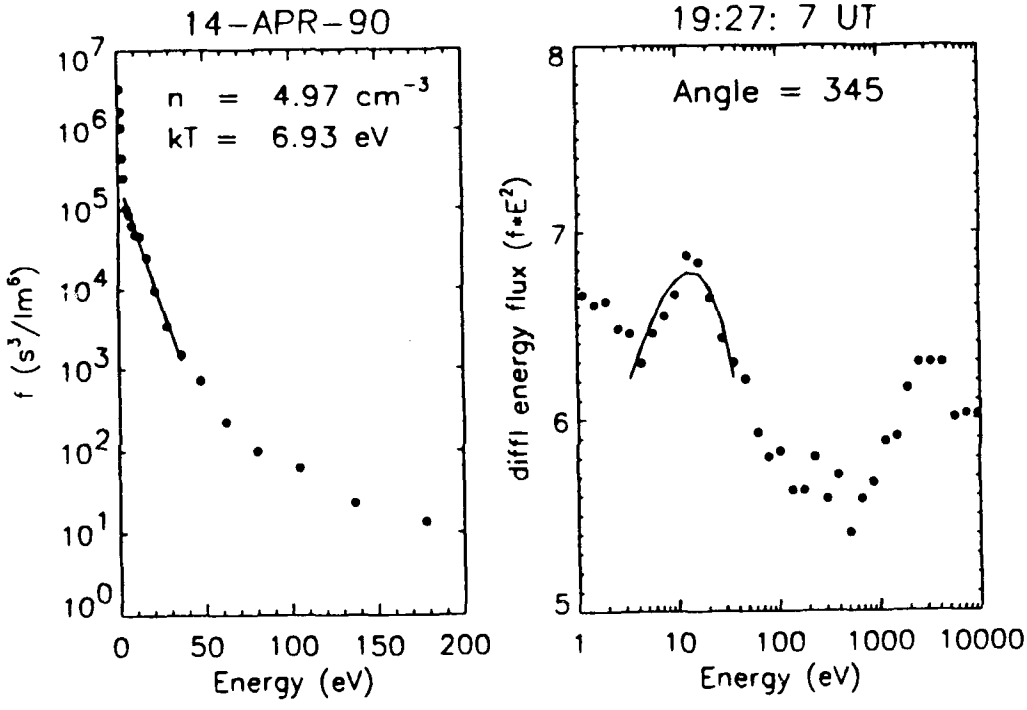

Figure 33 f vs Energy and Differential Energy Flux vs Energy Plots for 19:27:07 UT on April 14, 1990

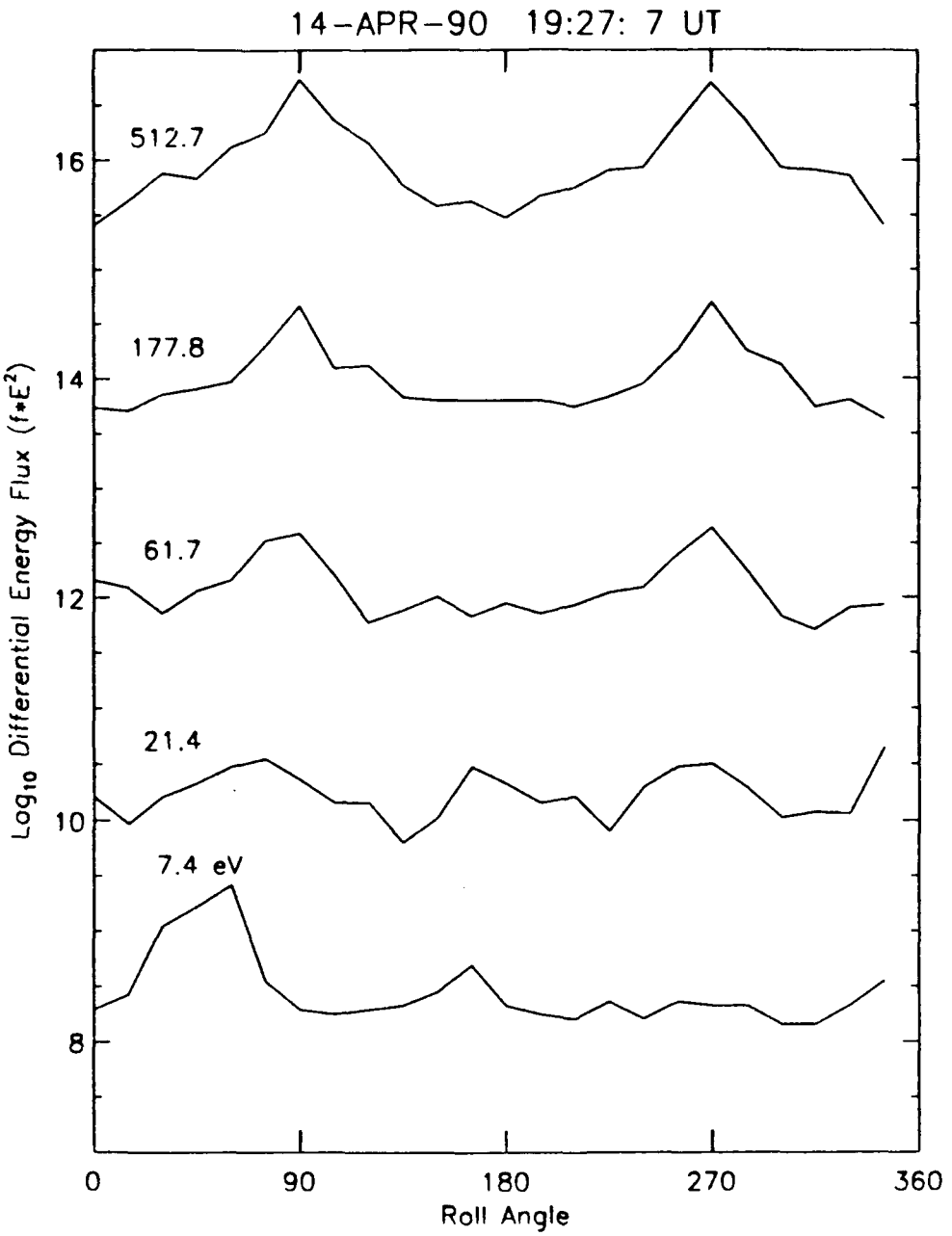

Figure 34 Stacked Line Plots of Diff. Energy Flux vs Roll Angle for 19:27:07 UT on April 14, 1990

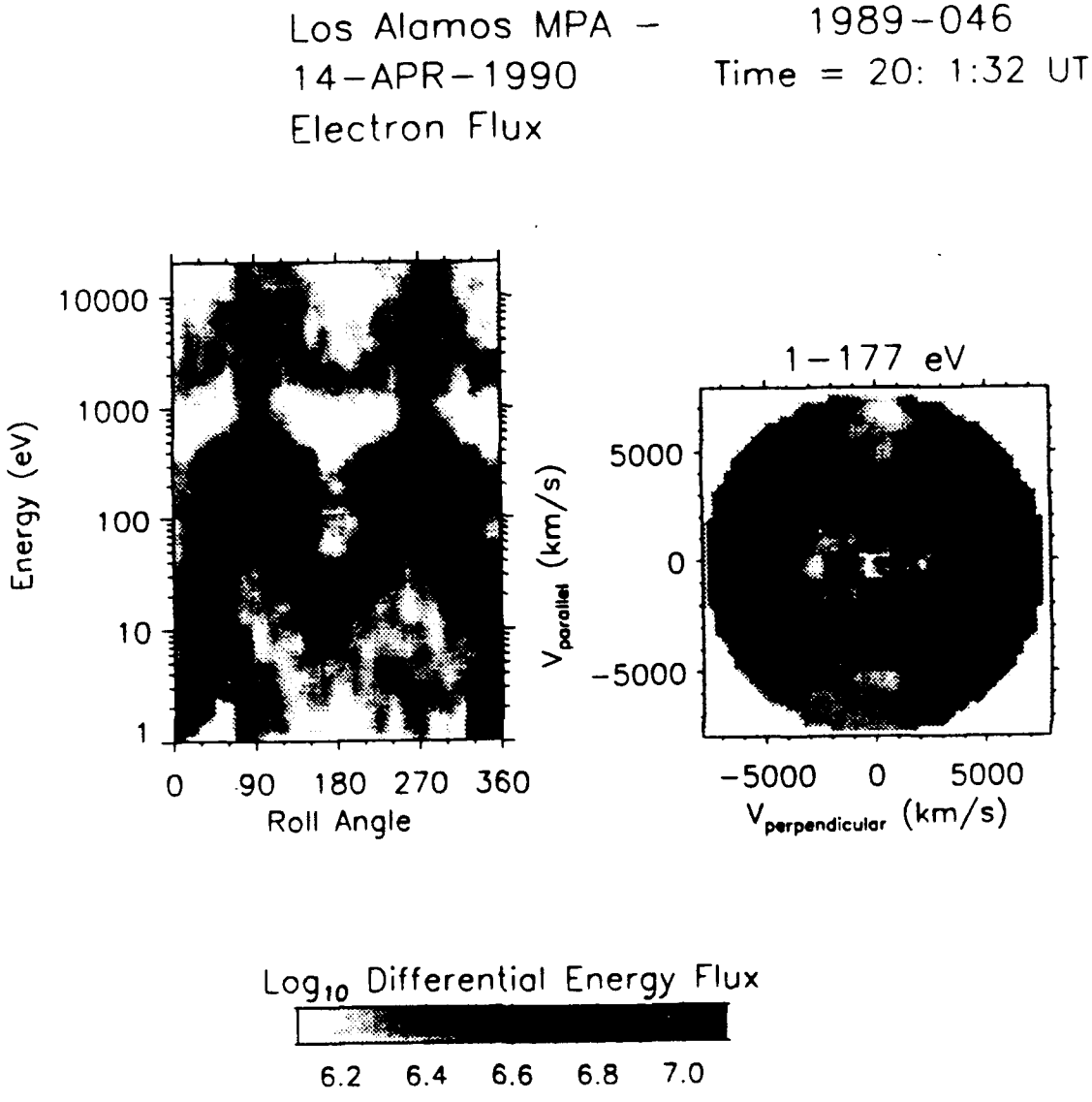

Figure 35 Energy versus Angle Spectrogram
for 20:01:32 UT on April 14, 1990

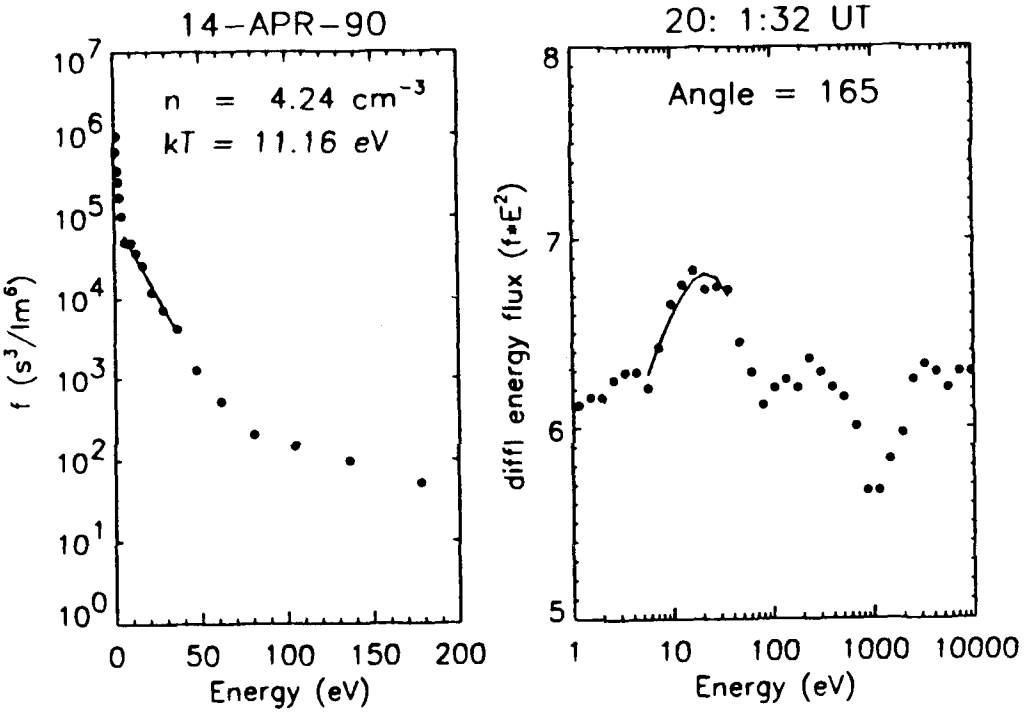

Figure 36 f vs Energy and Differential Energy Flux vs Energy Plots for 20:01:32 UT on April 14, 1990

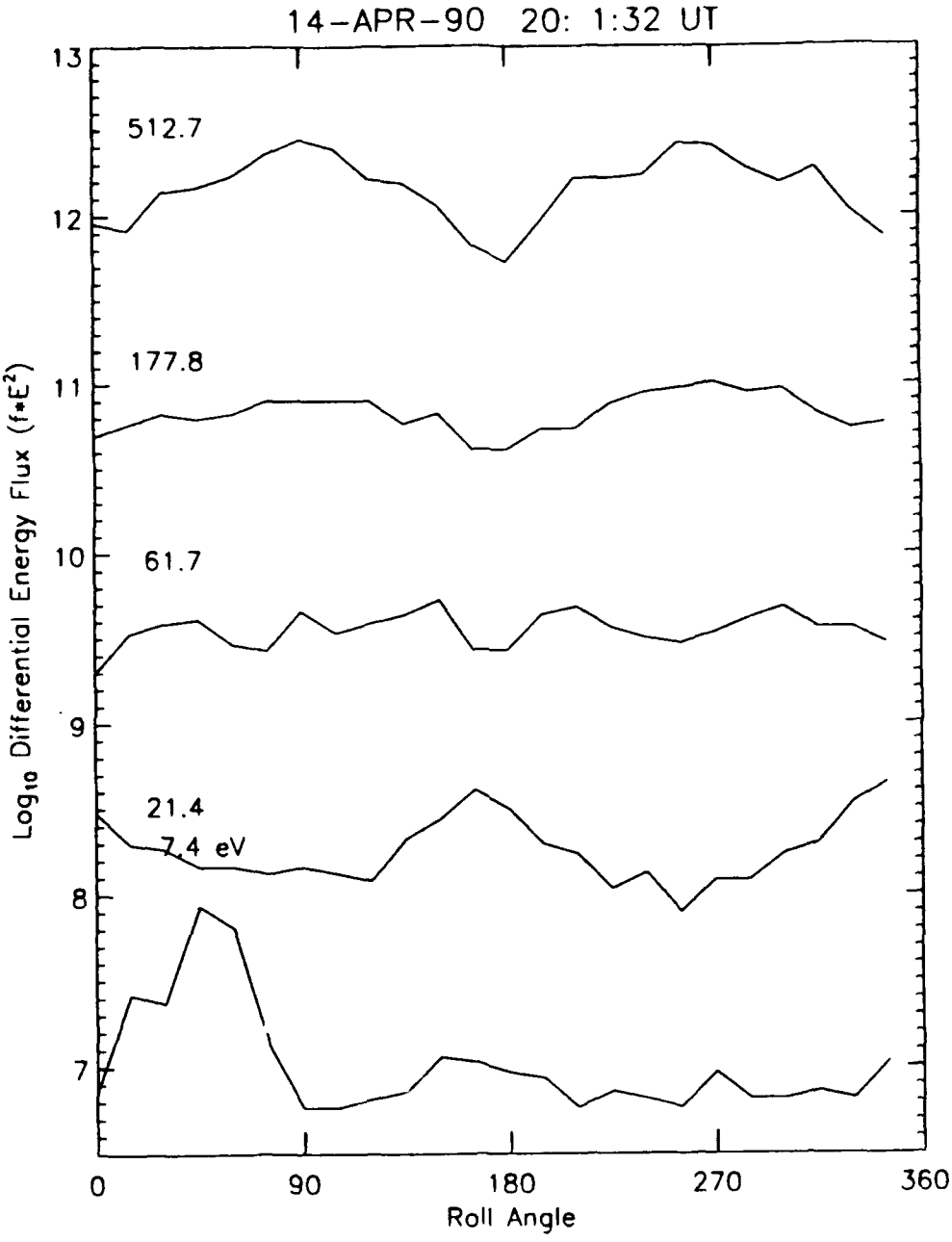

Figure 37 Stacked Line Plots of Diff. Energy Flux vs Roll Angle for 20:01:32 UT on April 14, 1990

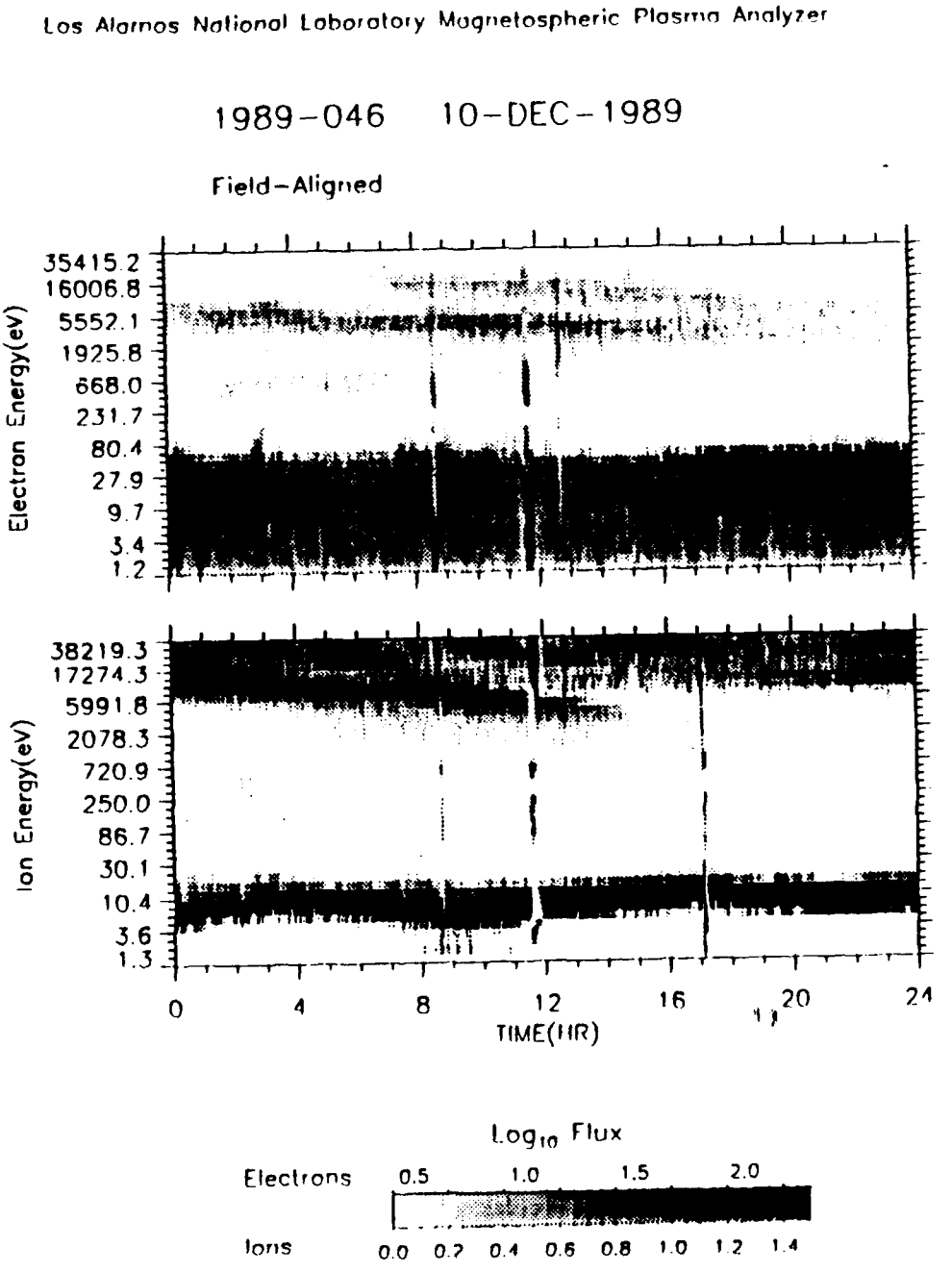

Figure 38 Energy vs Time Spectrogram--Field Aligned--12/10/89

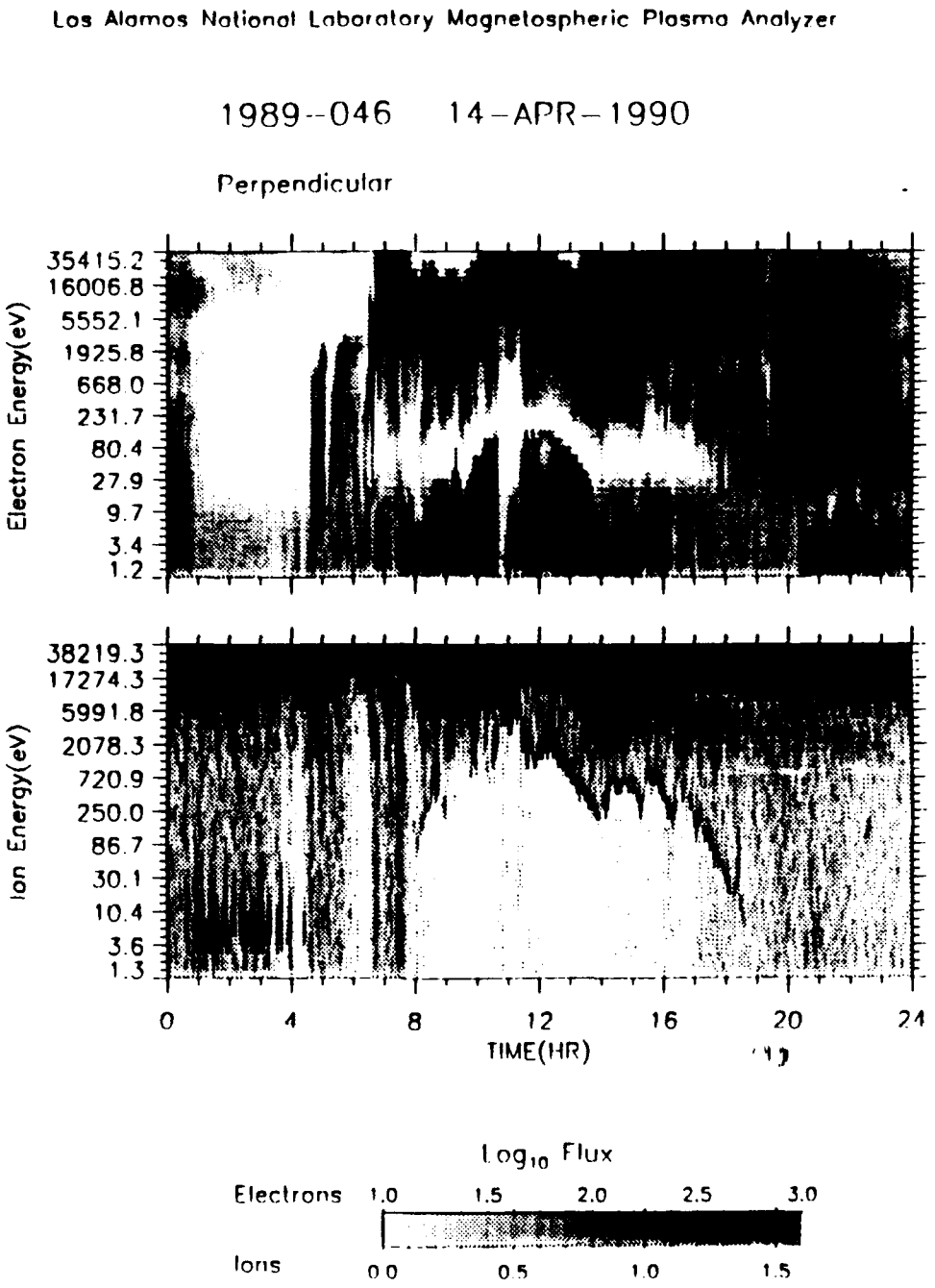

Figure 39 Energy vs Time Spectrogram--Perpendicular--12/10/89

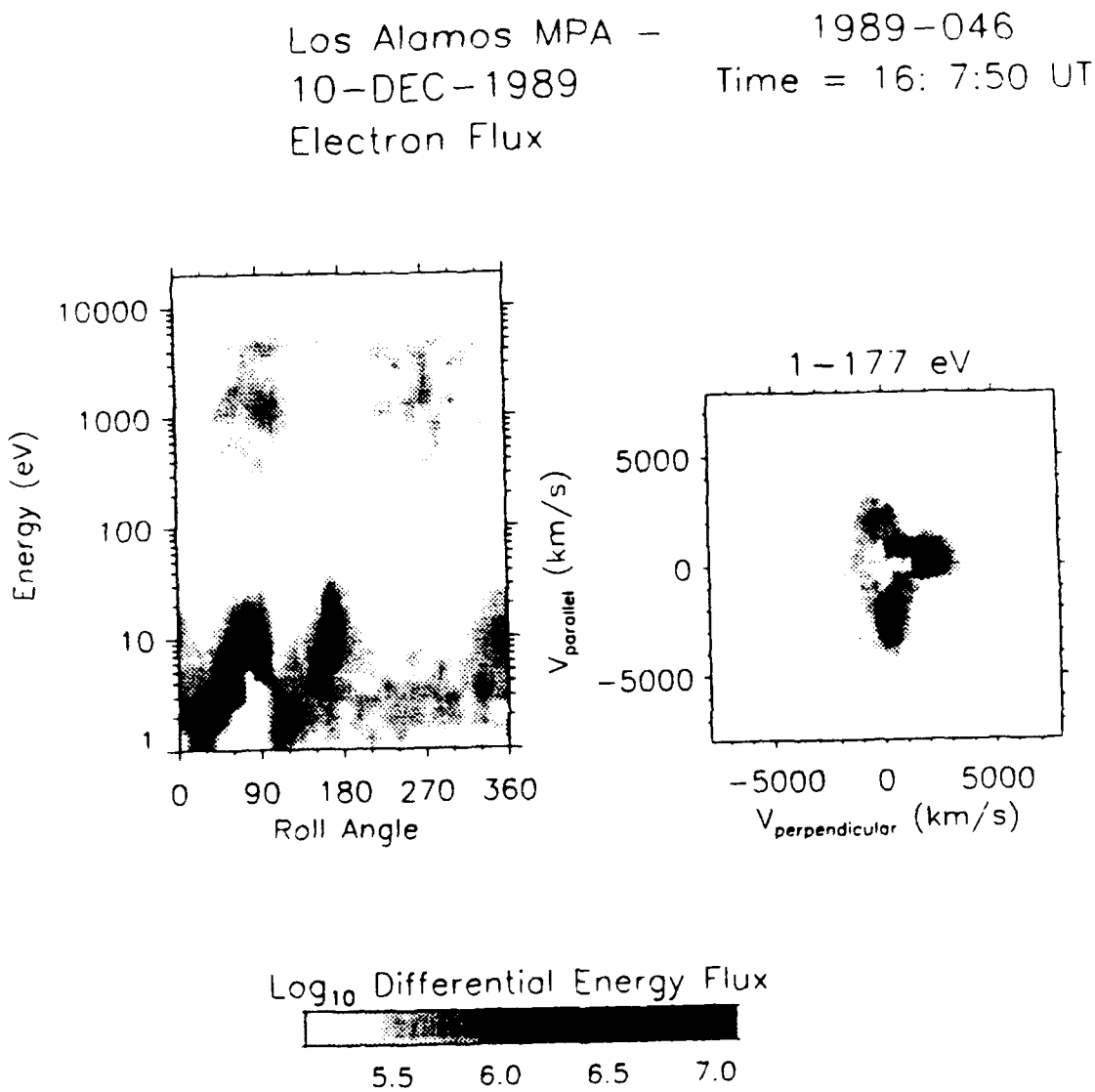

Figure 40 Energy versus Angle Spectrogram for 16:07:50 UT on December 10, 1989 (Spacecraft in Plasmasphere)

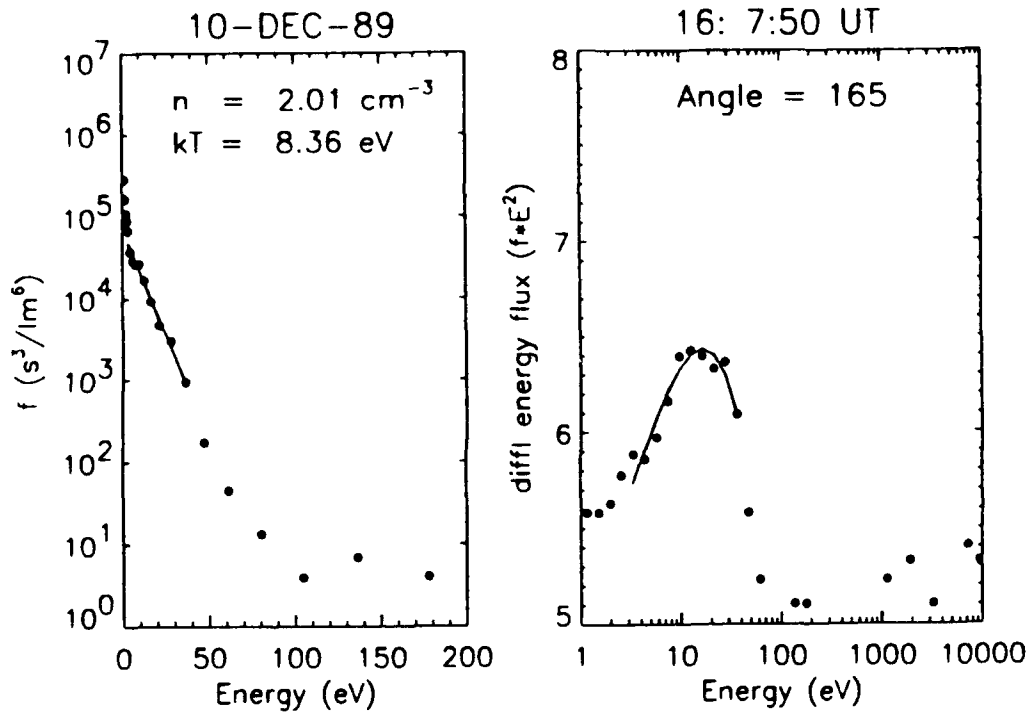

Figure 41 f vs Energy and Differential Energy Flux vs Energy Plots for 16:07:50 UT on December 10, 1989

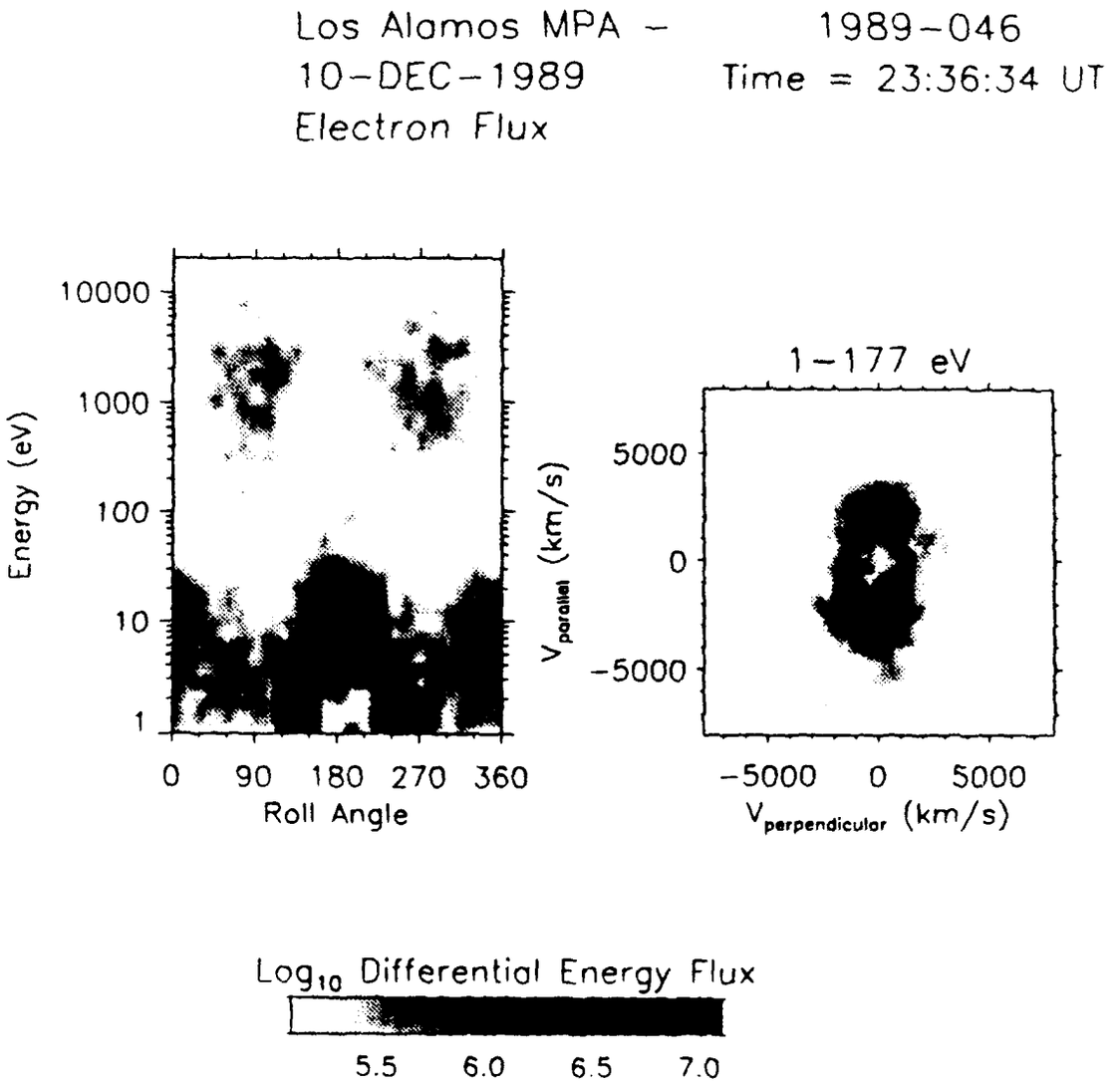

Figure 42 Energy versus Angle Spectrogram for 23:36:34 UT on December 10, 1989 (Spacecraft in Plasmasphere)

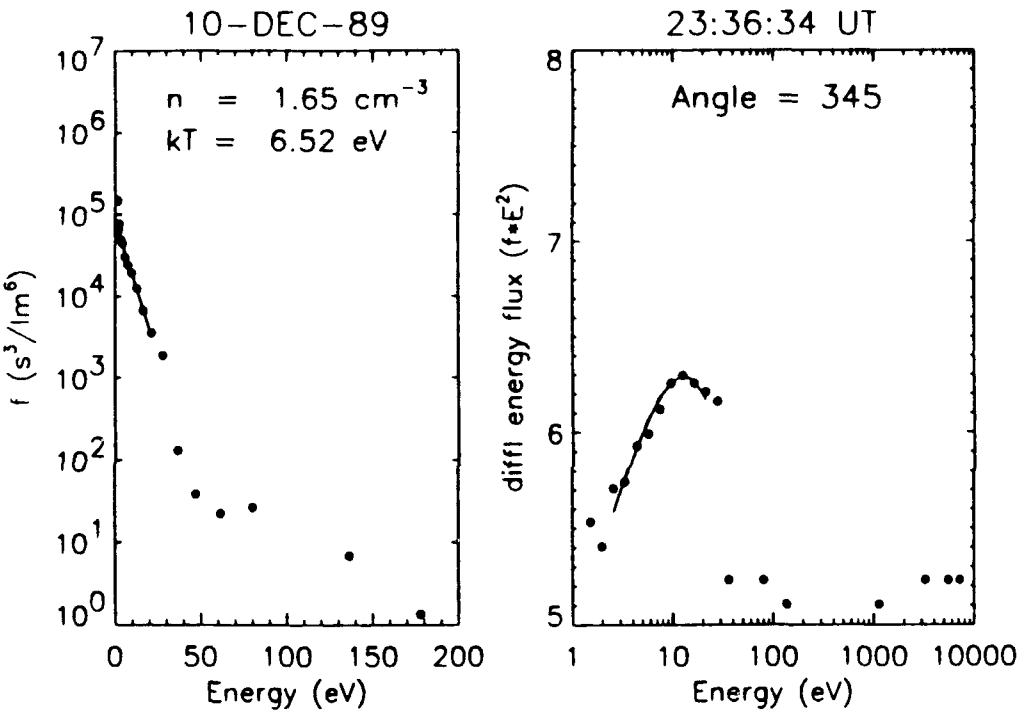

Figure 43 f vs Energy and Differential Energy Flux vs Energy Plots for 23:36:34 UT on December 10, 1989

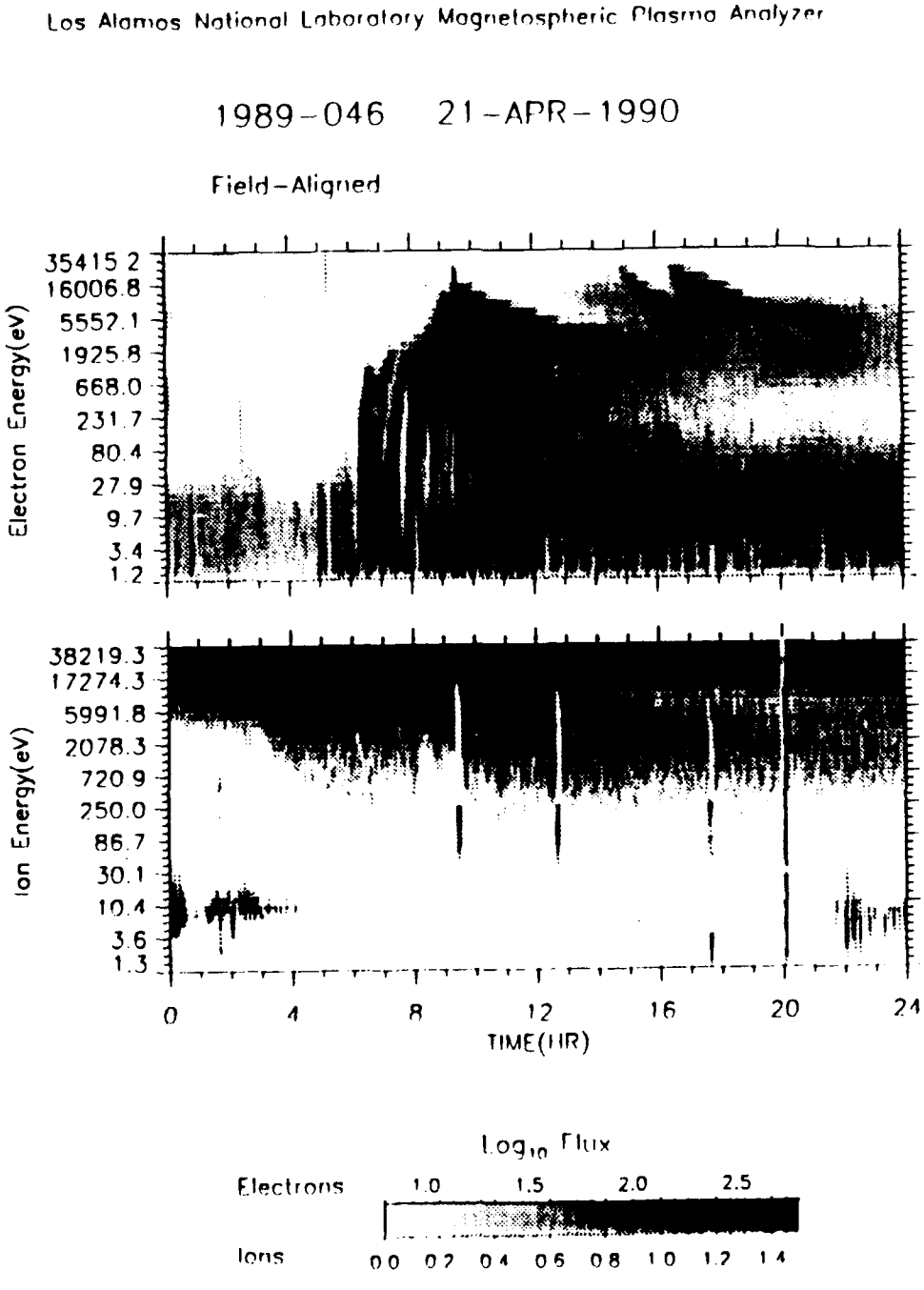

Figure 44 Energy vs Time Spectrogram--Field Aligned--4/21/90

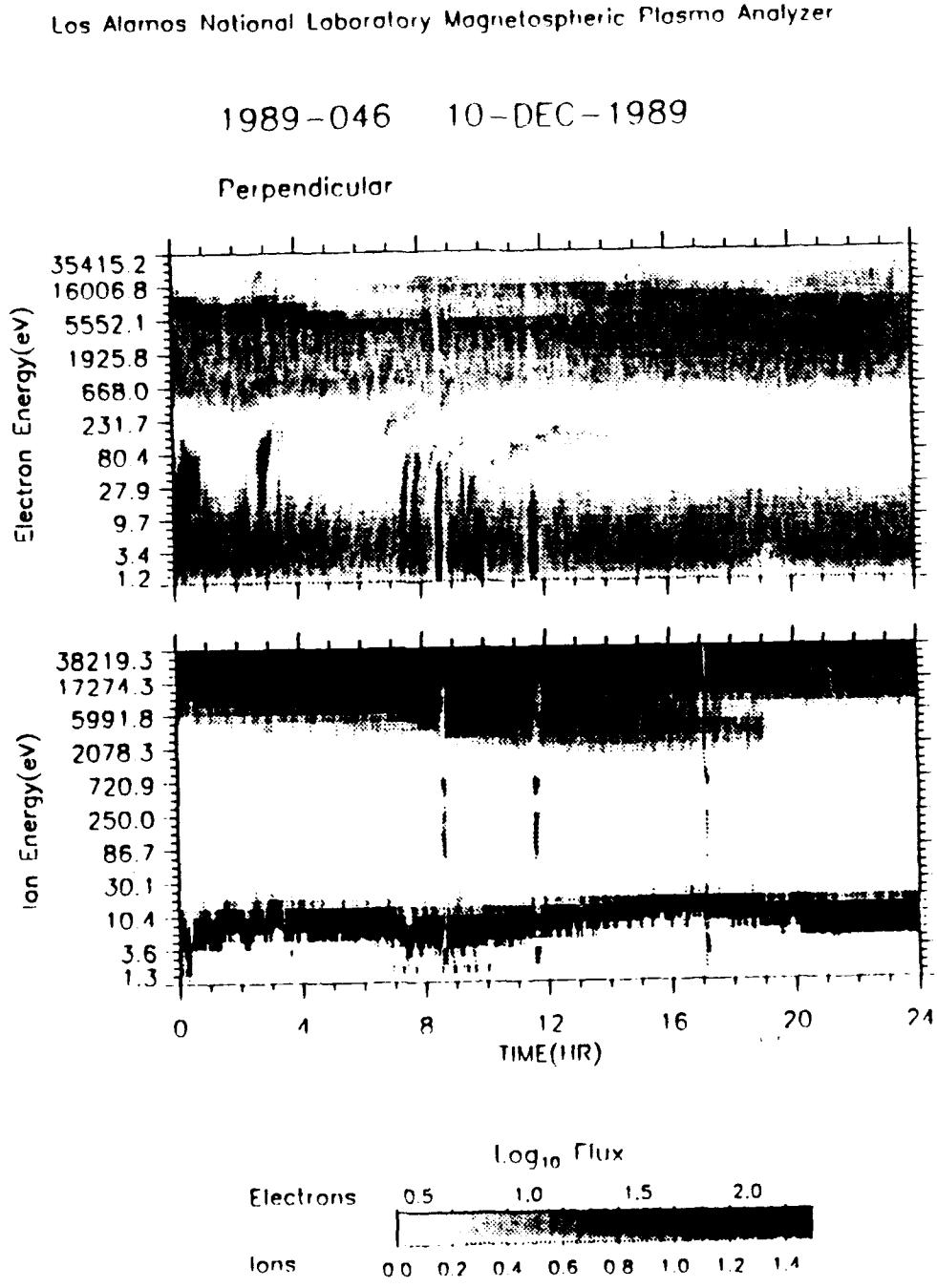

Figure 45 Energy vs Time Spectrogram--Perpendicular--4/21/90

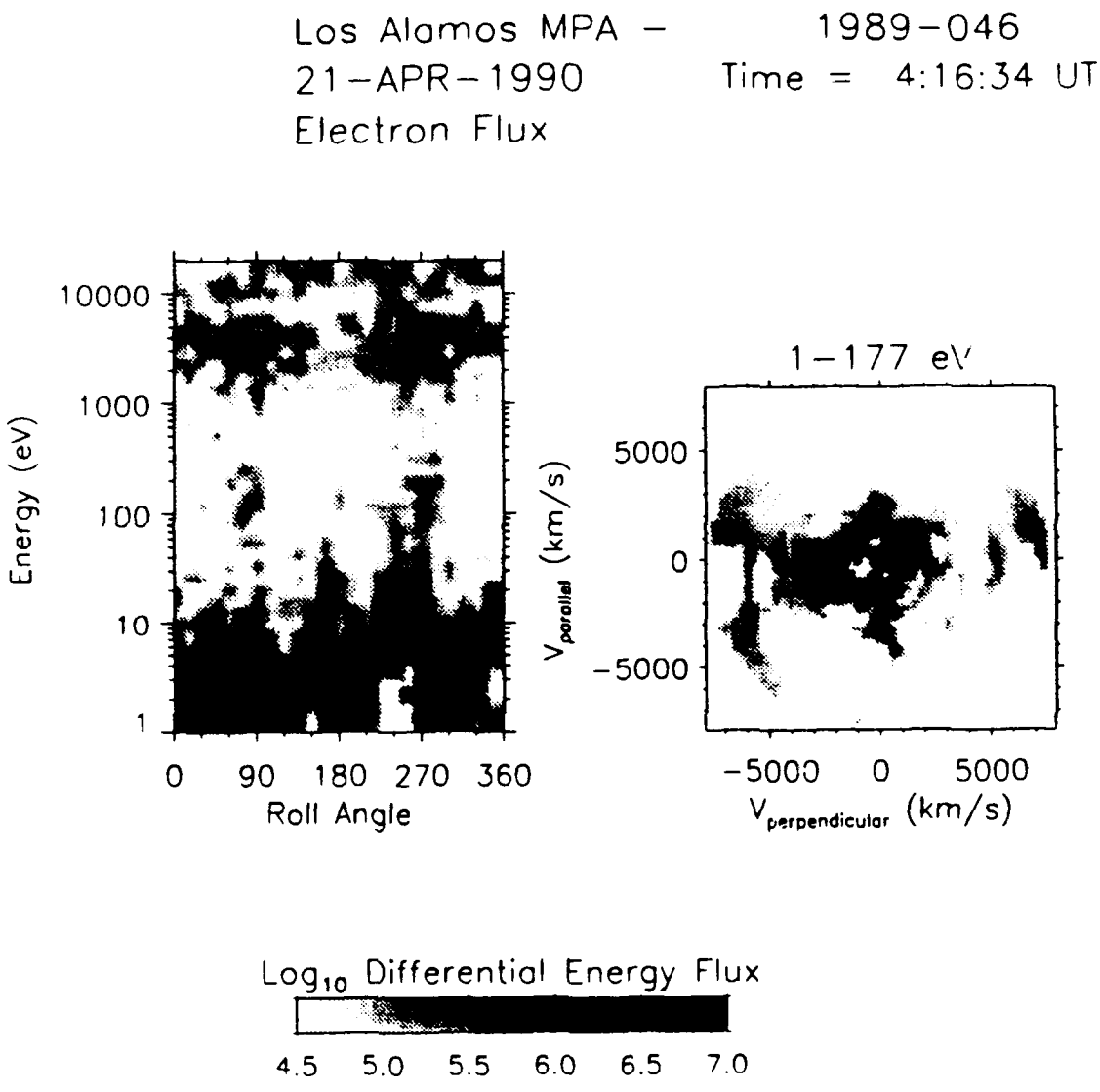

Figure 46 Energy versus Angle Spectrogram for 04:16:34 UT on April 21, 1990 (Spacecraft in Plasmasphere)

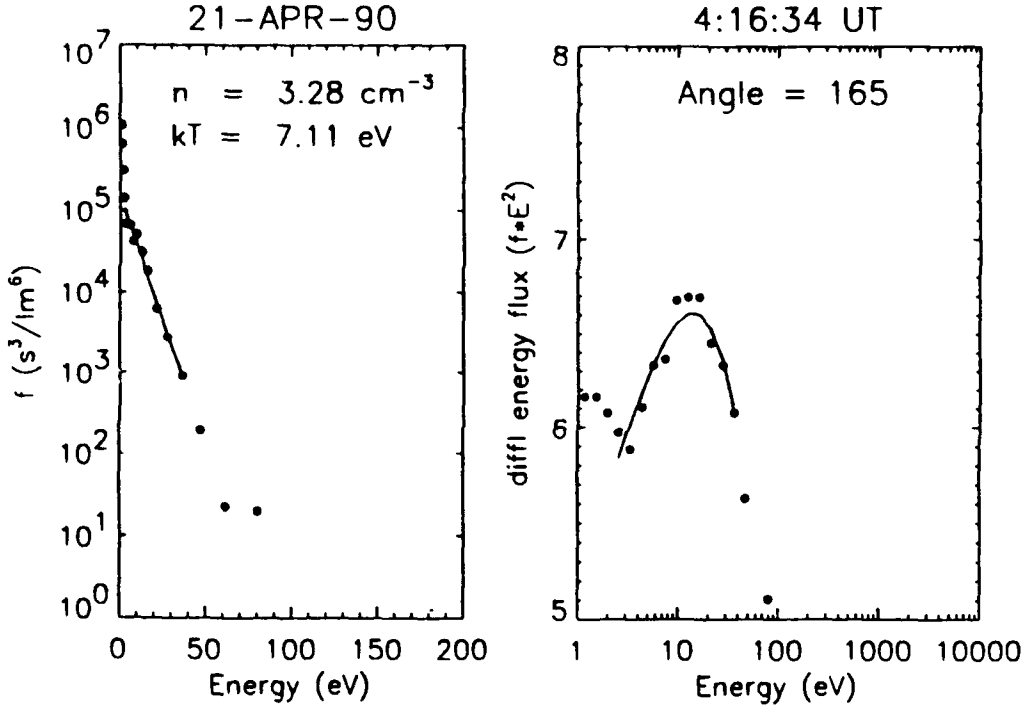

Figure 47 f vs Energy and Differential Energy Flux vs Energy Plots for 04:16:34 UT on April 21, 1990

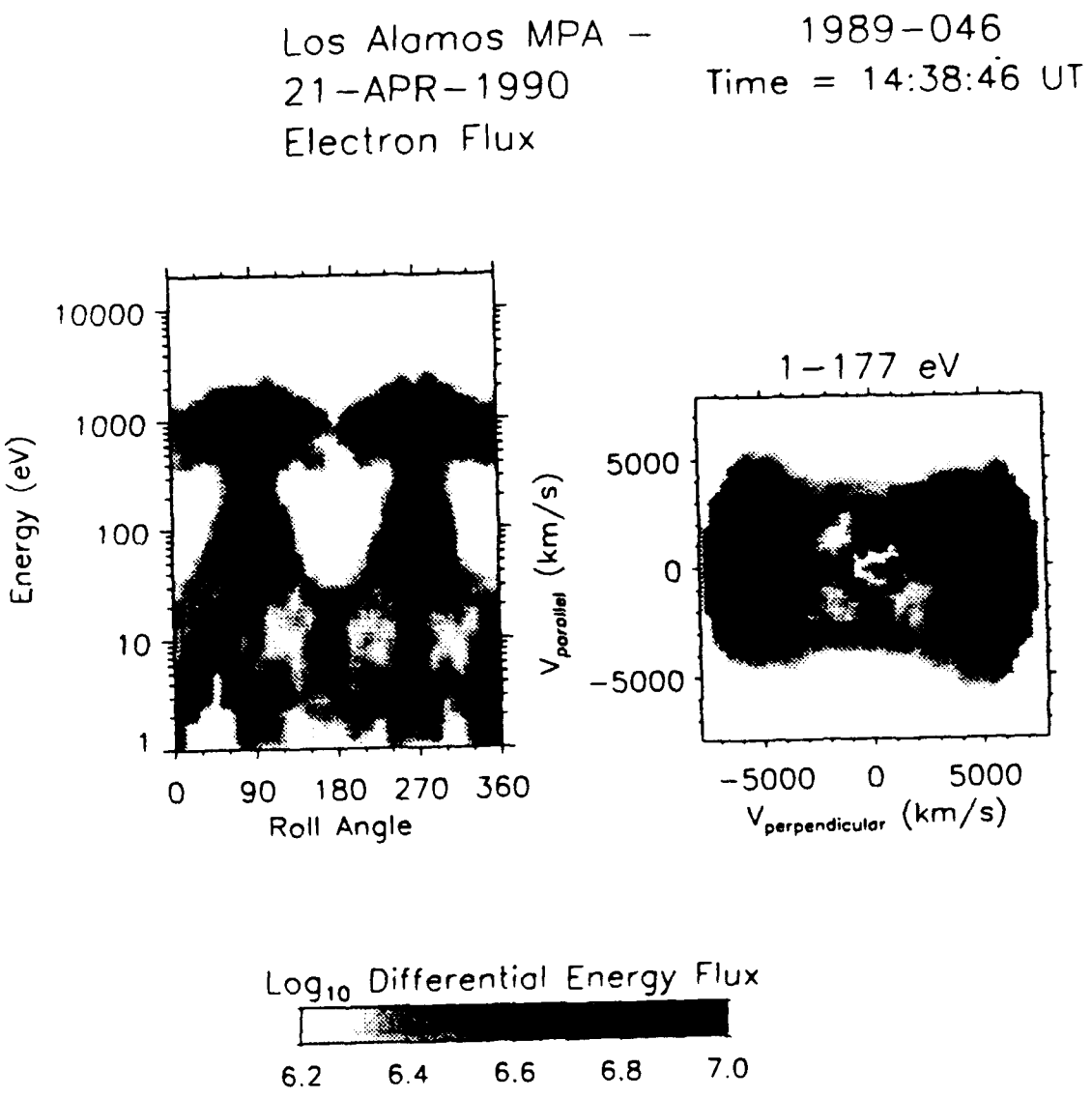

Figure 48 Energy versus Angle Spectrogram
for 14:38:46 UT on April 21, 1990

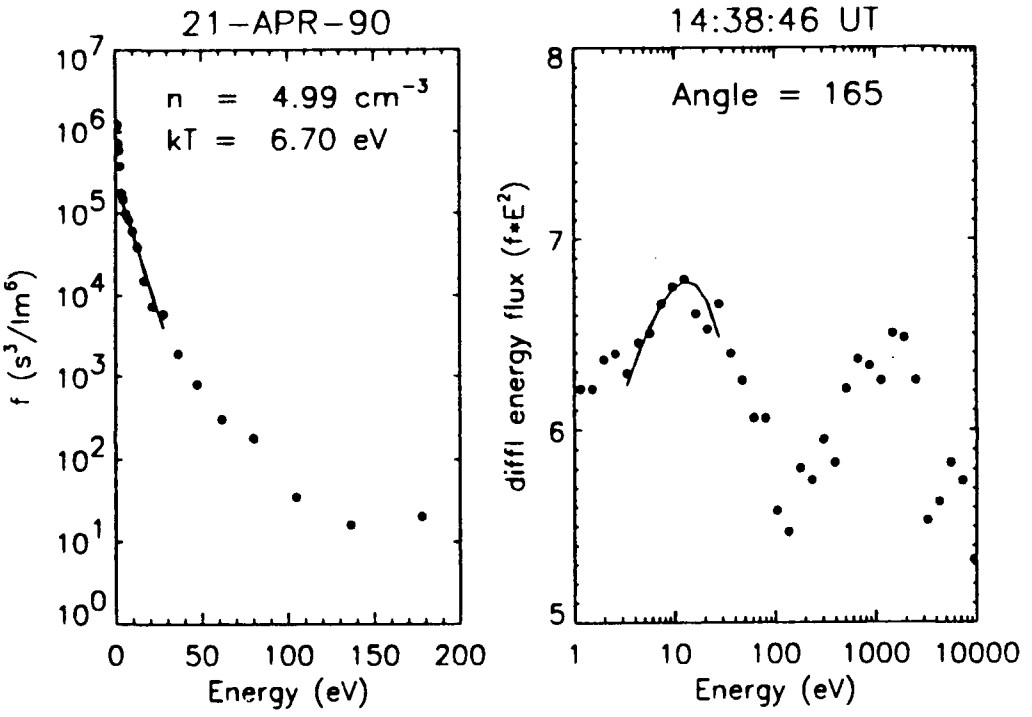

Figure 49 f vs Energy and Differential Energy Flux vs Energy Plots for 14:38:46 UT on April 21, 1990

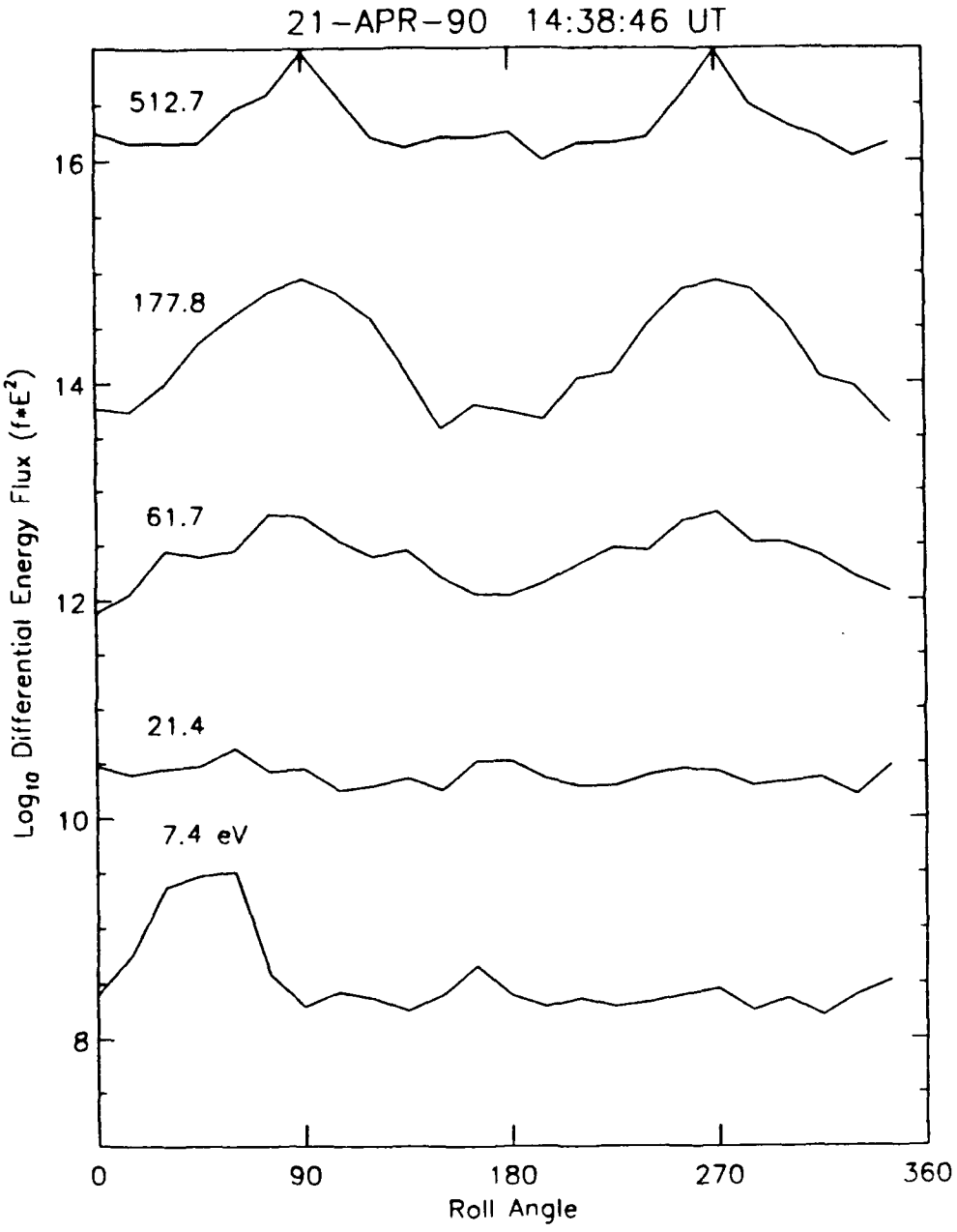

Figure 50 Stacked Line Plots of Diff. Energy Flux vs Roll Angle for 14:38:46 UT on April 21, 1990

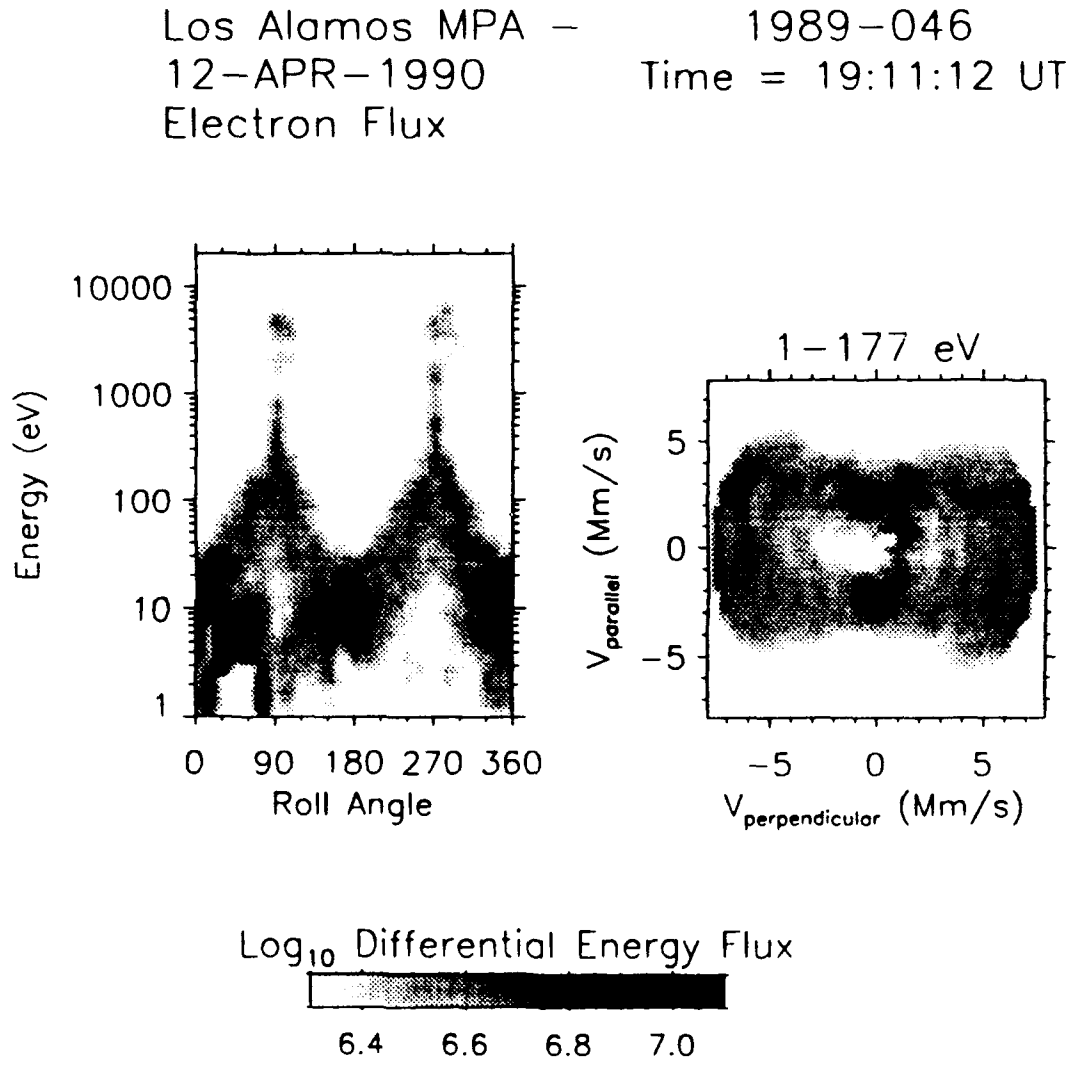

Figure 51 Energy versus Angle Spectrogram
for 19:11:12 UT on April 12, 1990

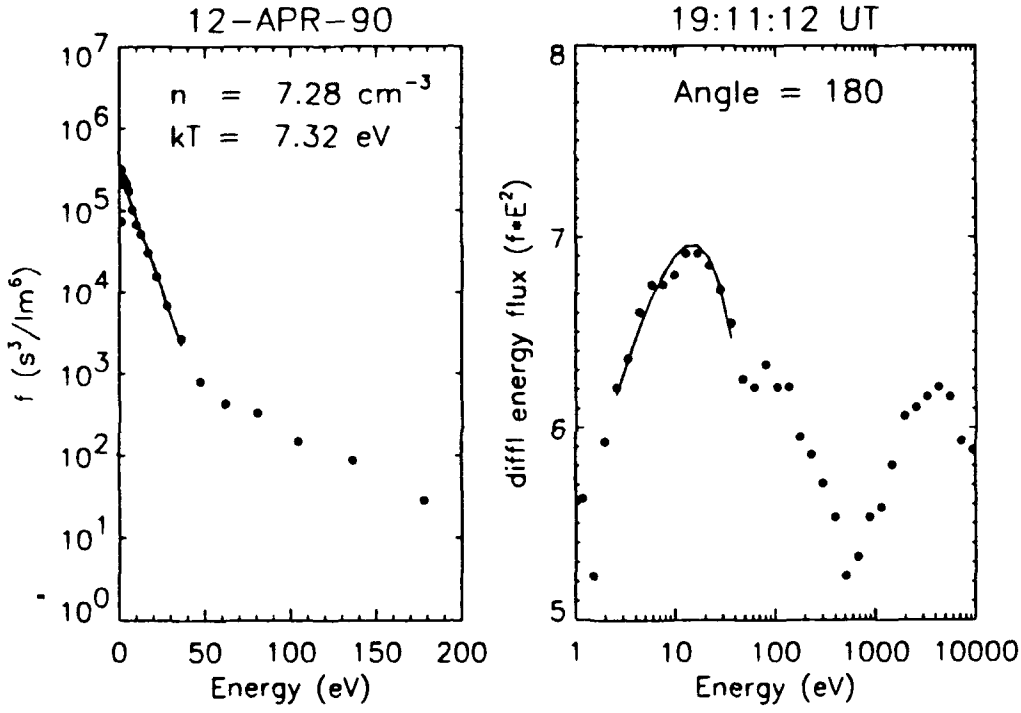

Figure 52 f vs Energy and Differential Energy Flux vs Energy Plots for 19:11:12 UT on April 12, 1990

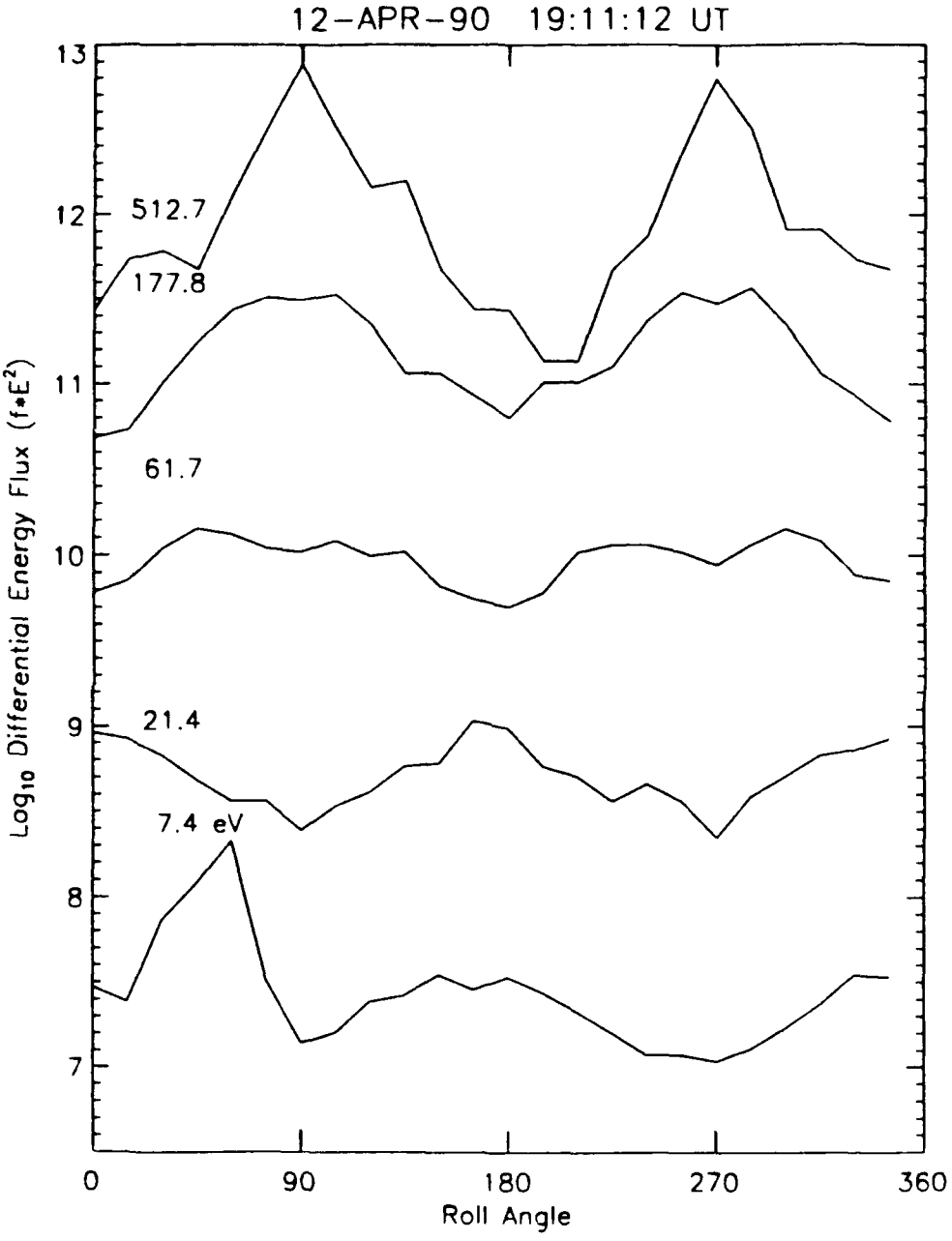

Figure 53 Stacked Line Plots of Diff. Energy Flux vs Roll Angle for 19:11:12 UT on April 12, 1990

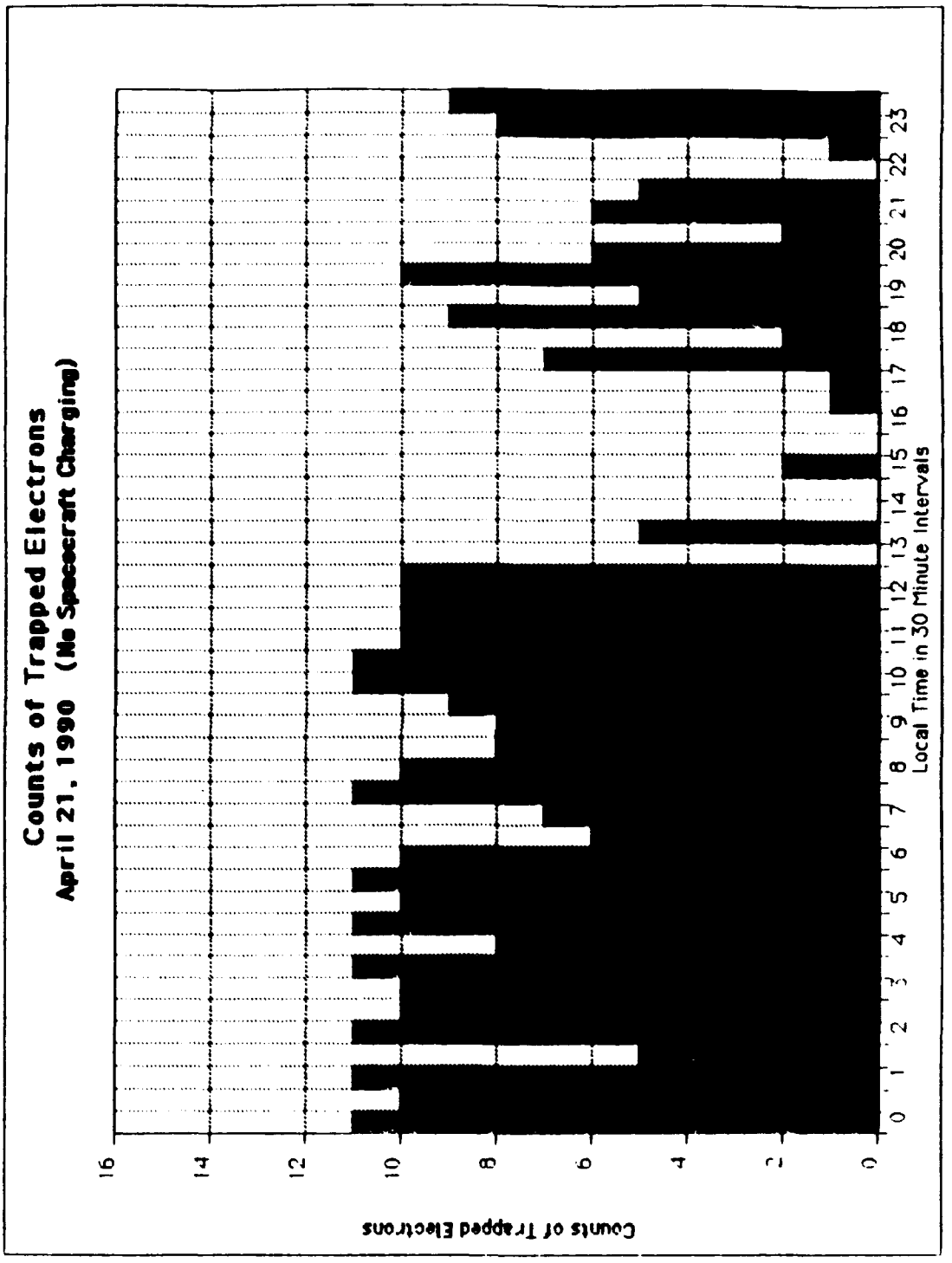

Figure 54 Counts of Trapped Electrons for April 21, 1990

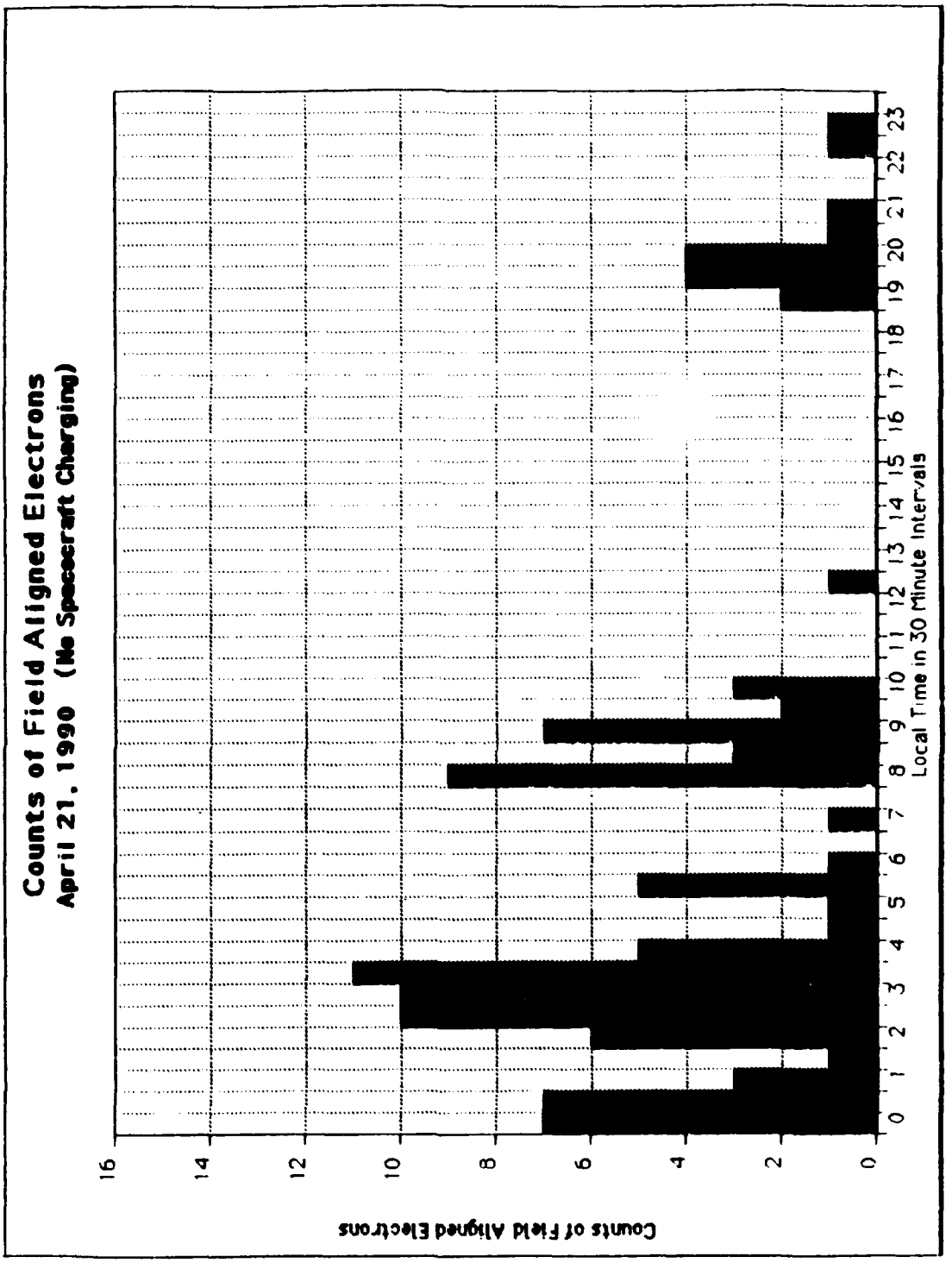

Figure 55 Counts of Field Aligned Electrons for April 21, 1990

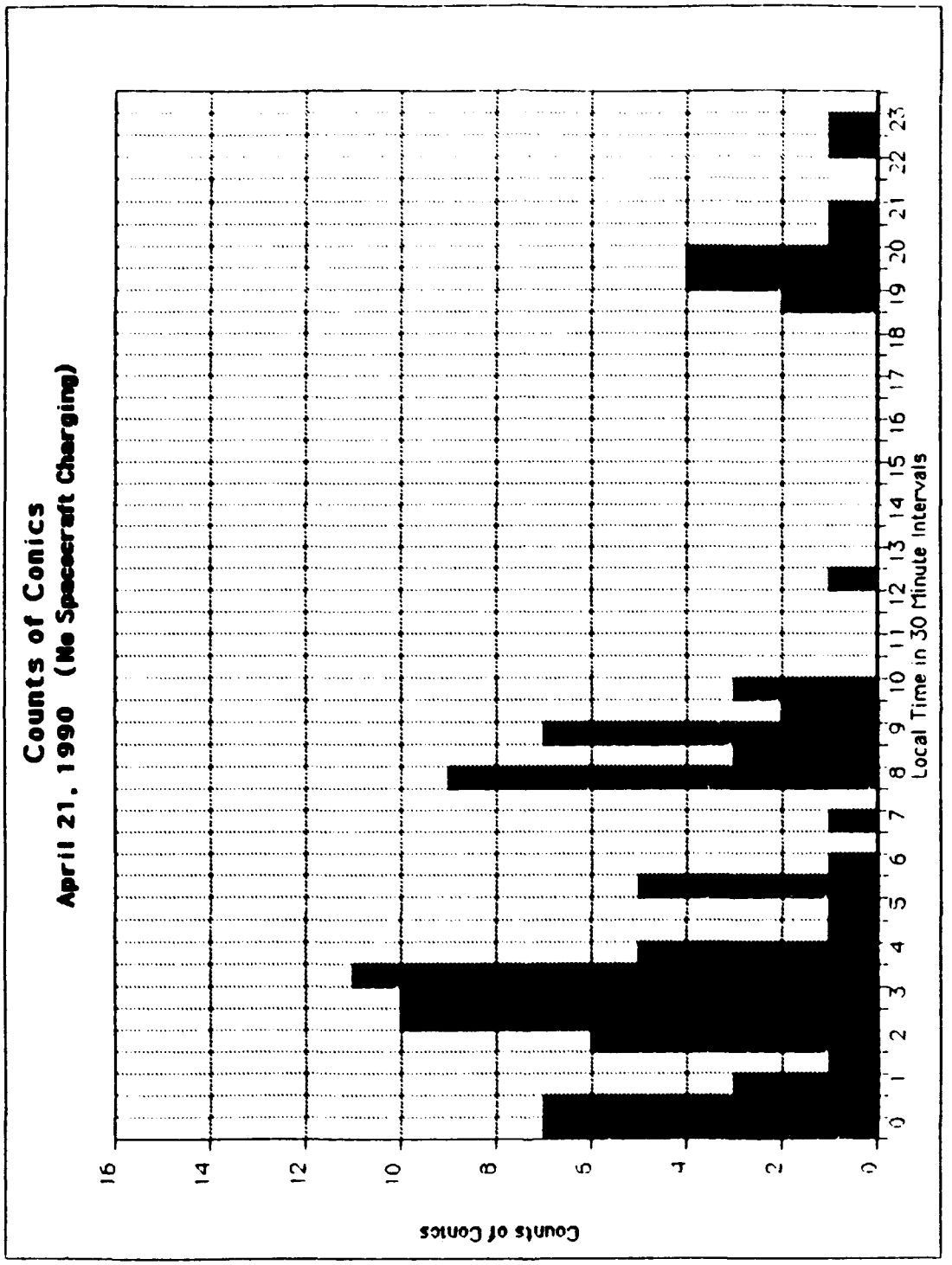

Figure 56 Counts of Conics for April 21, 1990

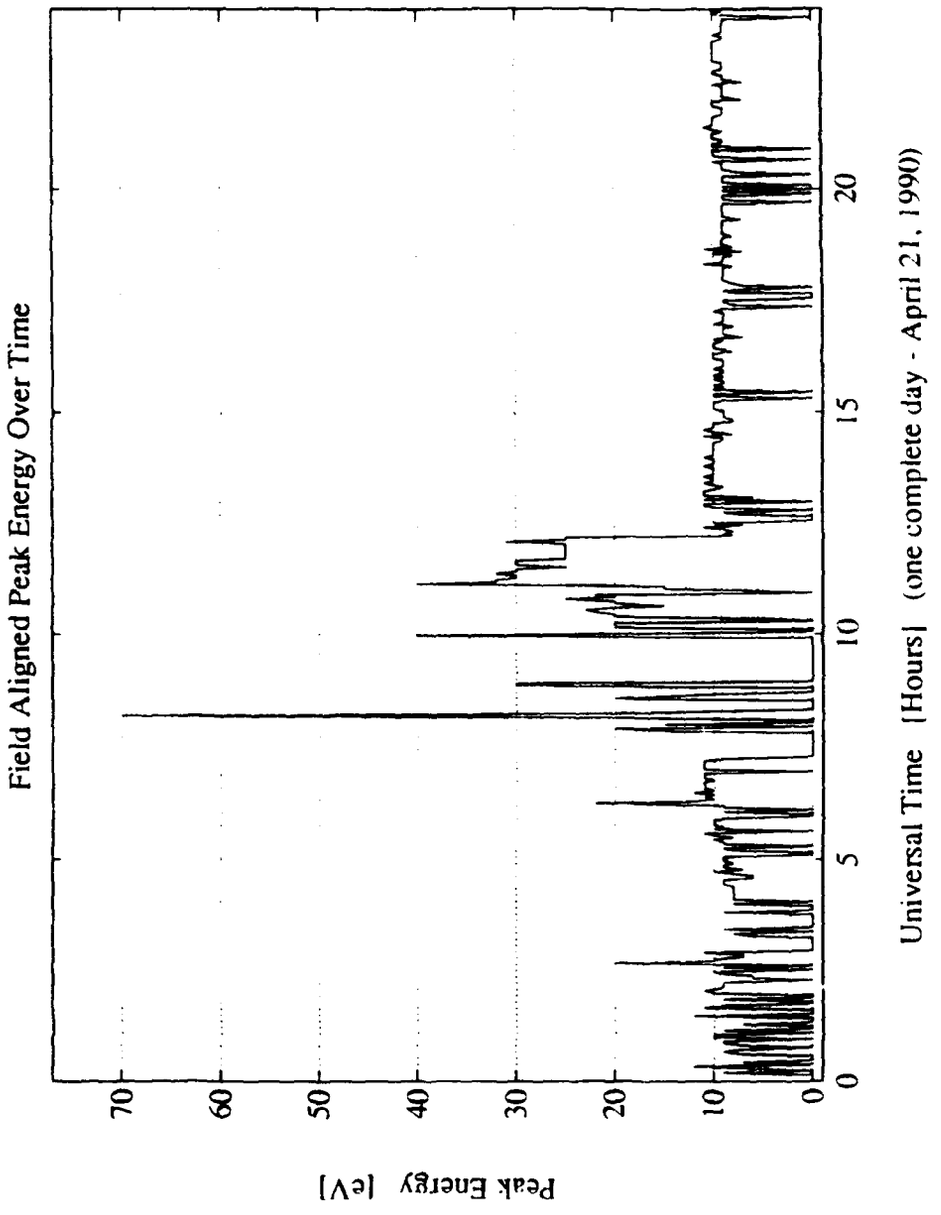

Figure 57 Peak Energy vs Time for Field Aligned Electron Distributions on April 21, 1990

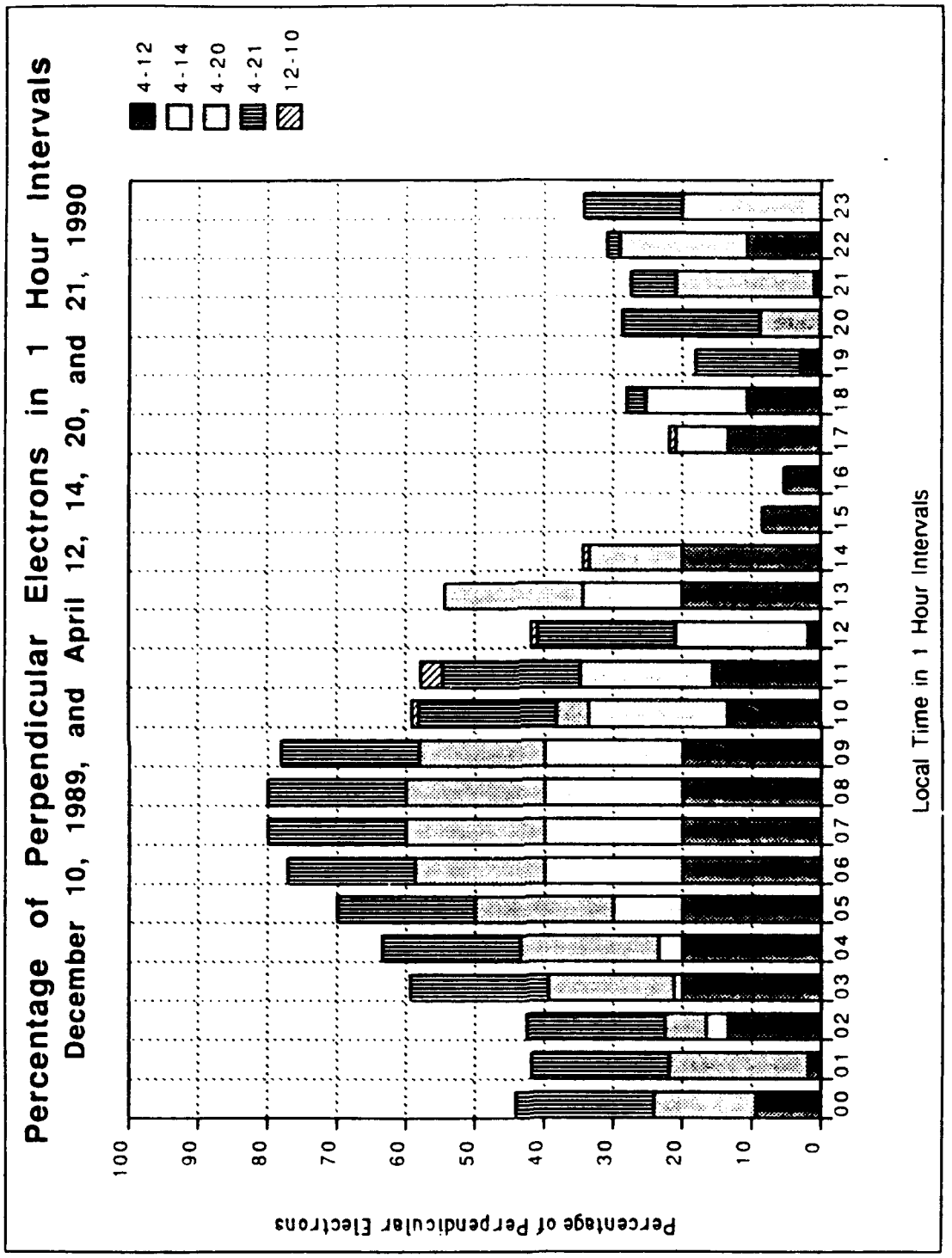

Figure 58 Percentage of Trapped Electrons for Five Days

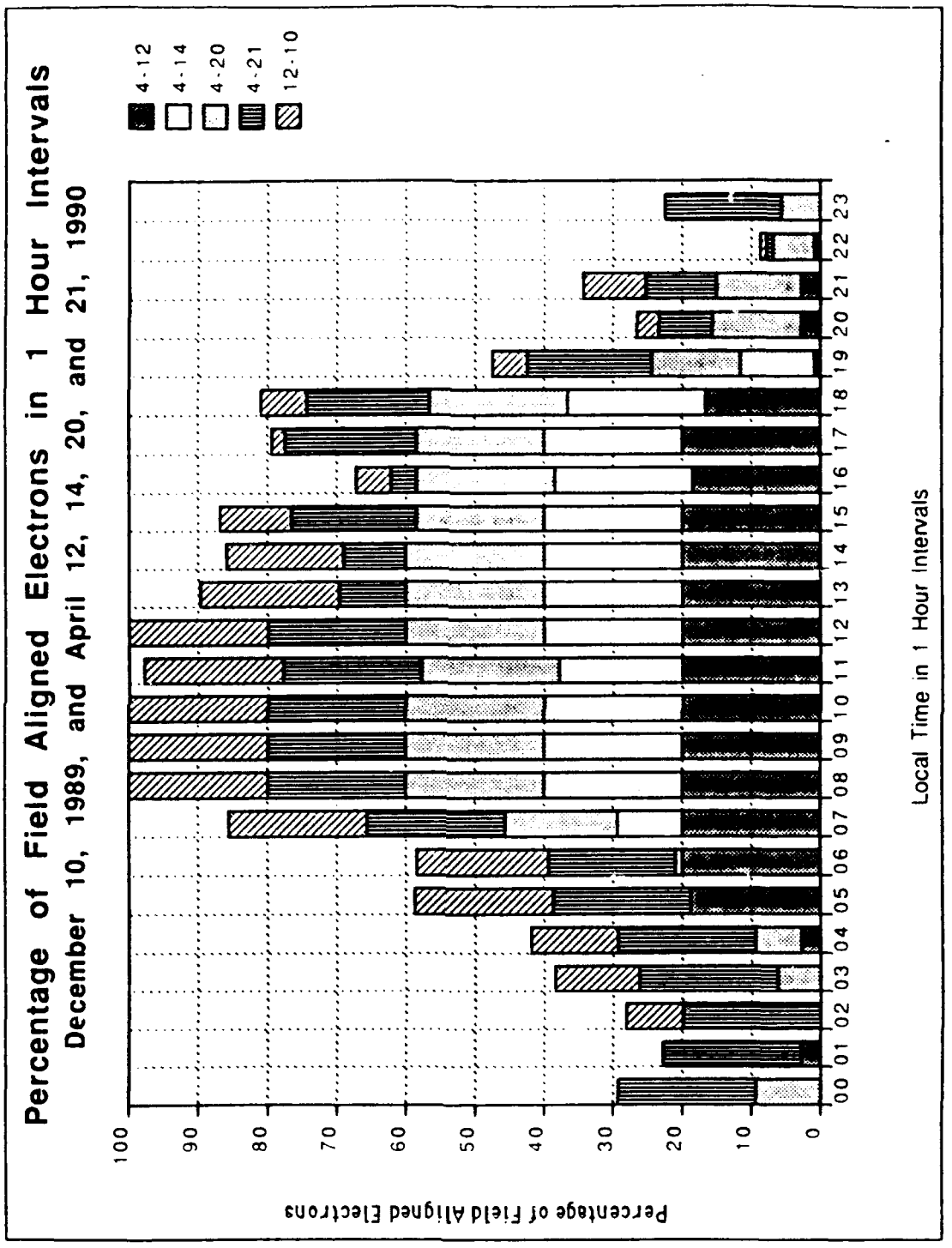

Figure 59 Percentage of Field Aligned Electrons for Five Days

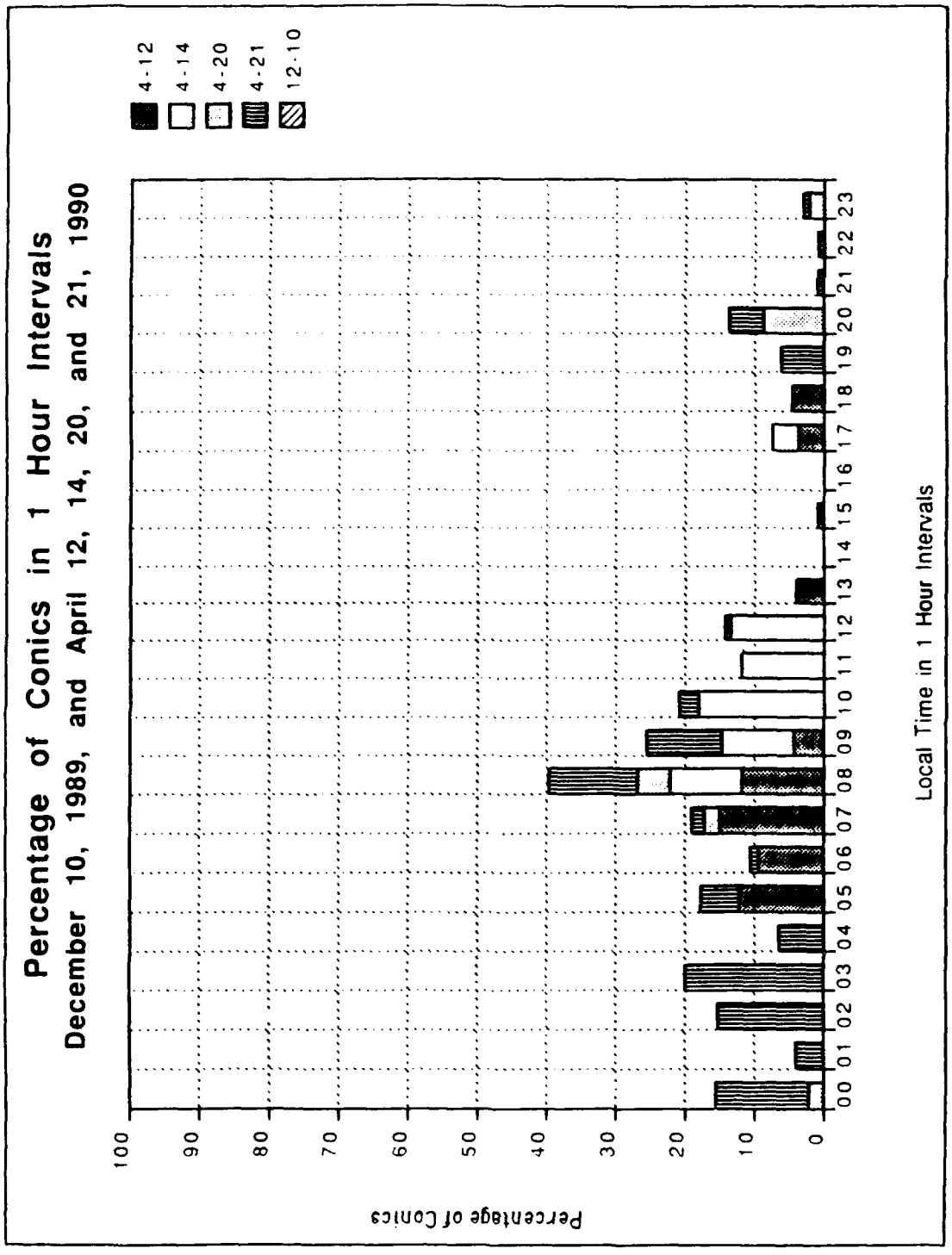

Figure 60 Percentage of Conics for Five Days

APPENDIX C OTHER STATISTICAL PLOTS

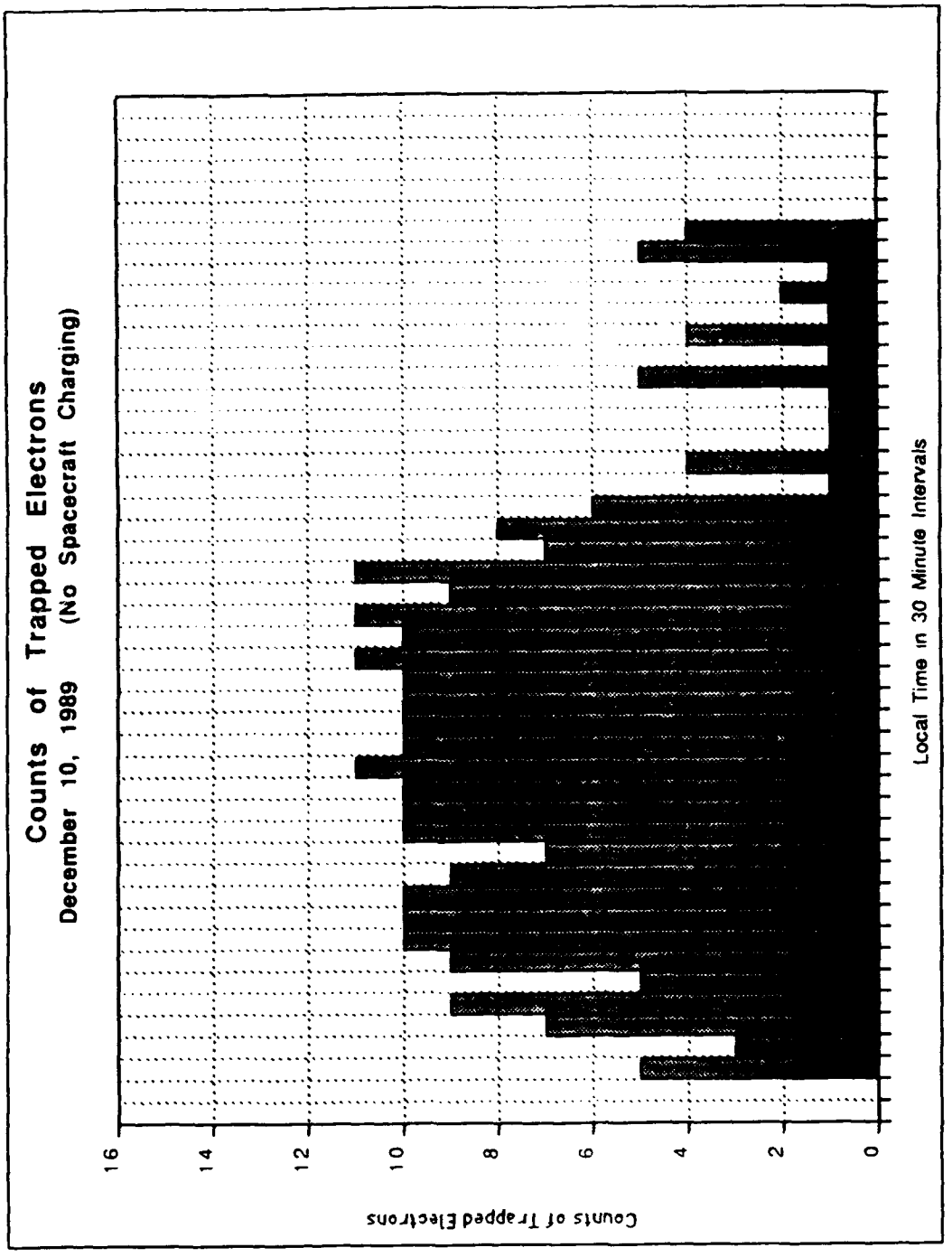

Counts of Trapped Electrons for December 10, 1989

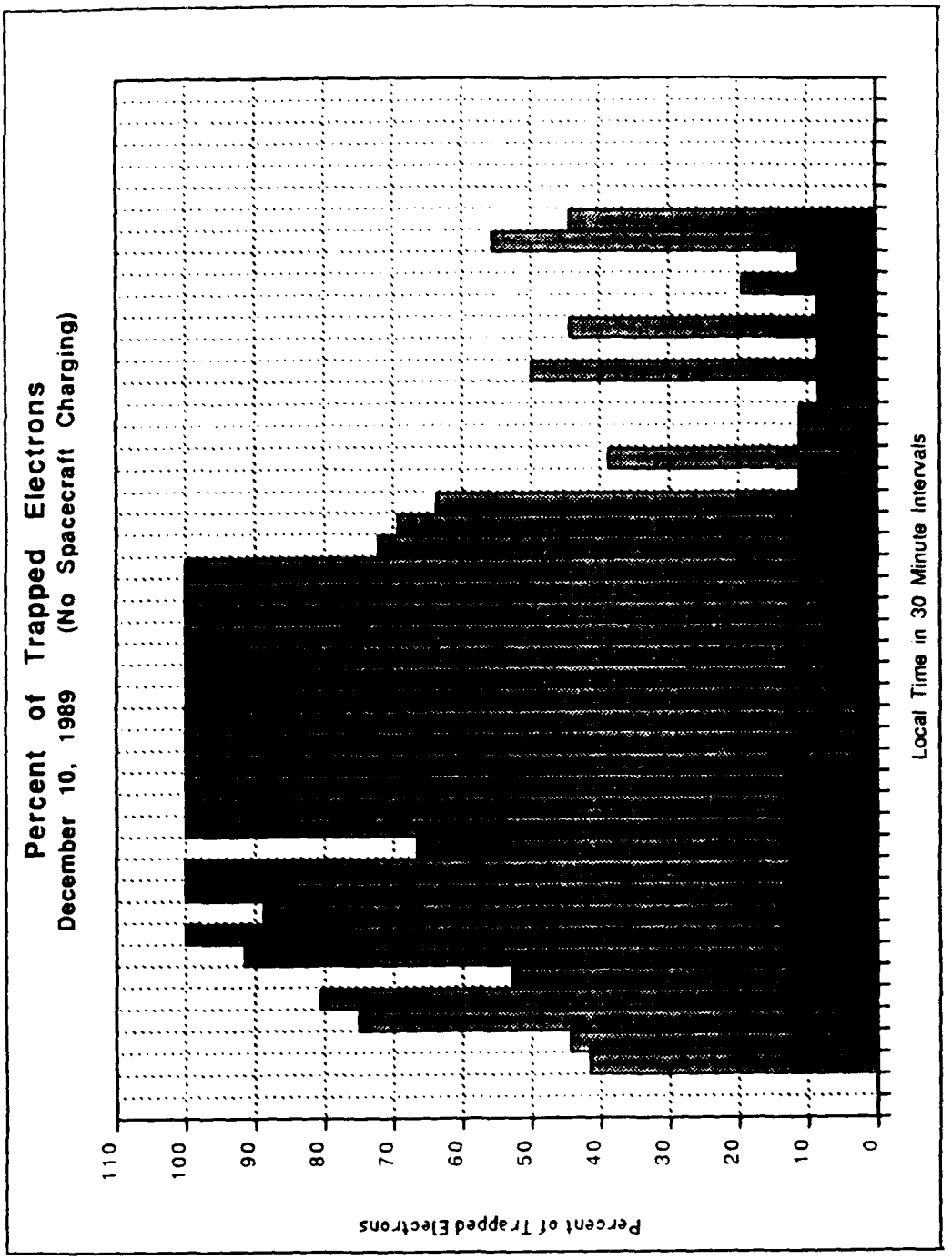

Percent of Trapped Electrons for December 10, 1989

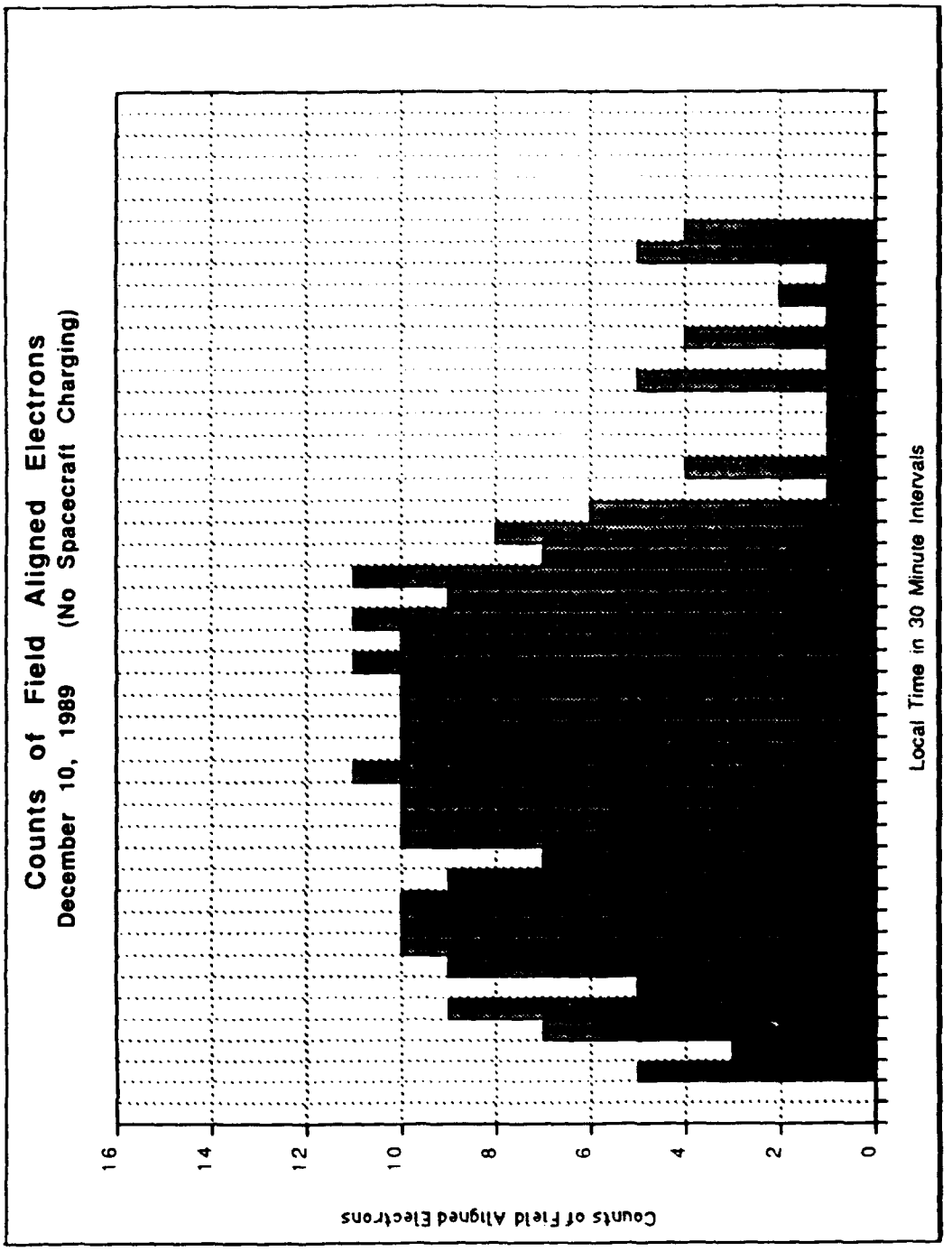

Counts of Field Aligned Electrons for December 10, 1989

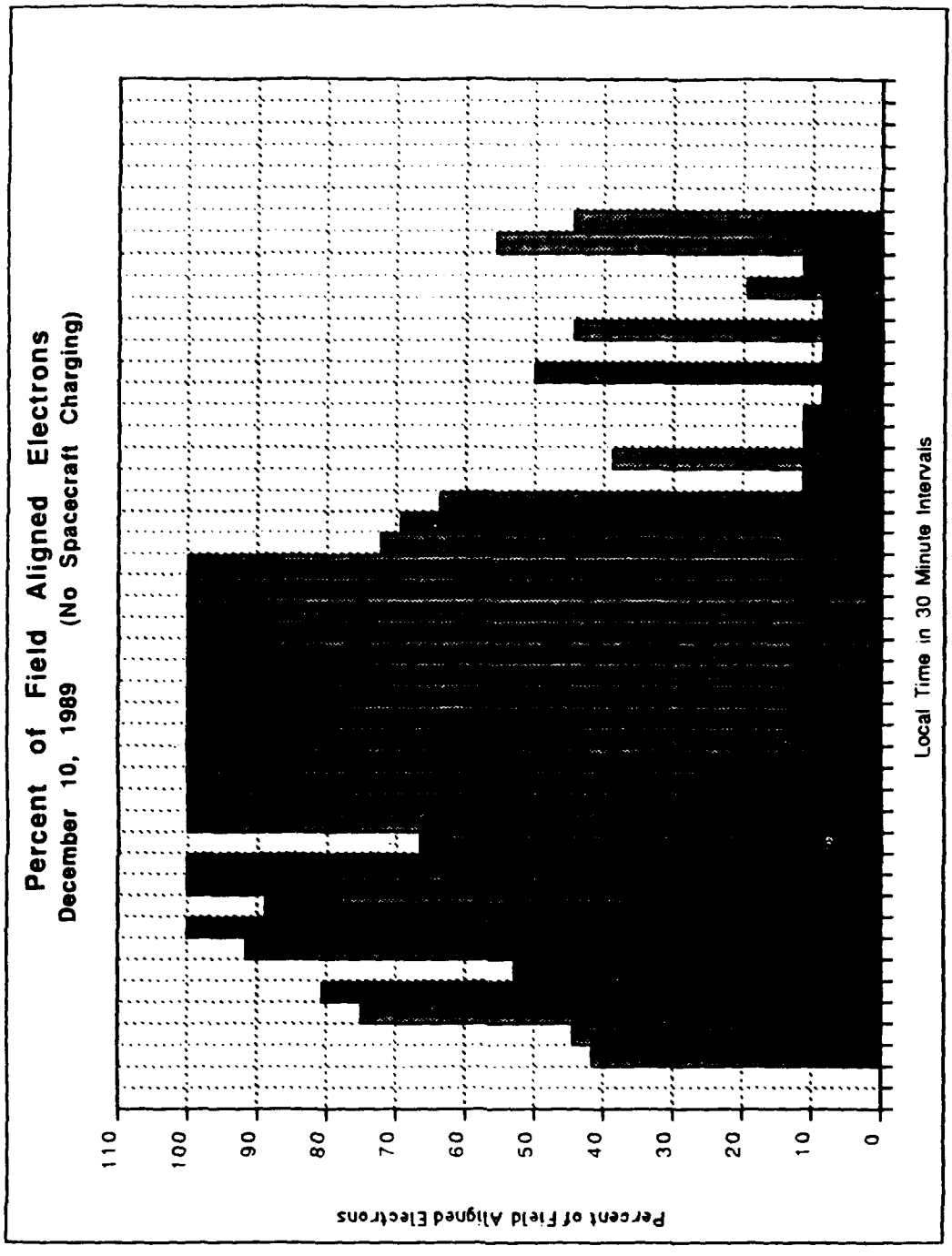

Percent of Field Aligned Electrons for December 10, 1989

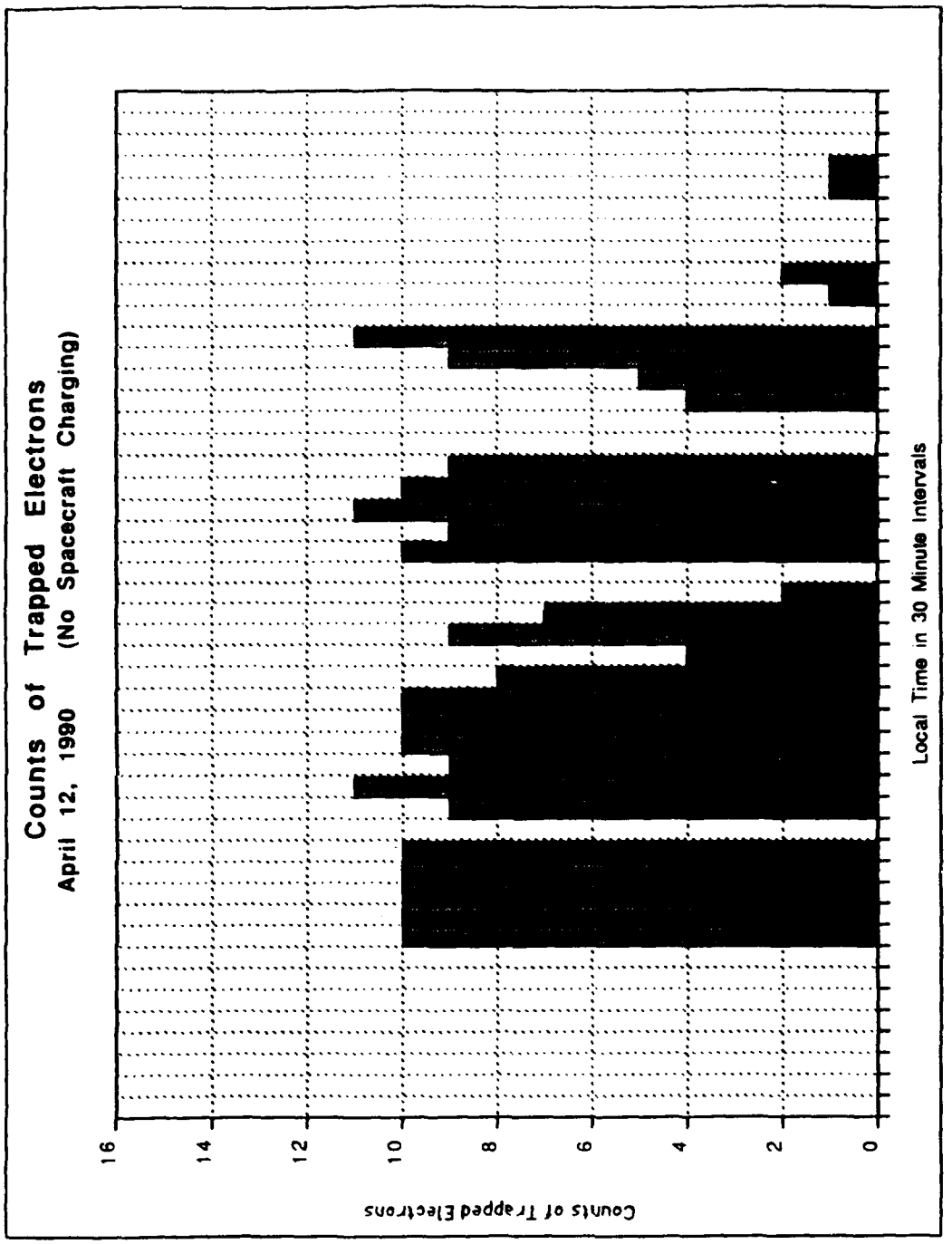

Counts of Trapped Electrons for April 12, 1990

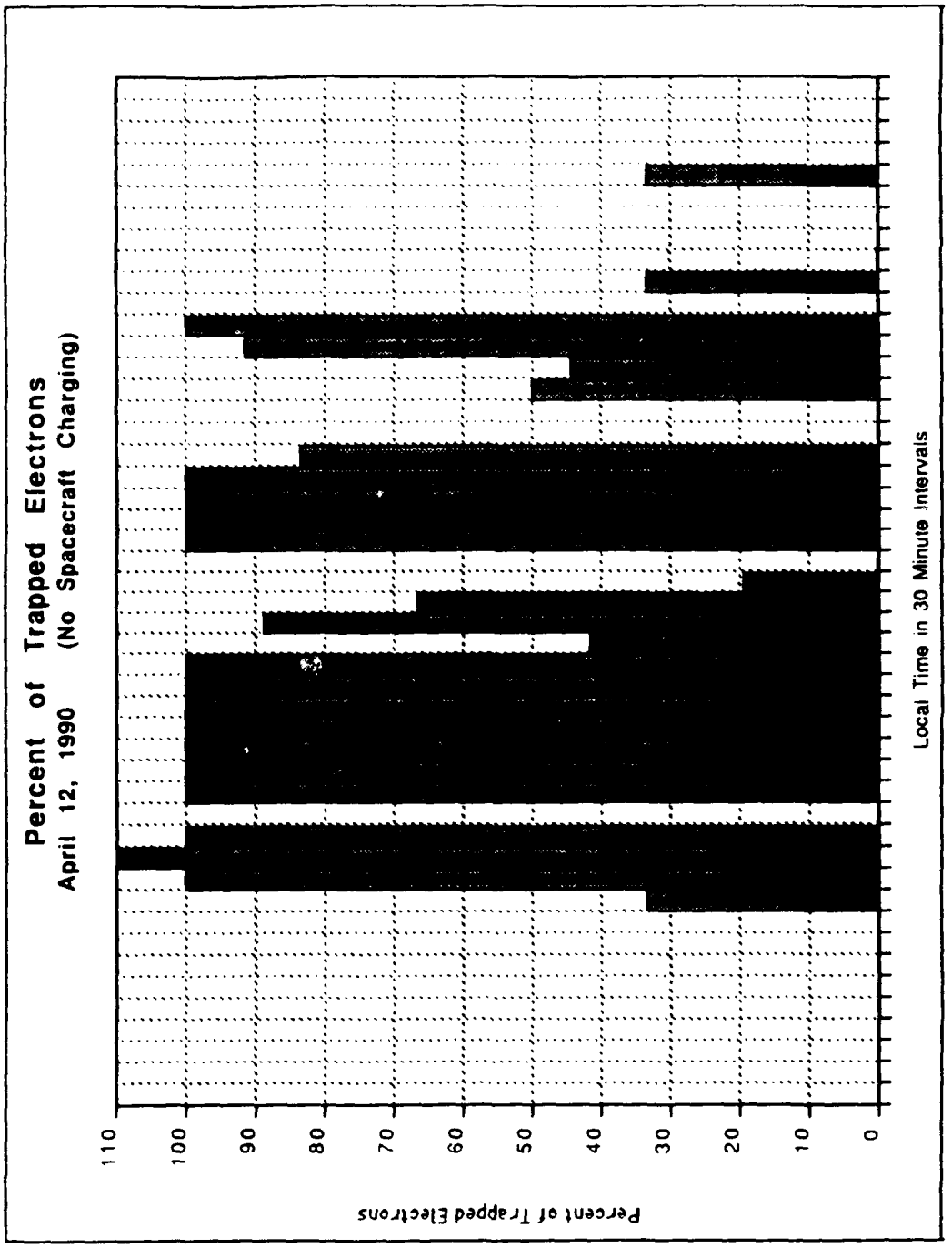

Percent of Trapped Electrons for April 12, 1990

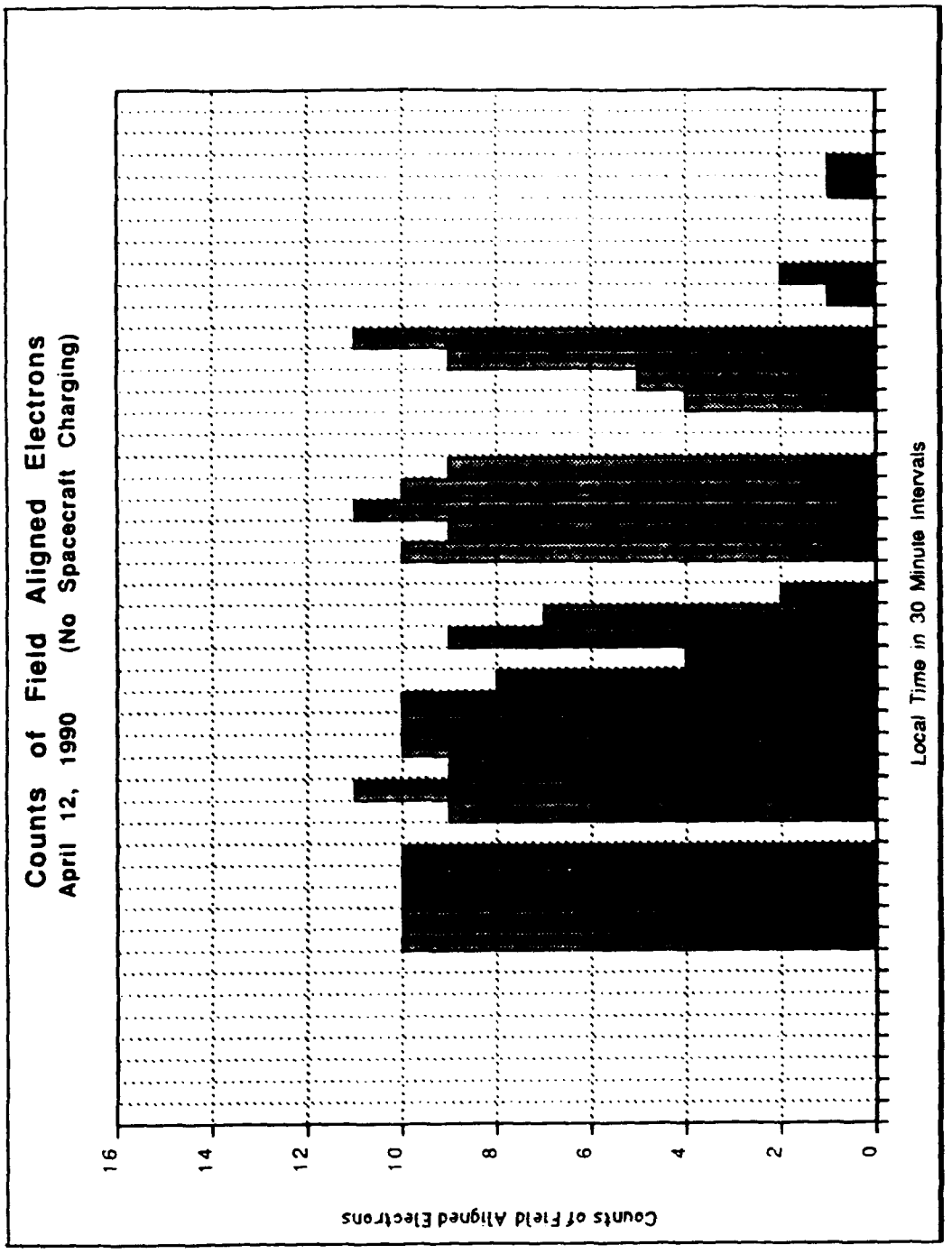

Counts of Field Aligned Electrons for April 12, 1990

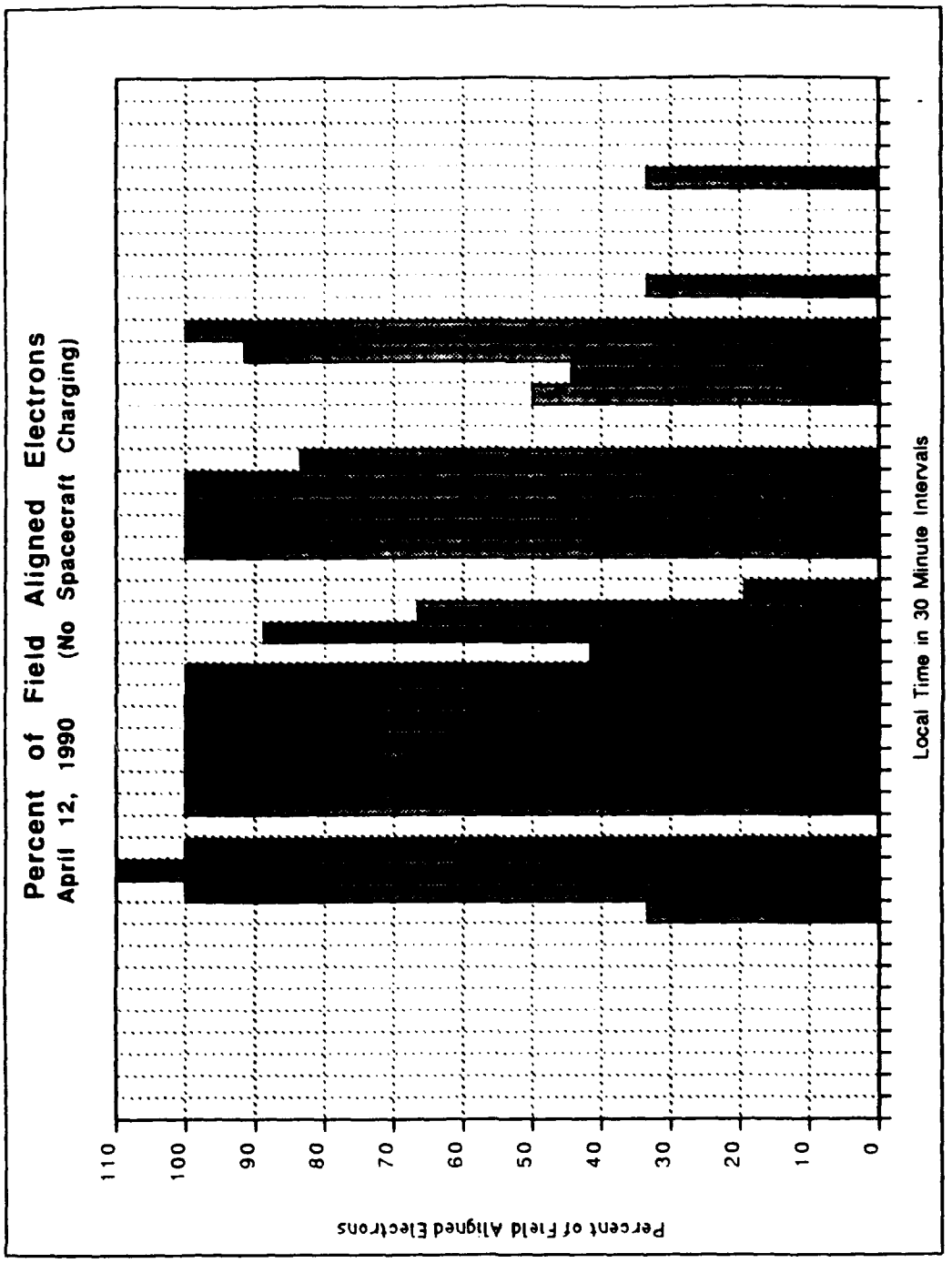

Percent of Field Aligned Electrons for April 12, 1990

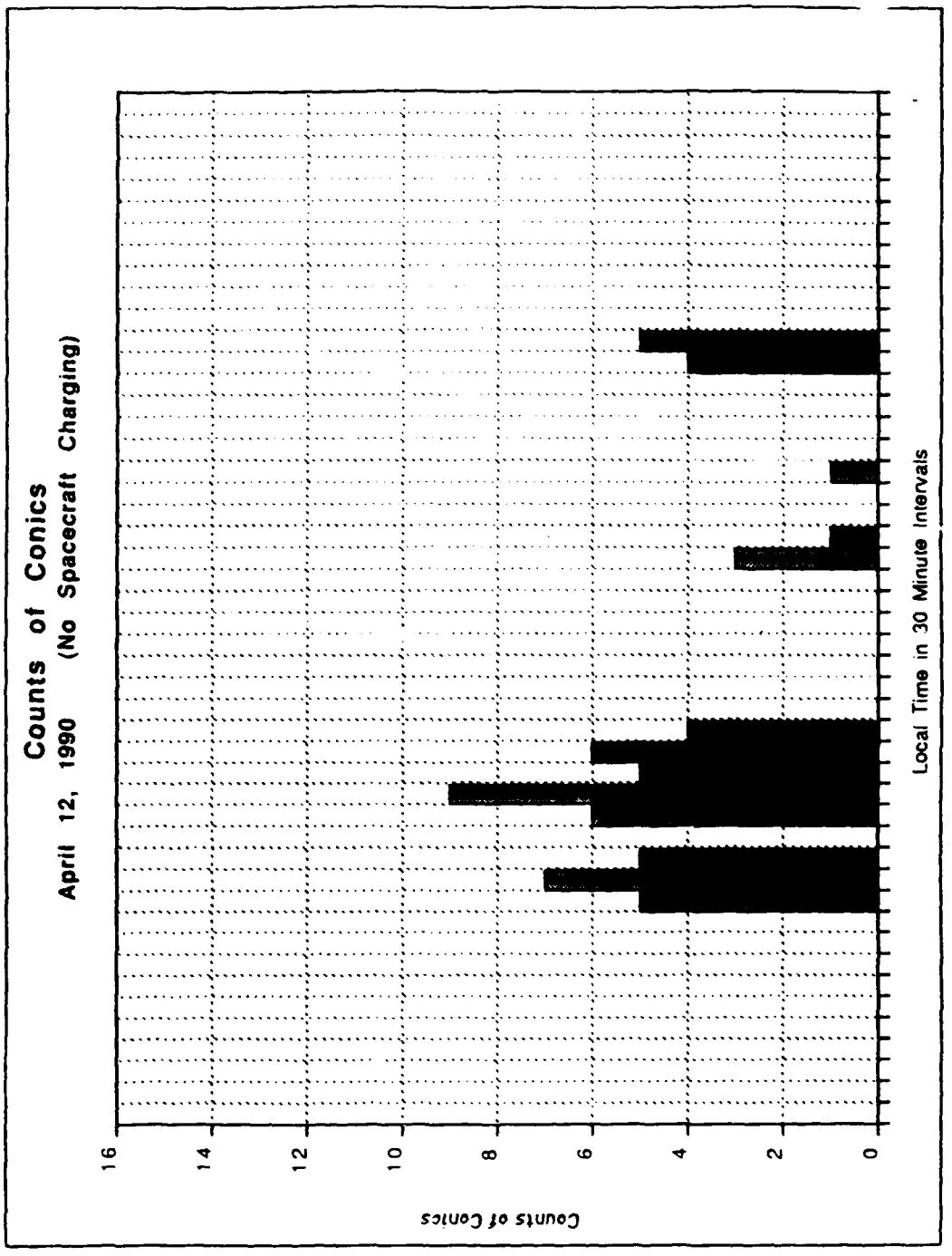

Counts of Conics for April 12, 1990

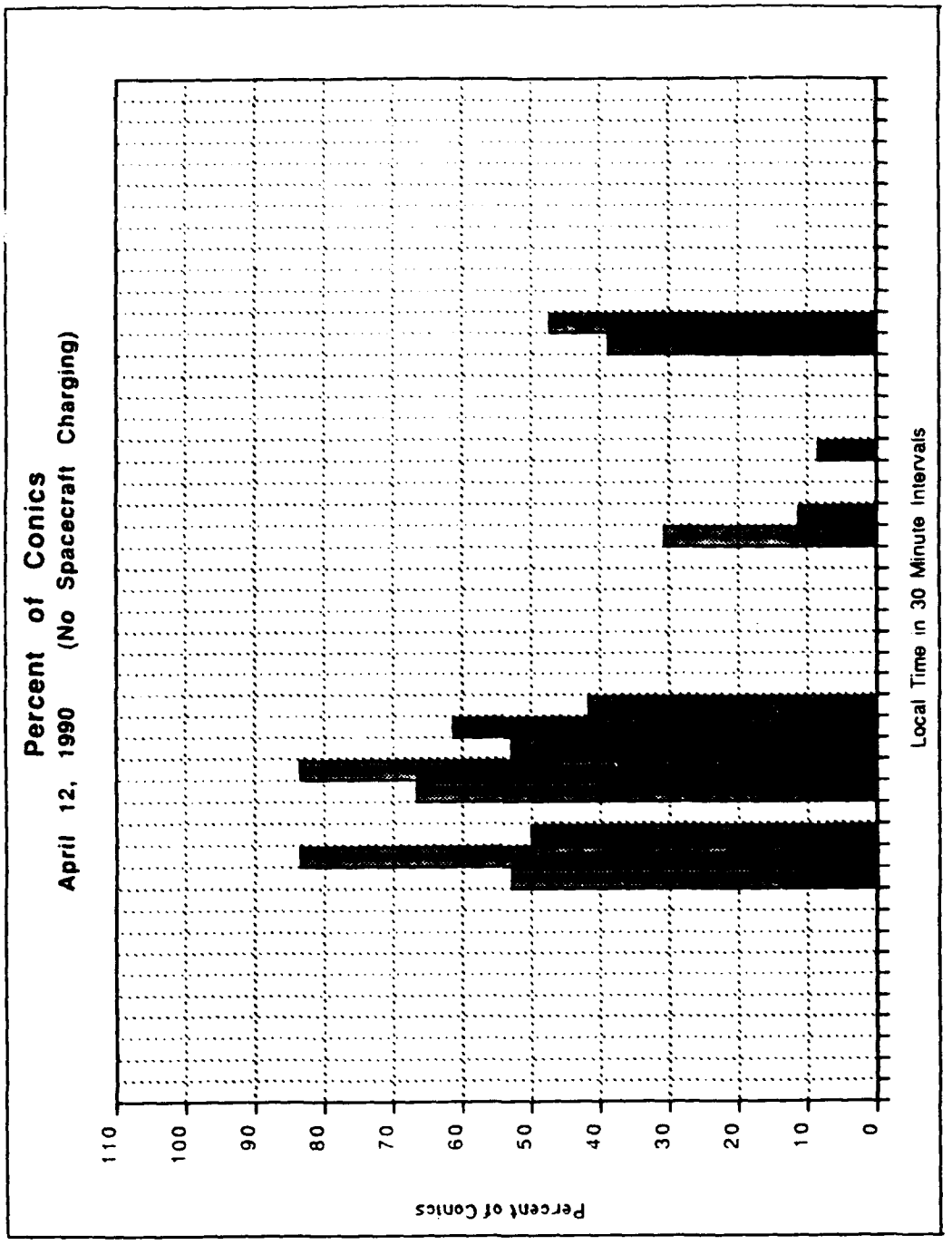

Percent of Conics for April 12, 1990

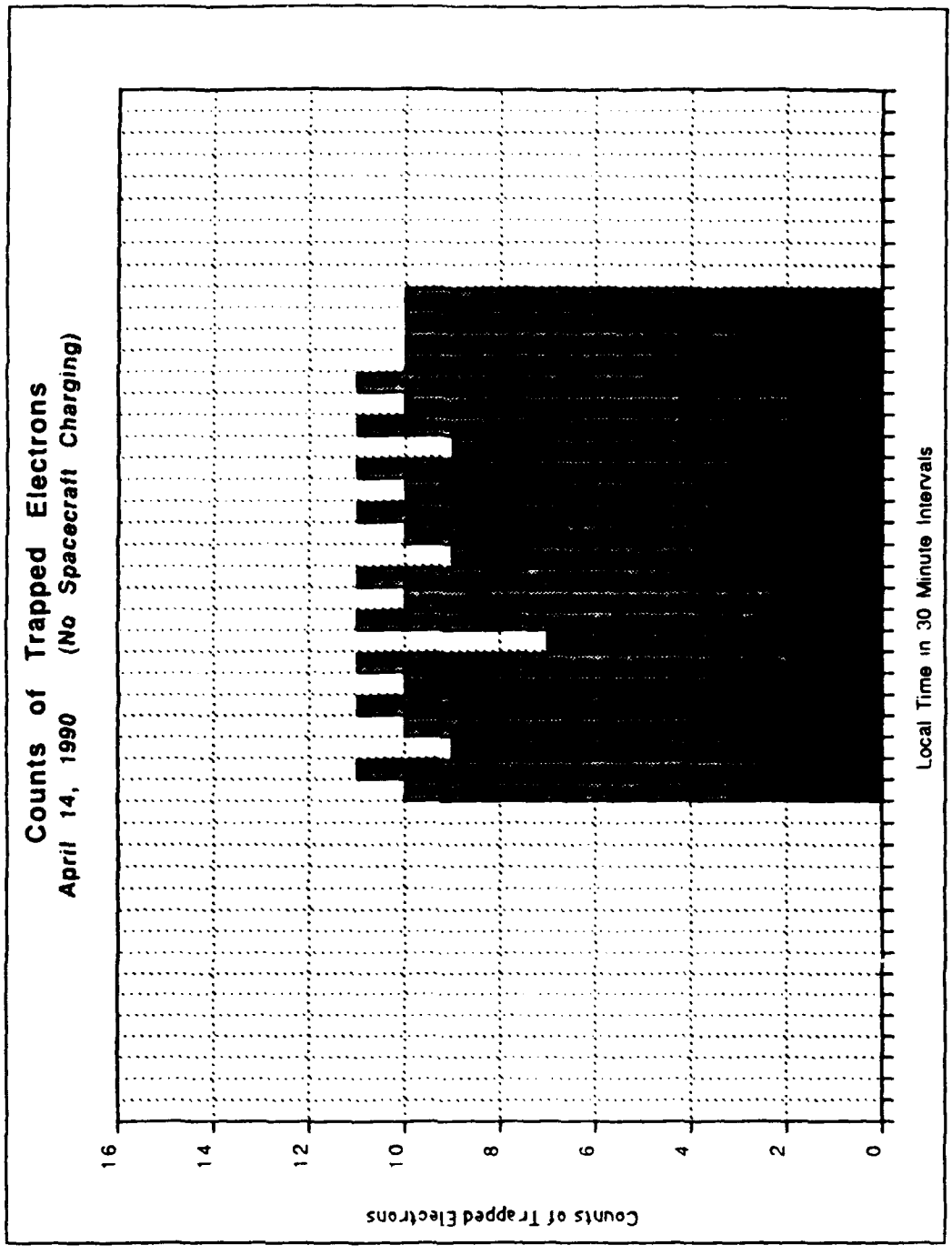

Counts of Trapped Electrons for April 14, 1990

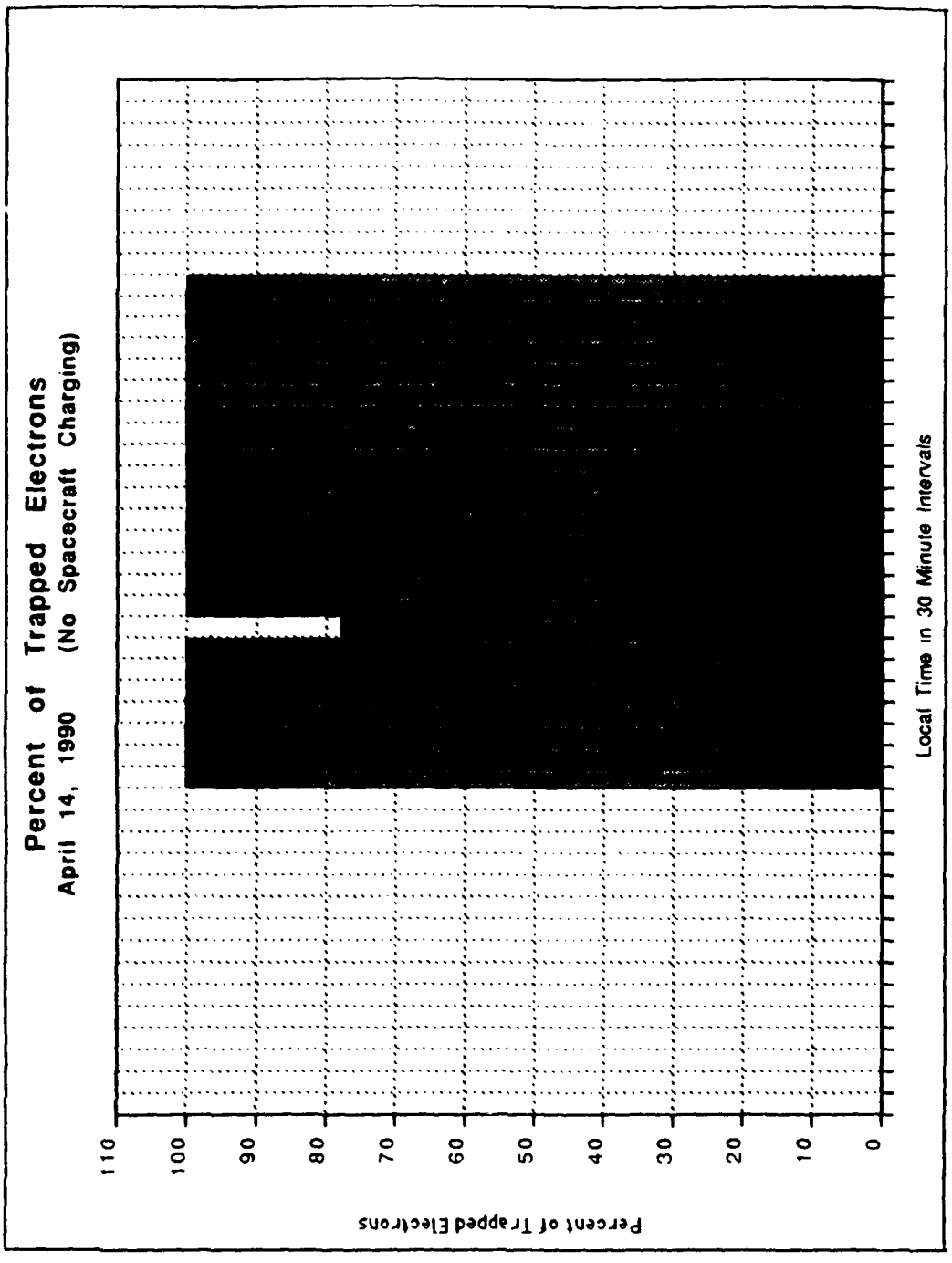

Percent of Trapped Electrons for April 14, 1990

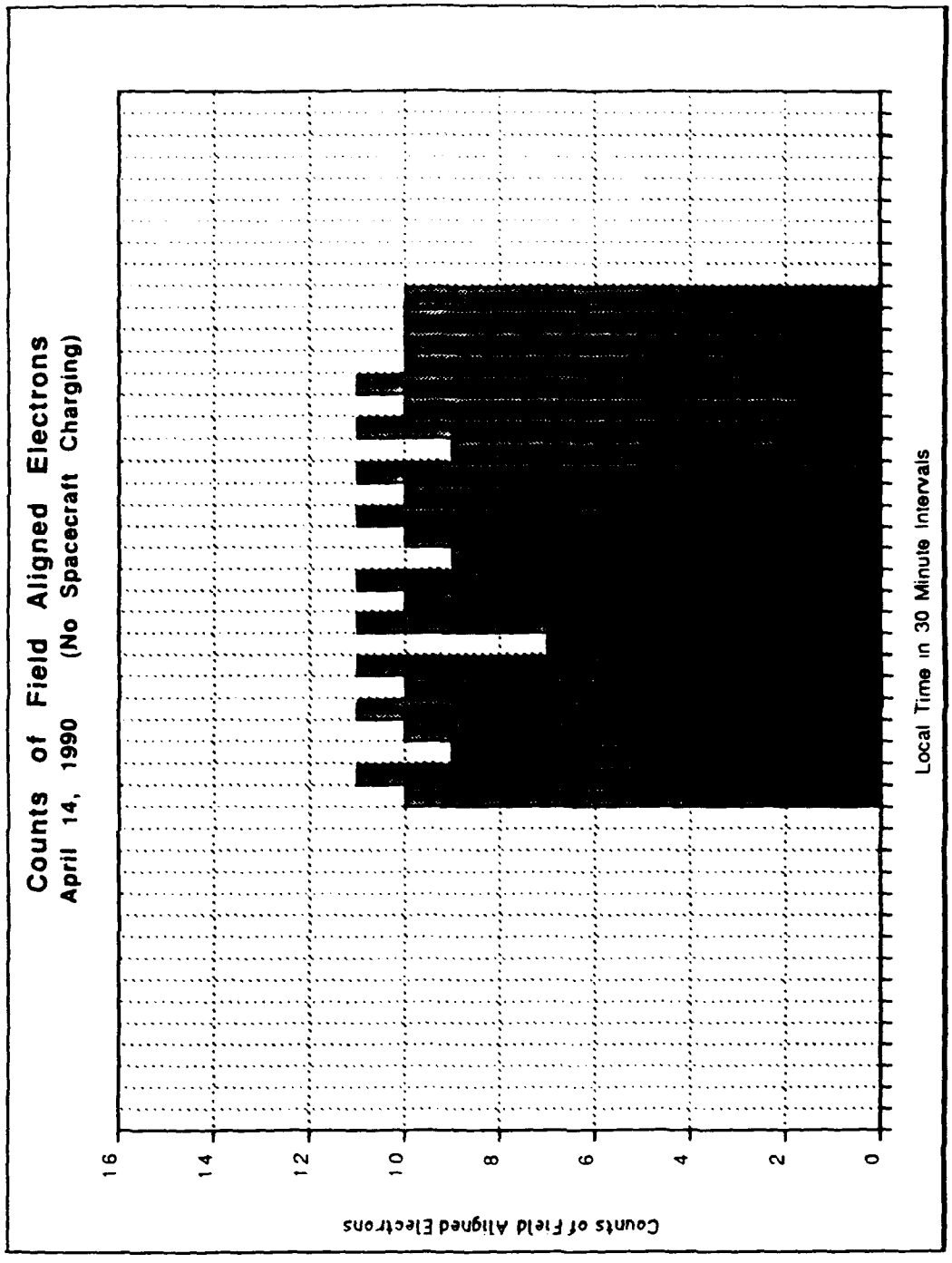

Counts of Field Aligned Electrons for April 14, 1990

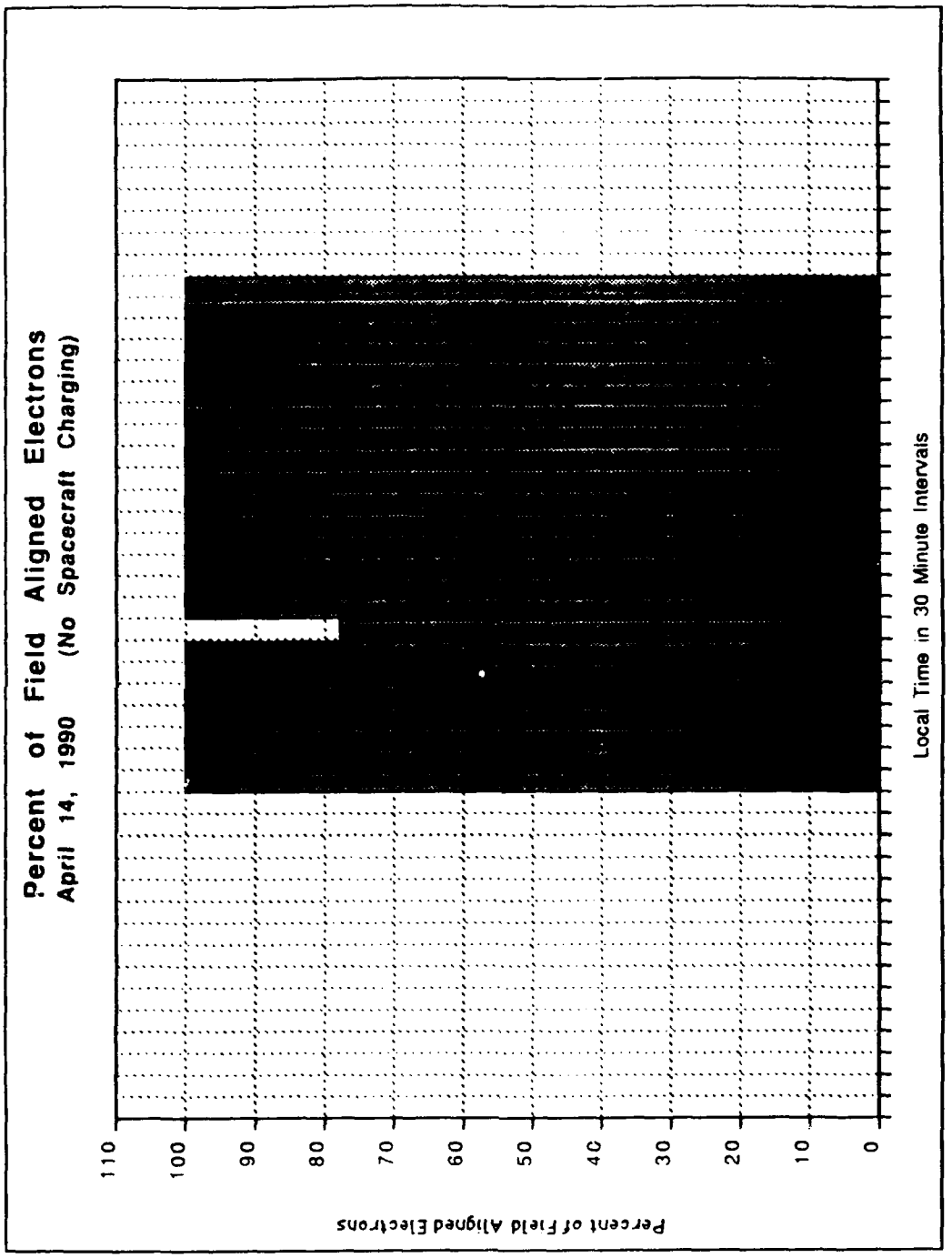

Percent of Field Aligned Electrons for April 14, 1990

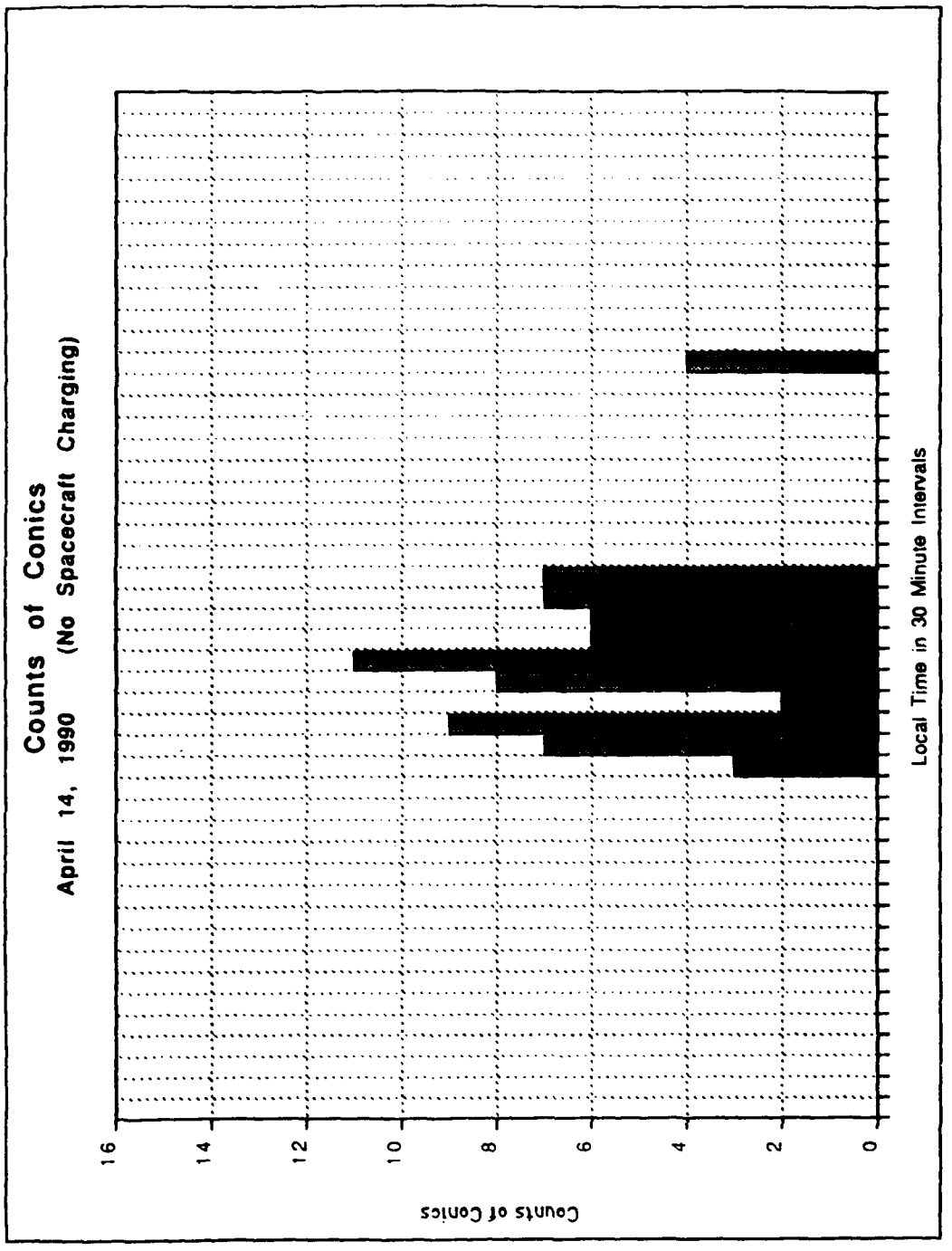

Counts of Conics for April 14, 1990

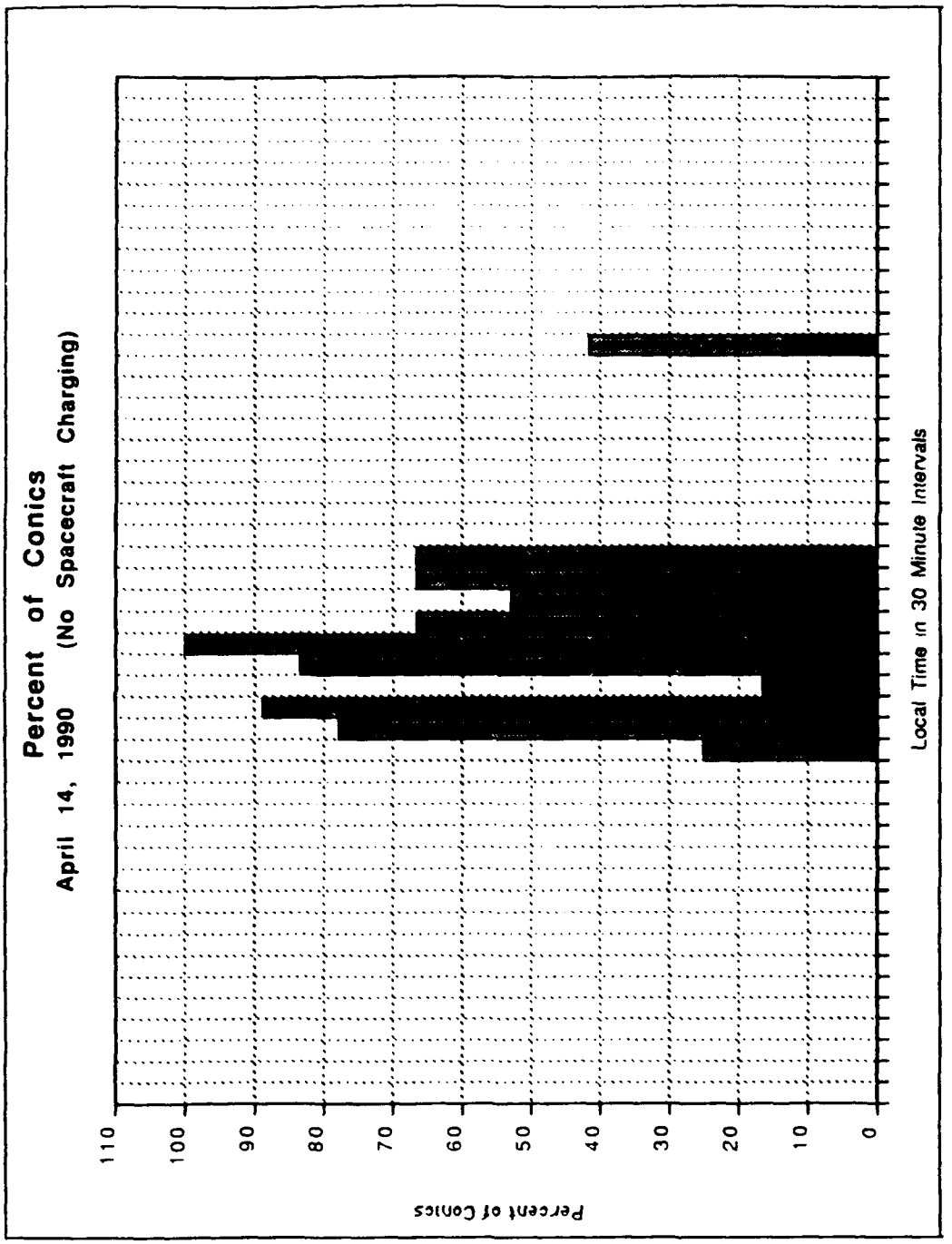

Percent of Conics for April 14, 1990

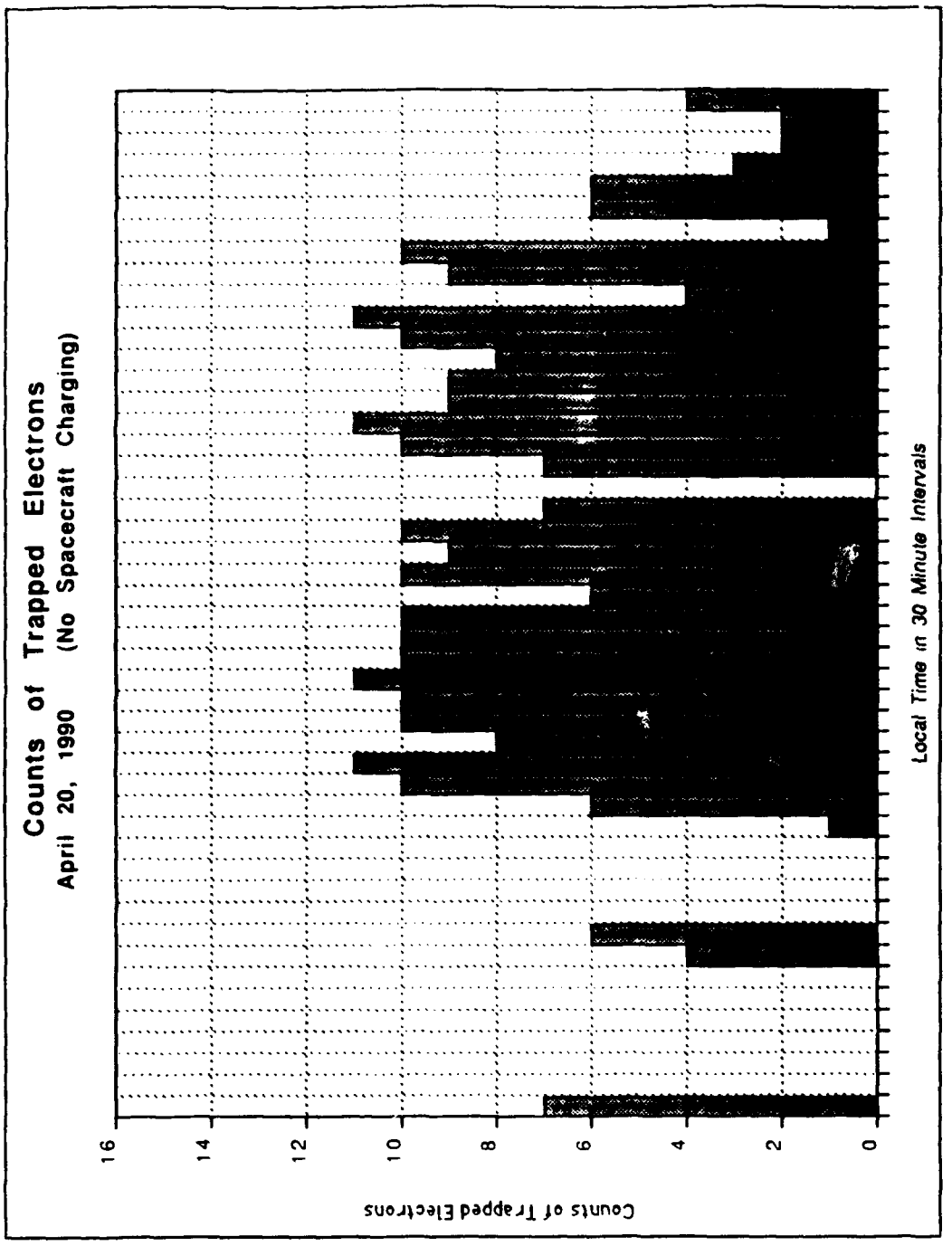

Counts of Trapped Electrons for April 20, 1990

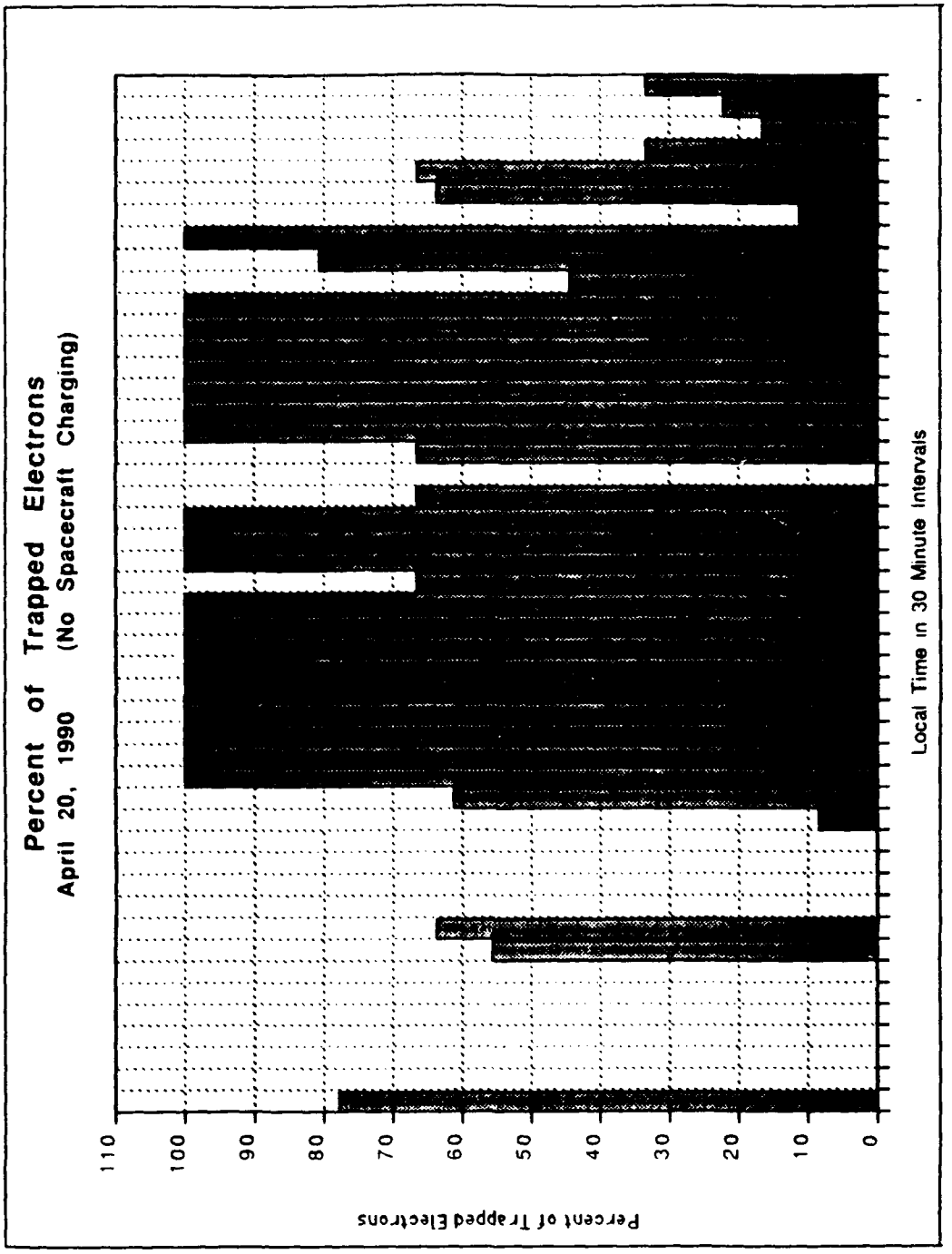

Percent of Trapped Electrons for April 20, 1990

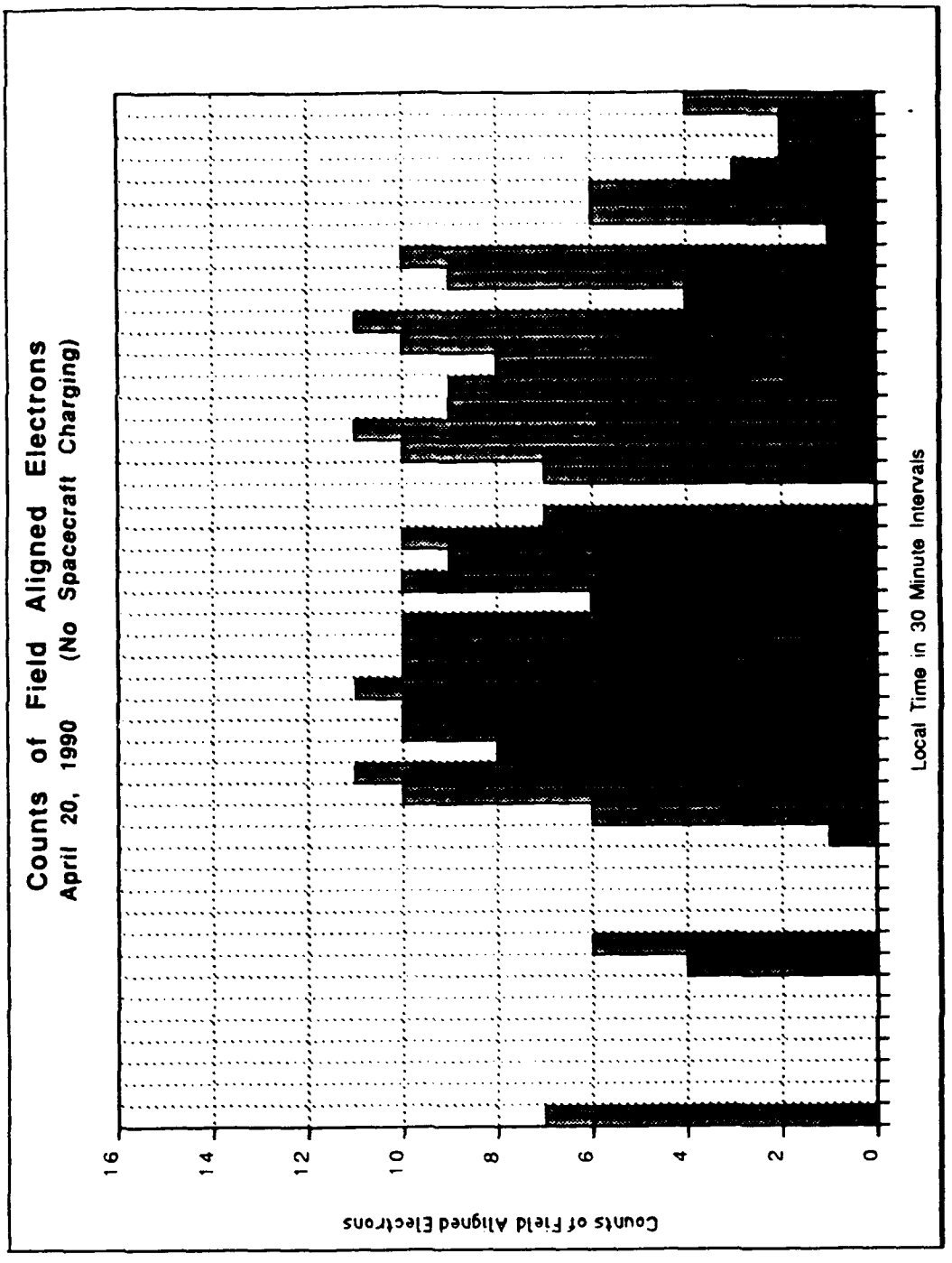

Counts of Field Aligned Electrons for April 20, 1990

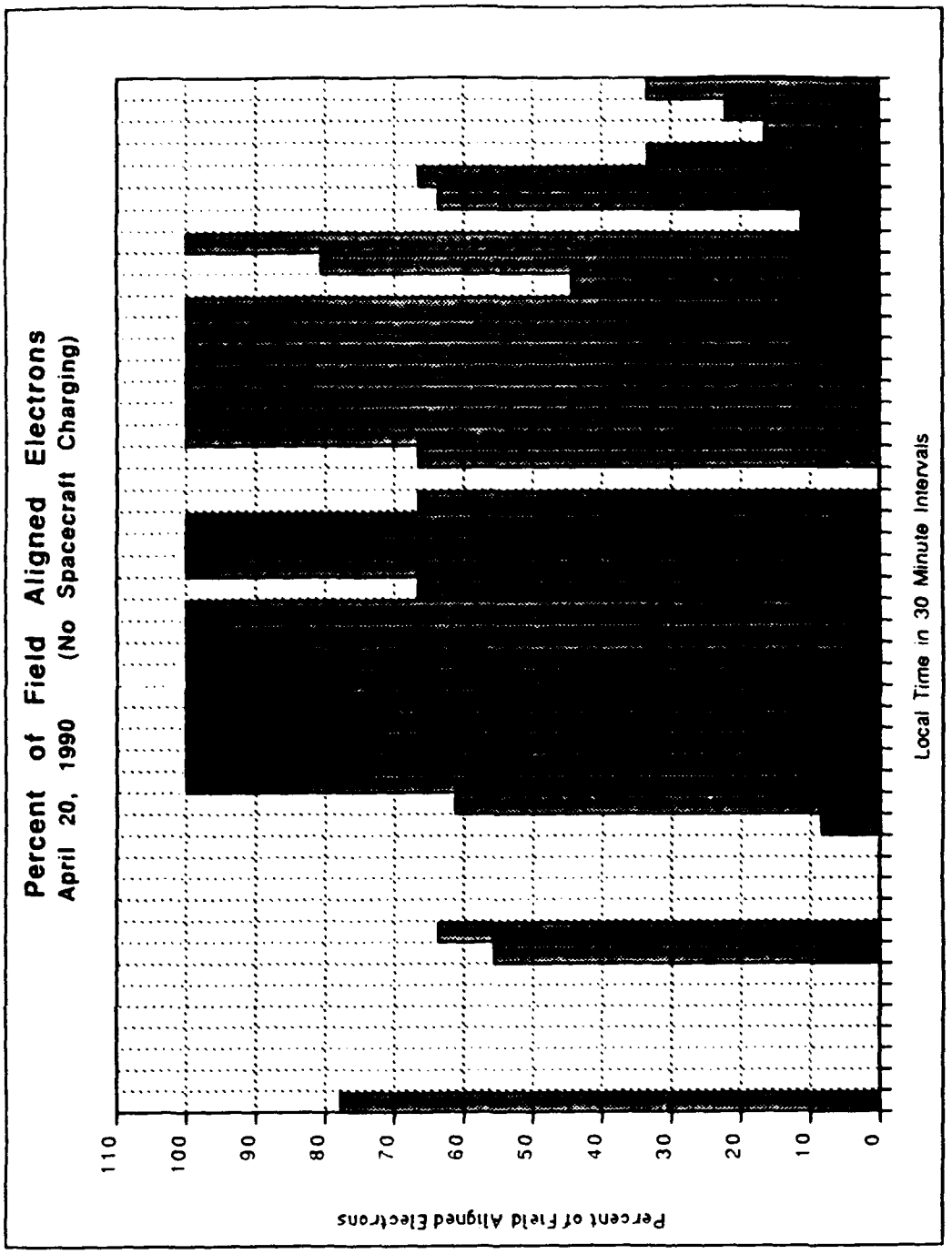

Percent of Field Aligned Electrons for April 20, 1990

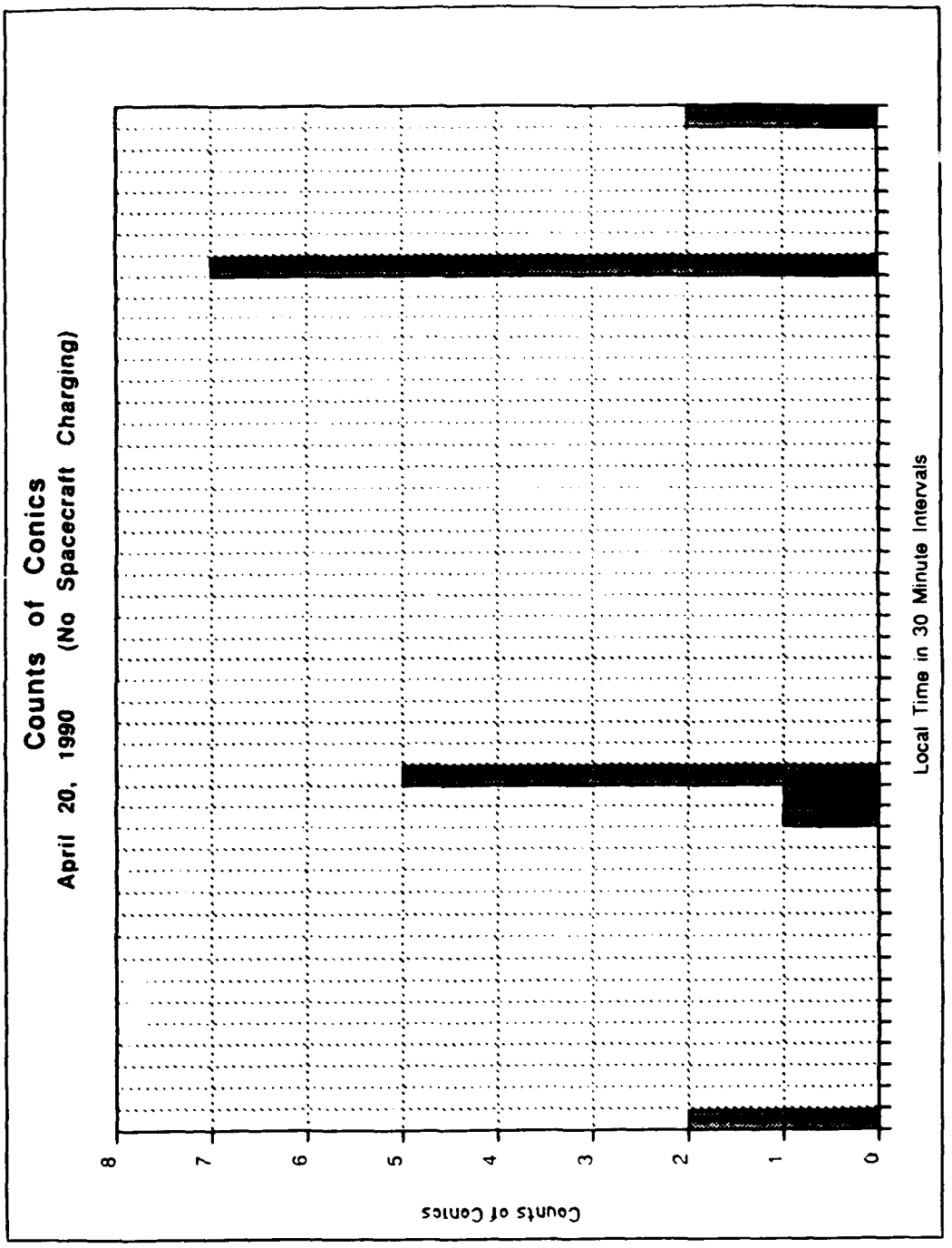

Counts of Conics for April 20, 1990

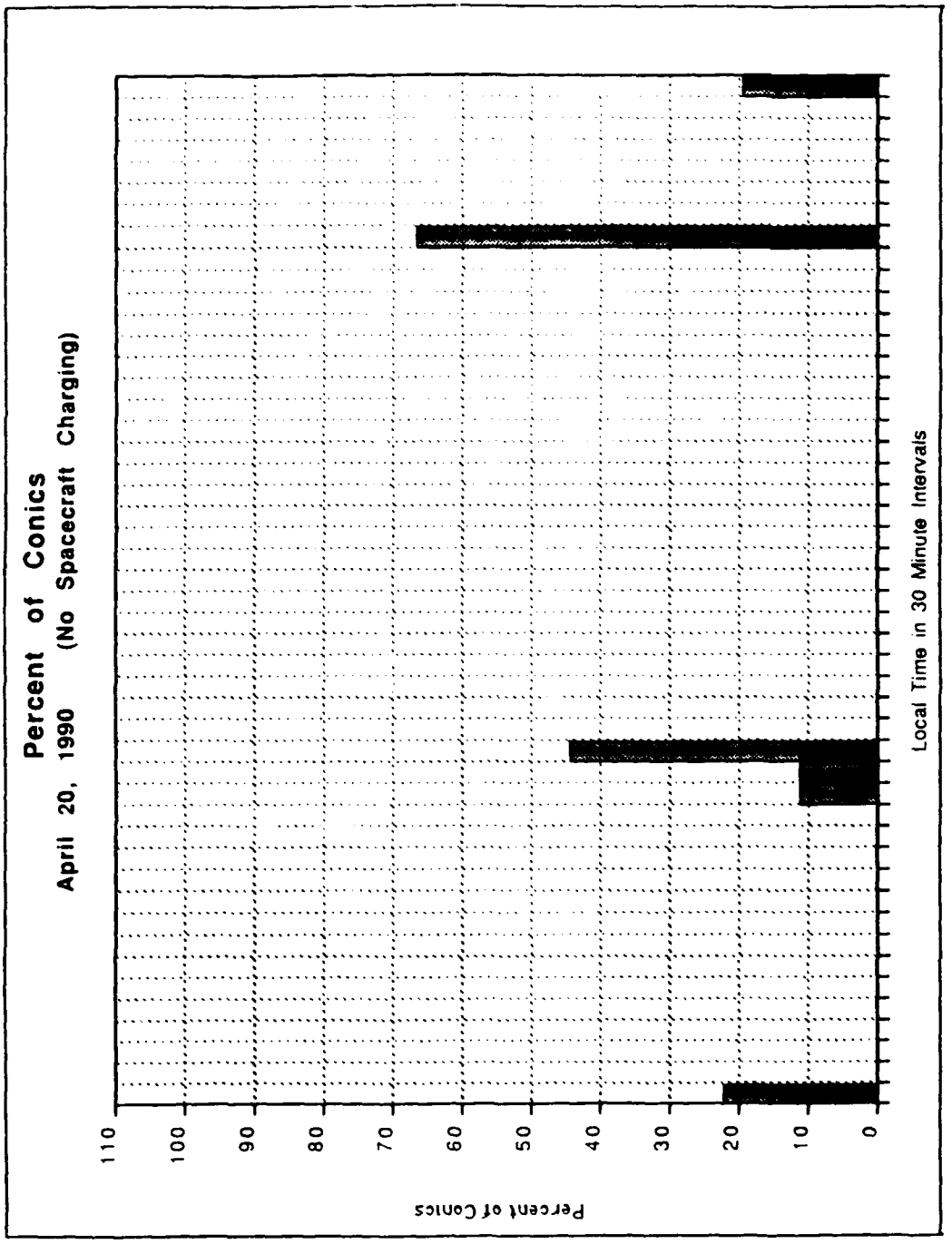

Percent of Conics for April 20, 1990

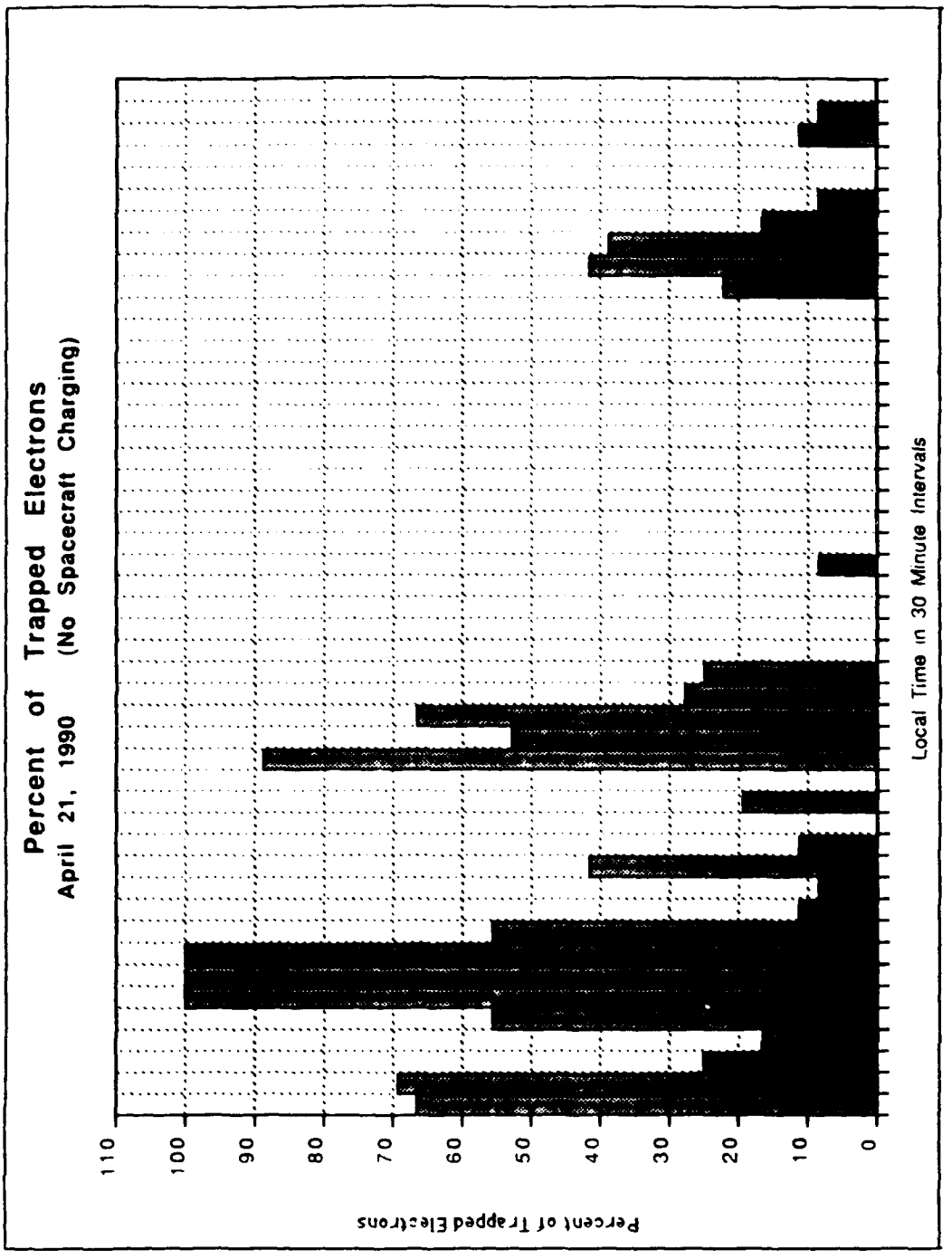

Percent of Trapped Electrons for April 21, 1990

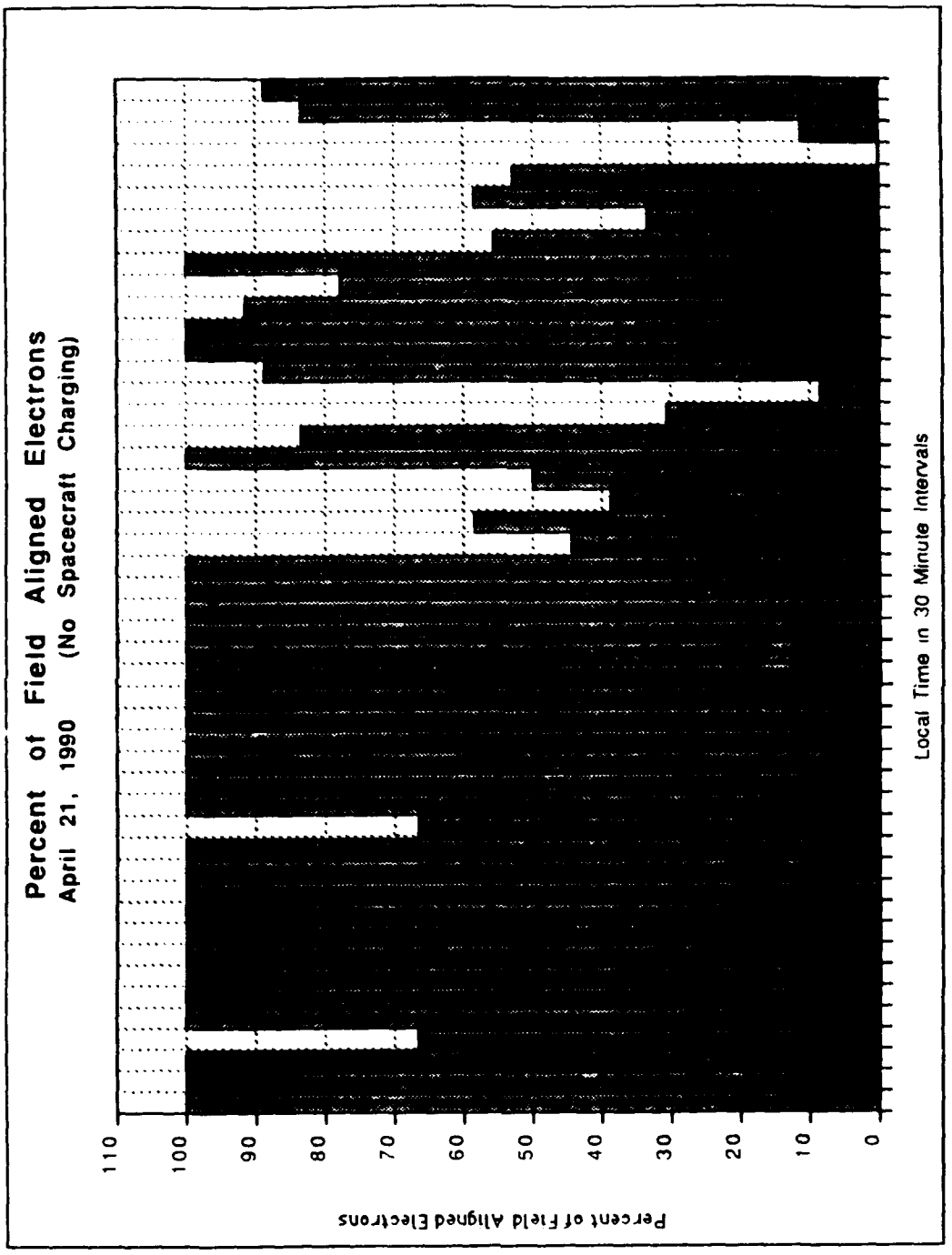

Percent of Field Aligned Electrons for April 21, 1990

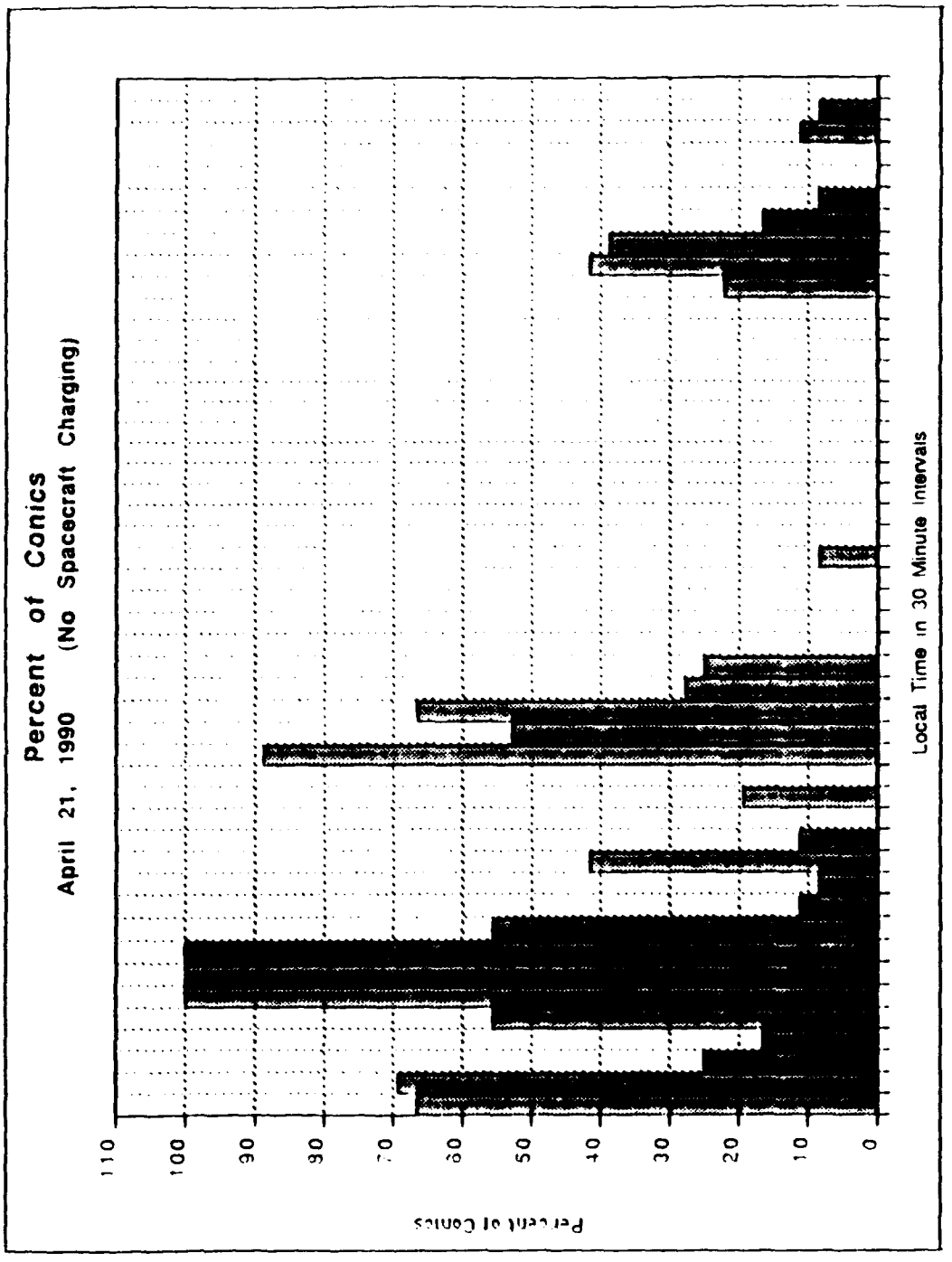

Percent of Conics for April 21, 1990

APPENDIX D PEAK ENERGY VERSUS TIME PLOTS

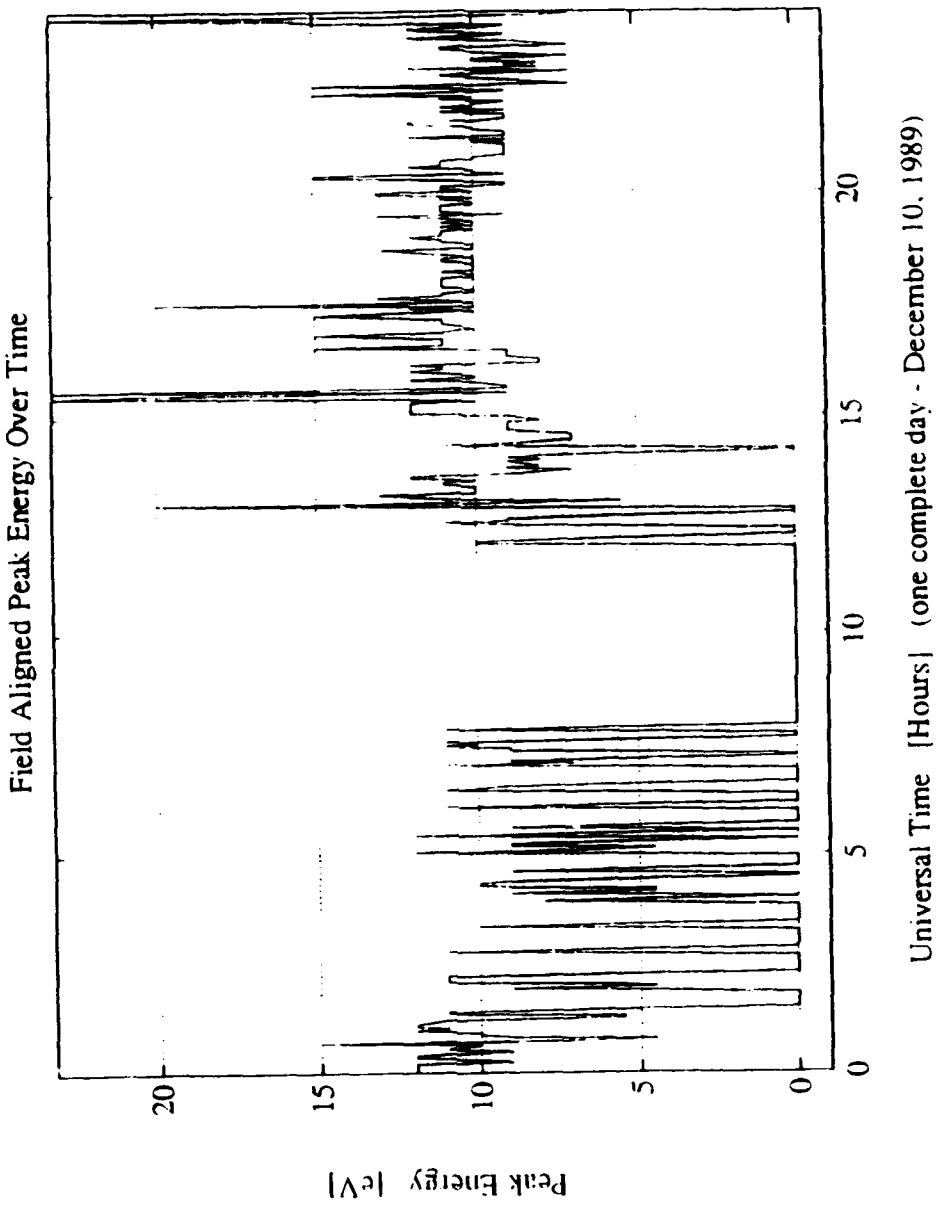

Peak Energy vs Time for Field Aligned Electron Distributions
December 10, 1989

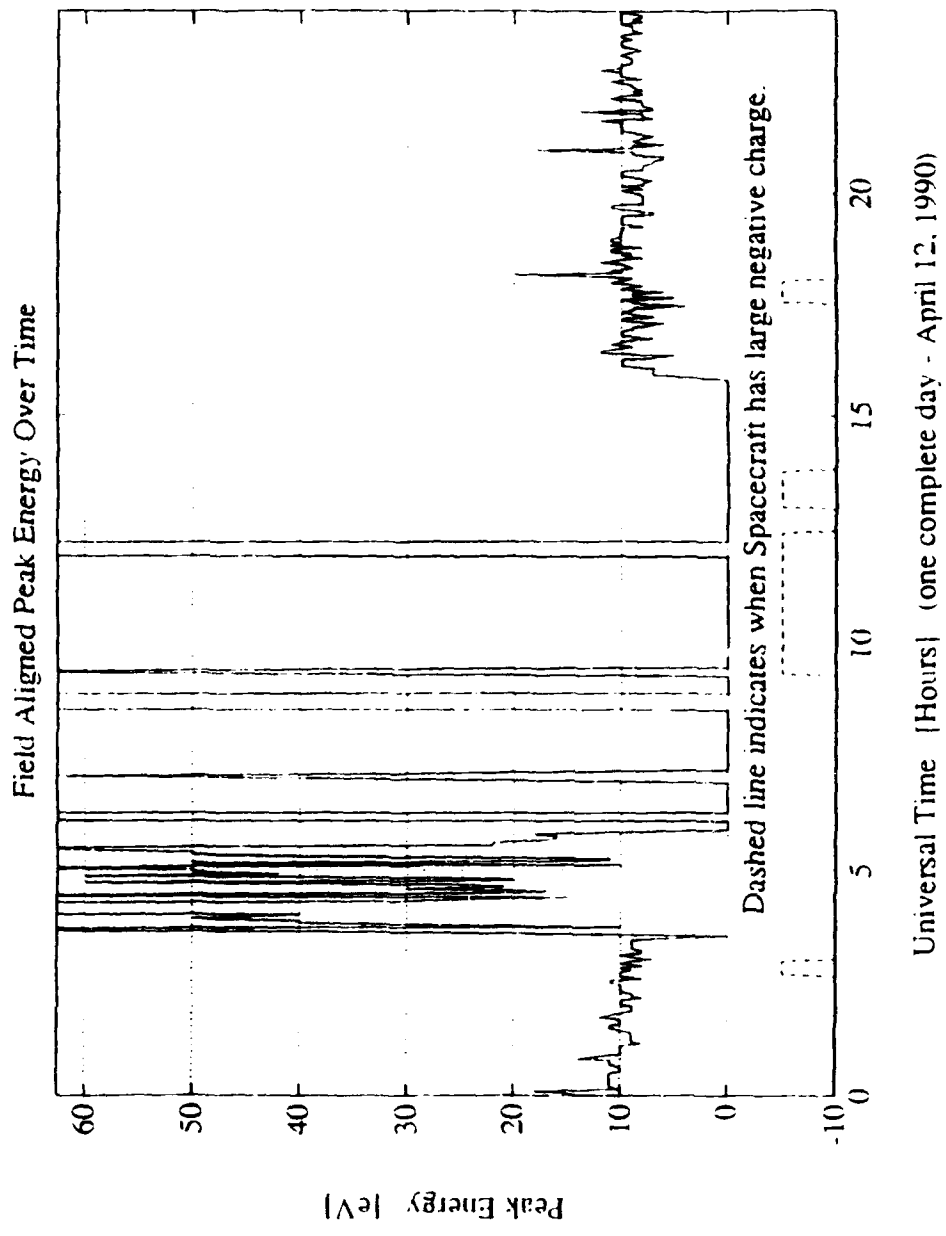

Peak Energy vs Time for Field Aligned Electron Distributions
April 12, 1990

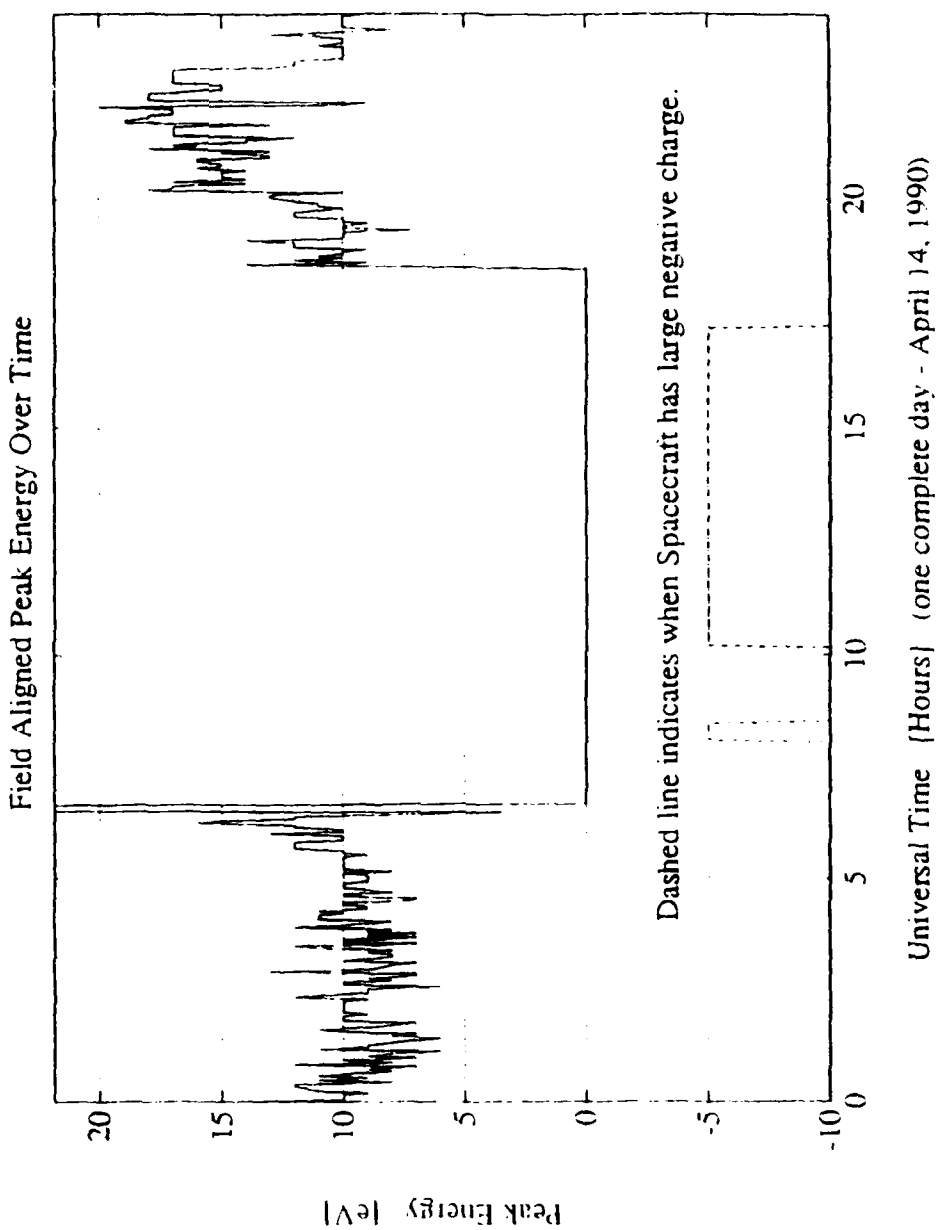

Peak Energy vs Time for Field Aligned Electron Distributions
April 14, 1990

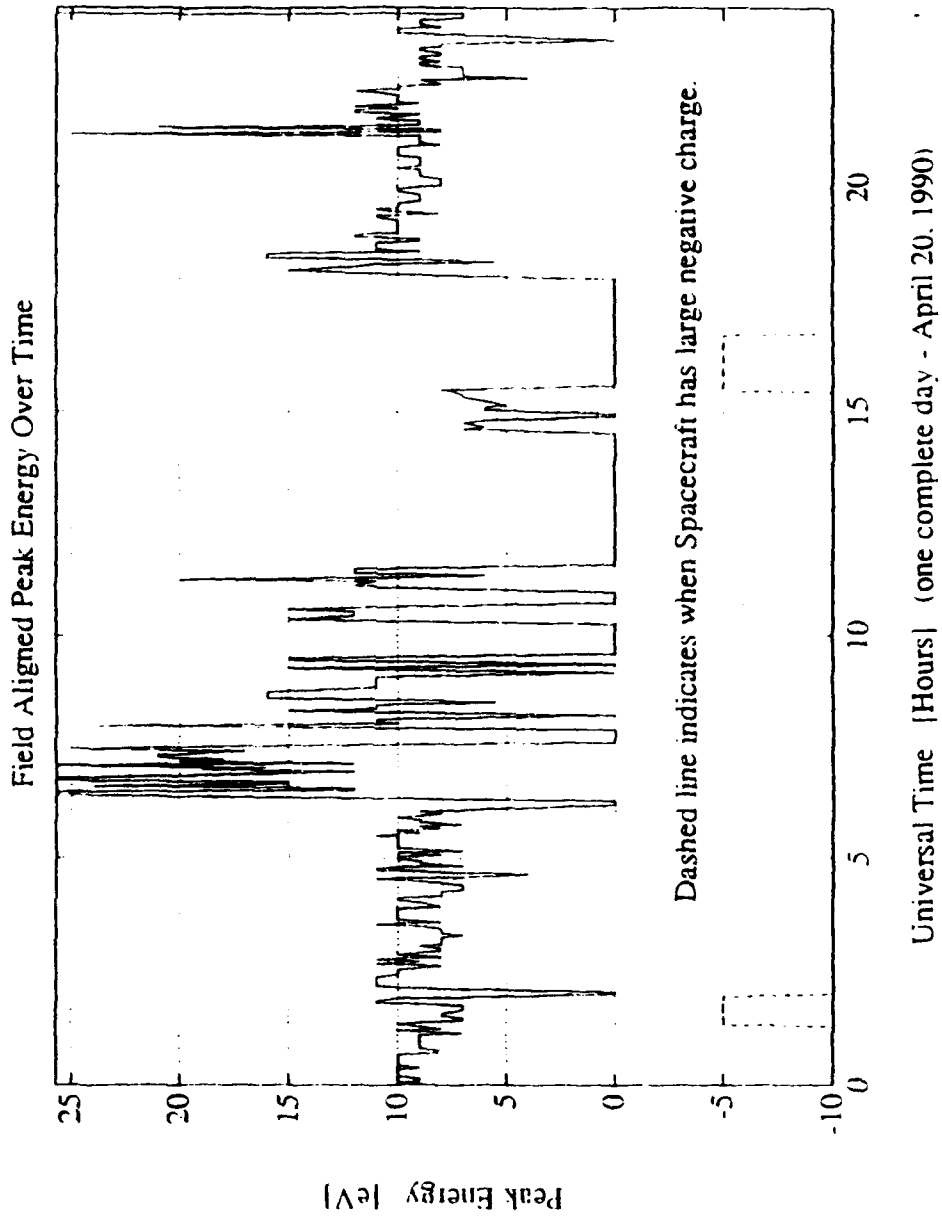

Peak Energy vs Time for Field Aligned Electron Distributions
April 20, 1990

LIST OF REFERENCES

Bame, S. J., *Magnetospheric Plasma Analyzer for Spacecraft with Constrained Resources* , Review of Science Instrumentation, Vol. 64, No. 4, pp. 1026-1033, April 1993.

Coates, A. J., *Ionospheric Photoelectrons Observed in the Magnetosphere at Distances up to 7 Earth Radii* , Planetary Space Science, Vol. 33, No. 11, pp.1267-1275, May 1985.

Chappell, C. R., *The Day Side of the Plasmasphere* , 1971.

Cicerone, Ralph J., *Thermalization and Transport of Photoelectrons: A Comparison of Theoretical Approaches* , Journal of Geophysical Research, Vol. 78, No. 28, pp. 6709-6728, 1973.

Cicerone, Ralph J., *Photoelectrons in the Ionosphere: Radar Measurements and Theoretical Computations* , Reviews of Geophysics and Space Physics, Vol. 12, No. 2, pp. 259-271, May 1974.

Doering, J. P., *High Resolution Daytime Photoelectron Energy Spectra from AE-E* . Geophysical Research Letters, Vol. 3., p. 129, 1976.

Dusenbery, P. B., *Generation of Ion- Conic Distribution by Upgoing Ionospheric electrons* , Journal Of Geophysical Research, Vol. 86, No. A9, pp. 7627-7638, September 1981.

Fiely, David Paul, *Survey of Spacecraft Charging Behavior for the Geosynchronous Satellite 1989-046* , Masters Thesis, Naval Postgraduate School, March 1992.

Galperin, Yu. I., *On the Sounding of the Magnetosphere by Photoelectrons* , Proceedings XVII Congress of I. A. F., Madrid, 1966.

List of References (Continued)

Johnstone, A. D., *Pitch Angle Diffusion of Low Energy Electrons by Whistler Mode Waves* , Journal Of Geophysical Research, Vol. 98, No. A4, pp. 5959-5967, April 1993.

Kennel, C. F., *VLF Electric Field Observations in the Magnetosphere* , Journal Of Geophysical Research, Vol. 75, pp. 6136-6152, January 1978.

Klumpar, D. M., *Direct Evidence for Two-Stage (Bimodal) Acceleration of Ionospheric Ions* , Journal Of Geophysical Research, Vol. 89, No. A12, pp. 10,779-10,787, December 1984.

Knudsen, W. C., *Eclipse and Non-Eclipse Differential Photoelectron Flux* , Journal Of Geophysical Research, Vol. 77, pp. 1221, 1972.

Krinberg, I. A., *Coulomb Collision-Induced Photoelectron Trapping by the Geomagnetic Field and Electron Gas Heating in the Plasmasphere* , Annales De Geophysique, t. 34, fasc. 2, pp. 89-96, 1978.

Lantto, Eric, *Detailed Analysis Case Studies of Trapped Plasmas at the Earth's Magnetic Equator* , Masters Thesis, Naval Postgraduate School, June 1993.

Lee, J. S., *Measurements of the Ambient Photoelectron Spectrum from Atmospheric Explorer: I. AE-E Measurements below 300 km During Solar Minimum Conditions* , Planetary Space Science, Vol. 28, pp.947-971, May 1980a.

Lee, J. S., *Measurements of the Ambient Photoelectron Spectrum from Atmospheric Explorer: II. AE-E Measurements from 300 to 1000 km During Solar Minimum Conditions* , Planetary Space Science, Vol. 28, pp.973-996, May 1980b.

List of References (Continued)

Mantas, George P., *Photoelectron Flux Buildup in the Plasmasphere* , Journal Of Geophysical Research, Vol. 83, No. A1, pp. 1-15, January 1978.

McComas, D. J., *Magnetospheric Plasma Analyzer (MPA): Initial Three-Spacecraft Observations from Geosynchronous Orbit* , Submitted to Journal of Geophysical Research, November 1992.

Olsen, Richard C., *Equatorially Trapped Plasma Populations* , Journal Of Geophysical Research, Vol. 86, No. A13, pp. 11,235-11,425, December 1981.

Oran E. S., *Photoelectron Flux in the Earth's Ionosphere* , Planetary Space Science, Vol. 26, p. 1161, 1978.

Peterson, W. K., *Measurement of magnetic Field Aligned Potential Differences Using High Resolution Conjugate Photoelectron Energy Spectra* , Geophysical Research Letters, Vol. 4., No. 9., pp. 373-376, September 1977b.

Peterson, W. K., *Conjugate Photoelectron Fluxes Observed on Atmosphere Explorer C* , Geophysical Research Letters, Vol. 4., No. 3., pp. 109-112, March 1977a.

Rao, B. C. N., *Photoelectron Flux in the Topside Ionosphere Measured by Retarding Potential Analyzers* , Journal Of Geophysical Research, Vol. 74, p. 1715, 1969.

Sharp, R. D., *Observation of an Ionospheric Acceleration Mechanism Producing Energetic (keV) Ions Primarily Normal to the Geomagnetic Field Direction* , Journal Of Geophysical Research, Vol. 82, No. 22, pp. 3324-3328, August 1977.

Shawhan, S. D., *Conjugate Photoelectron Impact Ionisation* , Journal of Atmospheric and Terrestrial Physics, Vol. 32, p. 1885, 1970.

List of References (Continued)

Singhal, R. P., *Analytical Yield Spectrum Approach to Photoelectron Fluxes in the Earth's Atmosphere* , American Geophysical Union, pp. 6847-6852, April 1984.

Takahashi, T., *Energy Degradation and Transport of Photoelectrons Escaping from the Upper Ionosphere* , Repts. Ionosphere Space Research, Japan, Vol. 27, No. 79, 1973.

Takahashi, T., *Degradation and Transport of Photoelectrons in the Plasmasphere* , Sciences Repts., Tohoku University, May 1974.

Tascione, Thomas F., *Introduction to the Space Environment* , pp. 45-100, Orbit Book Company, 1988.

Wrenn, Gordon L., *Satellite Measurements of Photoelectron Fluxes* , Exposé Présenté dans le Cadre du Symposium "Aurora and Airglow," Kyoto, October 1973.

BIBLIOGRAPHY

Braccio, Peter G, *Survey of Trapped Plasmas at the Earth's Magnetic Equator* , Masters Thesis, Naval Postgraduate School, December 1991.

Horwitz, J. L., *Core Plasma In the Magnetosphere* , Reviews of Geophysics, Vol. 25, No. 3, April 1987.

Kintner, Paul M., *A Search for the Plasma Processes Associated with Perpendicular Heating* , Journal Of Geophysical Research, Vol. 89, No. A2, February 1984.

Khazanov, G. V., *Analytic Description of the Electron Temperature Behavior in the Upper Ionosphere and the Plasmasphere* , Geophysical Research Letters, Vol. 19, No. 19, October 1992.

Krinberg, I. A., *The Influence of the Ionosphere-Plasmasphere Coupling Upon the Latitude Variations of Ionospheric Parameters*, Annales De Geophysique, t. 34, fasc.4, 1980.

McMahan, W. J., *The 2 to 5 eV Energy Spectra of Thermospheric Photoelectrons: Measurements in Apparent Conflict with Theory* , Journal Of Geophysical Research, Vol. 88, No. A11, November 1983.

Olsen, Richard C., *Energy Transfer at the Convection Boundary* , Submitted to Journal Of Geophysical Research, March 1993.

Scott, Lewis J., *On the Consequences of Bi-Maxwellian Distributions on Parallel Electric Fields* , Masters Thesis, Naval Postgraduate School, December 1991.

Bibliography (Continued)

Yamauchi, M., *A Narrow Region of Electron Beams at the Poleward Edge of the Cusp* , Journal Of Geophysical Research, Vol. 98, No. A5, May 1993.

INITIAL DISTRIBUTION LIST

1.	Defense Technical Information Center Cameron Station Alexandria, Virginia 22304-6145	2
2.	Superintendent Attn: Library, Code 52 Naval Postgraduate School Monterey, California 93943-5000	2
3.	Department Chairman, Code PH Department of Physics Naval Postgraduate School Monterey, California 93943-5000	1
4.	Dr. R. C. Olsen, Code PH/OS Department of Physics Naval Postgraduate School Monterey, California 93943-5000	5
5.	Dr. D. J. McComas Mail Stop D438, SST-8, LANL Los Alamos, New Mexico 87545	1
6.	Dr. M. Thomsen Mail Stop D438, SST-8, LANL Los Alamos, New Mexico 87545	1
7.	Mr. Gracen Joiner, Code 1114SP Office of Naval Research 800 N. Quincy Street Arlington, Virginia 22217	1
8.	Lcdr. J. S. Laszakovits, USN Portsmouth Naval Shipyard Kittery, Maine	2